EUROPEAN ORGANISATION FOR NUCLEAR RESEARCH (CERN)

Submitted to: PRC

CERN-EP-2024-196
July 26, 2024

Jet radius dependence of dijet momentum balance and suppression in Pb+Pb collisions at 5.02 TeV with the ATLAS detector

The ATLAS Collaboration

This paper describes a measurement of the jet radius dependence of the dijet momentum balance between leading back-to-back jets in 1.72 nb^{-1} of Pb+Pb collisions collected in 2018 and 255 pb^{-1} of pp collisions collected in 2017 by the ATLAS detector at the LHC. Both data sets were collected at $\sqrt{s_{\text{NN}}} = 5.02$ TeV. Jets are reconstructed using the anti-k_t algorithm with jet radius parameters $R = 0.2$, 0.3, 0.4, 0.5 and 0.6. The dijet momentum balance distributions are constructed for leading jets with transverse momentum p_{T} from 100 to 562 GeV for $R =$ 0.2, 0.3 and 0.4 jets, and from 158 to 562 GeV for $R = 0.5$ and 0.6 jets. The absolutely normalized dijet momentum balance distributions are constructed to compare measurements of the dijet yields in Pb+Pb collisions directly to the dijet cross sections in pp collisions. For all jet radii considered here, there is a suppression of more balanced dijets in Pb+Pb collisions compared to pp collisions, while for more imbalanced dijets there is an enhancement. There is a jet radius dependence to the dijet yields, being stronger for more imbalanced dijets than for more balanced dijets. Additionally, jet pair nuclear modification factors are measured. The subleading jet yields are found to be more suppressed than leading jet yields in dijets. A jet radius dependence of the pair nuclear modification factors is observed, with the suppression decreasing with increasing jet radius. These measurements provide new constraints on jet quenching scenarios in the quark-gluon plasma.

Contents

1 Introduction

The physics aim of the heavy-ion program at the Large Hadron Collider (LHC) [1] is to produce the quark–gluon plasma (QGP) and measure its properties. The QGP is an ultra hot and ultra dense state of matter in which quarks and gluons are no longer confined in color-neutral hadrons (for a recent review, see Ref. [2]). To understand the properties of the QGP at short distances, high transverse momentum (p_{T}) probes such as jets are used [3]. Jets traversing the QGP experience *jet quenching*, characterized by a reduction in the overall jet energy compared to expectations from pp collisions. This phenomenon is understood to arise from radiative and collisional energy loss, reducing the jet p_{T} by moving the energy of the initial parton to wider angles, with some of it ending up outside the jet cone [4]. Jet quenching is typically quantified by the overall rate of jets in a given centrality[1] interval in Pb+Pb collisions and at a given p_{T} compared to geometric expectations based on measured cross sections in pp, commonly known as the *nuclear modification factor*,

$$R_{\mathrm{AA}} = \frac{1}{N_{\mathrm{evt}}^{\mathrm{AA}}} \frac{\mathrm{d}N_{\mathrm{jet}}^{\mathrm{AA}}}{\mathrm{d}p_{\mathrm{T}}} \Bigg/ \left(\langle T_{\mathrm{AA}} \rangle \frac{\mathrm{d}\sigma_{\mathrm{jet}}^{pp}}{\mathrm{d}p_{\mathrm{T}}} \right), \tag{1}$$

where $N_{\mathrm{evt}}^{\mathrm{AA}}$ is the total number of minimum-bias Pb+Pb events and $\langle T_{\mathrm{AA}} \rangle$ is the mean nuclear thickness function [5] for the centrality interval. This normalization accounts for the geometric enhancement in hard scattering rates in Pb+Pb collisions with respect to pp collisions. The jet yield in Pb+Pb collisions is $N_{\mathrm{jet}}^{\mathrm{AA}}$, and the jet cross section in pp collisions is $\sigma_{\mathrm{jet}}^{pp}$, both measured as a function of the jet p_{T}. In the most

---

[1] Centrality characterizes the degree to which the colliding nuclei overlap. The most central collisions have a large overlap and the highest particle multiplicities, while the most peripheral collisions have only a minimal overlap and have particle multiplicities closer to those of pp collisions at the same nucleon–nucleon collision energy.

central Pb+Pb collisions, R_{AA} is observed to be approximately 0.5, dependent on the jet p_{T}, up to a p_{T} of approximately 1 TeV [6–9]. Measurements of the suppression of jets of different radii are of great interest to understand where the lost energy is with respect to the jet axis, how the energy is distributed among the jet particles, and to measure the possible response of the QGP to the presence of the jet [10, 11]. For $p_{\mathrm{T}} > 400$ GeV in central collisions, CMS has measured no significant dependence of the jet R_{AA} on the jet radius [12]. At much lower momentum ($p_{\mathrm{T}} < 100$ GeV), measurements from ATLAS [13] found a decrease in jet quenching (an increased jet yield) with increasing jet radius, with a moderate dependence on the jet radius. In contrast, recent measurements from ALICE [14] in a similar momentum region suggest that jet quenching *increases* for larger radii jets at fixed p_{T}. For recent reviews of jet quenching, see Refs. [3, 15].

Jets are largely produced in pairs in $2 \longrightarrow 2$ partonic scattering processes. The quantum chromodynamics (QCD) evolution of the partons after the scattering gives rise to back-to-back jets, referred to here as “dijets”. The two jets are expected to experience asymmetric energy loss due to traversing unequal path lengths in the QGP [16], driven by the geometry of the overlapping nuclei and the relative orientation of the jet trajectories through the QGP. Measurements of the azimuthal anisotropy of jets [17] have shown that the geometry of the overlapping nuclei affects the relative rates of jets measured in Pb+Pb collisions. Additionally, jets are also expected to experience jet-by-jet fluctuations in the energy-loss process [18]. While single jets can be used to study jet quenching, dijets can also be used as a complementary probe. The measurement of the p_{T} balance of dijets provides a way to constrain the relative importance of fluctuations and geometry in jet quenching. The shape modification of jets in dijets has been less studied than for single jets, where the jet shape is the distribution of charged-particle transverse momentum as a function of the angular distance to the jet axis. Studying jet shapes, CMS observed a redistribution of the charged-particle transverse momentum with an enhancement at larger angular distances with respect to the jet axis, when comparing Pb+Pb to pp collisions [19]. In this context, measurements of the jet radius dependence of the dijet balance are especially interesting and can provide different sensitivity to the location of the lost energy than is available with single jet measurements.

To compare the transverse momenta of the two jets that comprise a dijet, the leading dijet momentum balance

$$x_{\mathrm{J}} \equiv p_{\mathrm{T},2}/p_{\mathrm{T},1} \tag{2}$$

is measured. The leading dijet is constructed using the two highest-p_{T} jets out of the set of jets in an event, $p_{\mathrm{T},1}$ is the transverse momentum of the highest-p_{T} (leading) jet, and $p_{\mathrm{T},2}$, of the second-highest-p_{T} (subleading) jet.

In pp collisions, the showering process in vacuum and higher-order scattering processes can lead to imbalanced dijet transverse momenta. However, the most probable situation is that the jets are nearly balanced in p_{T} [20, 21]. Previous dijet measurements in Pb+Pb collisions have shown that jets are more likely to be more imbalanced in Pb+Pb collisions than in pp collisions [20–23].

Early dijet publications reported only the dijet momentum balance normalized by the measured dijet yields [20, 22, 23], to study the changes in the shape of the x_{J} distribution as a function of the heavy-ion collision centrality. Reference [21] addressed the absolute rate at which $R = 0.4$ dijets are produced in Pb+Pb collisions, assessing whether leading dijets are suppressed at levels similar to those for inclusive jets [6]. This paper extends the studies of Ref. [21] by varying the jet radius parameter, with leading dijets being measured in Pb+Pb and pp collisions at $\sqrt{s_{\mathrm{NN}}} = 5.02$ TeV. The measurements use 1.72 nb^{-1} of Pb+Pb collisions collected in 2018 and 255 pb^{-1} of pp data collected in 2017 with the ATLAS detector [24] at the LHC.

Jets are reconstructed using the anti-k_t algorithm [25] with radius parameters $R = 0.2, 0.3, 0.4, 0.5$ and 0.6. The analysis is conducted independently for each of the jet radius values. In each case, the leading dijets are constructed from the two highest-p_{T} jets in the event and are required to have the two jets nearly back-to-back in azimuth with $|\phi_1 - \phi_2| > 7\pi/8$ and $|y| < 2.1$[2]. Leading jets are reported with p_{T} values from 100 to 562 GeV for $R = 0.2, 0.3$ and 0.4 and from 158 to 562 GeV for $R = 0.5$ and 0.6. To be consistent with Refs. [20, 21], subleading jets are reported down to x_{J} values of 0.32 for each leading jet p_{T} selection. Events in which the two highest-p_{T} jets do not meet the selection criteria are discarded.

The primary observable for this measurement is the two-dimensional yield of leading dijets (N_{pair}) meeting the selection criteria described above:

$$\frac{\mathrm{d}^2 N_{\mathrm{pair}}}{\mathrm{d}p_{\mathrm{T},1}\mathrm{d}p_{\mathrm{T},2}}. \tag{3}$$

Analogously to R_{AA} in Eq. (1), the pair nuclear modification factors for dijets as a function of the leading and subleading jet p_{T} can be defined as:

$$R_{\mathrm{AA}}^{\mathrm{pair}}(p_{\mathrm{T},1}) = \frac{\frac{1}{\langle T_{\mathrm{AA}}\rangle N_{\mathrm{evt}}^{\mathrm{AA}}} \int_{0.32\times p_{\mathrm{T},1}}^{p_{\mathrm{T},1}} \frac{\mathrm{d}^2 N_{\mathrm{pair}}^{\mathrm{AA}}}{\mathrm{d}p_{\mathrm{T},1}\mathrm{d}p_{\mathrm{T},2}} \mathrm{d}p_{\mathrm{T},2}}{\frac{1}{L_{pp}} \int_{0.32\times p_{\mathrm{T},1}}^{p_{\mathrm{T},1}} \frac{\mathrm{d}^2 N_{\mathrm{pair}}^{pp}}{\mathrm{d}p_{\mathrm{T},1}\mathrm{d}p_{\mathrm{T},2}} \mathrm{d}p_{\mathrm{T},2}} \tag{4}$$

and

$$R_{\mathrm{AA}}^{\mathrm{pair}}(p_{\mathrm{T},2}) = \frac{\frac{1}{\langle T_{\mathrm{AA}}\rangle N_{\mathrm{evt}}^{\mathrm{AA}}} \int_{p_{\mathrm{T},2}}^{p_{\mathrm{T},2}/0.32} \frac{\mathrm{d}^2 N_{\mathrm{pair}}^{\mathrm{AA}}}{\mathrm{d}p_{\mathrm{T},1}\mathrm{d}p_{\mathrm{T},2}} \mathrm{d}p_{\mathrm{T},1}}{\frac{1}{L_{pp}} \int_{p_{\mathrm{T},2}}^{p_{\mathrm{T},2}/0.32} \frac{\mathrm{d}^2 N_{\mathrm{pair}}^{pp}}{\mathrm{d}p_{\mathrm{T},1}\mathrm{d}p_{\mathrm{T},2}} \mathrm{d}p_{\mathrm{T},1}}. \tag{5}$$

where $\langle T_{\mathrm{AA}}\rangle$ and $N_{\mathrm{evt}}^{\mathrm{AA}}$ are defined the same way as in Eq. (1), L_{pp} is the integrated luminosity of the pp collisions [26], and N_{pair}^{pp} and $N_{\mathrm{pair}}^{\mathrm{AA}}$ are the dijet yields in pp and Pb+Pb collisions, respectively. By integrating over $p_{\mathrm{T},2}$ ($p_{\mathrm{T},1}$), one can access information from $R_{\mathrm{AA}}^{\mathrm{pair}}(p_{\mathrm{T},1})$ ($R_{\mathrm{AA}}^{\mathrm{pair}}(p_{\mathrm{T},2})$) about the differential rate of dijet production in leading (subleading) jet p_{T} bins. Comparison of these two quantities at a fixed jet p_{T} provides information about the suppression of leading and subleading jets in a dijet. These quantities were first shown in Ref. [21].

Additionally, projections of the two-dimensional ($p_{\mathrm{T},1}, p_{\mathrm{T},2}$) distributions can be used to construct x_{J} distributions as a function of $p_{\mathrm{T},1}$ and $p_{\mathrm{T},2}$. The x_{J} values, as defined in Eq. (2), are reported for $0.32 < x_{\mathrm{J}} < 1.0$ for selections in $p_{\mathrm{T},1}$. This paper presents results of the *absolutely normalized* x_{J} distributions in pp collisions:

$$\frac{1}{L_{pp}} \frac{\mathrm{d}N_{\mathrm{pair}}^{pp}}{\mathrm{d}x_{\mathrm{J}}} \tag{6}$$

and in Pb+Pb collisions:

$$\frac{1}{\langle T_{\mathrm{AA}}\rangle N_{\mathrm{evt}}^{\mathrm{AA}}} \frac{\mathrm{d}N_{\mathrm{pair}}^{\mathrm{AA}}}{\mathrm{d}x_{\mathrm{J}}}. \tag{7}$$

---

[2] ATLAS uses a right-handed coordinate system with its origin at the nominal interaction point (IP) in the center of the detector, and the z-axis along the beam pipe. The x-axis points from the IP to the center of the LHC ring, and the y-axis points upward. Cylindrical coordinates (r, ϕ) are used in the transverse plane, ϕ being the azimuthal angle around the z-axis. The pseudorapidity is defined in terms of the polar angle θ as $\eta = -\ln\tan(\theta/2)$. The rapidity is defined as $y = 0.5\ln[(E + p_z)/(E - p_z)]$ where E and p_z are the energy and z-component of the momentum along the beam direction, respectively. Transverse momentum and transverse energy are defined as $p_{\mathrm{T}} = p\sin\theta$ and $E_{\mathrm{T}} = E\sin\theta$, respectively. The angular distance between two objects with relative differences $\Delta\eta$ in pseudorapidity and $\Delta\phi$ in azimuth is given by $\Delta R = \sqrt{(\Delta\eta)^2 + (\Delta\phi)^2}$.

Similarly, the *dijet-yield-normalized* x_{J} distributions are defined as:

$$\frac{1}{N_{\mathrm{pair}}}\frac{\mathrm{d}N_{\mathrm{pair}}}{\mathrm{d}x_{\mathrm{J}}}, \tag{8}$$

with a normalization that was used in previous dijet measurements [20–23].

The absolutely normalized x_{J} distributions allow a direct comparison between the dijet rates measured in Pb+Pb and pp collisions. This comparison is quantified by the ratio:

$$J_{\mathrm{AA}} \equiv \frac{1}{\langle T_{\mathrm{AA}}\rangle N_{\mathrm{evt}}^{\mathrm{AA}}}\frac{\mathrm{d}N_{\mathrm{pair}}^{\mathrm{AA}}}{\mathrm{d}x_{\mathrm{J}}} \Bigg/ \left(\frac{1}{L_{pp}}\frac{\mathrm{d}N_{\mathrm{pair}}^{pp}}{\mathrm{d}x_{\mathrm{J}}}\right). \tag{9}$$

Finally, the absolutely normalized x_{J} distributions can be integrated over the measurement range of $0.32 < x_{\mathrm{J}} < 1.0$ (and the corresponding ranges in $p_{\mathrm{T},1}$ and $p_{\mathrm{T},2}$) to construct the absolutely normalized dijet yields in Pb+Pb collisions:

$$\frac{1}{\langle T_{\mathrm{AA}}\rangle N_{\mathrm{evt}}^{\mathrm{AA}}}\int_{0.32\times p_{\mathrm{T},1}}^{p_{\mathrm{T},1}} \frac{\mathrm{d}^2N_{\mathrm{pair}}^{\mathrm{AA}}}{\mathrm{d}p_{\mathrm{T},1}\mathrm{d}p_{\mathrm{T},2}}\mathrm{d}p_{\mathrm{T},2} \tag{10}$$

and the dijet cross sections in pp collisions:

$$\frac{1}{L_{pp}}\int_{0.32\times p_{\mathrm{T},1}}^{p_{\mathrm{T},1}} \frac{\mathrm{d}^2N_{\mathrm{pair}}^{pp}}{\mathrm{d}p_{\mathrm{T},1}\mathrm{d}p_{\mathrm{T},2}}\mathrm{d}p_{\mathrm{T},2}. \tag{11}$$

2 ATLAS detector

The ATLAS detector [24] at the LHC is a multipurpose particle detector with a forward–backward symmetric cylindrical geometry and a near-4π coverage in solid angle. It consists of an inner tracking detector surrounded by a thin superconducting solenoid, electromagnetic and hadron calorimeters, and a muon spectrometer. The inner-detector system is immersed in a 2 T axial magnetic field and provides charged-particle tracking in $|\eta| < 2.5$. The high-granularity silicon pixel detector covers the vertex region and typically provides four measurements per track, with the first hit typically being in the insertable B-layer installed before Run 2 [27, 28]. It is followed by the silicon microstrip tracker (SCT), which usually provides eight measurements per track. These silicon detectors are complemented by the transition radiation tracker, a drift-tube-based detector, which surrounds the SCT and has coverage up to $|\eta| = 2.0$.

The calorimeter system covers the pseudorapidity range $|\eta| < 4.9$. In the region $|\eta| < 3.2$, electromagnetic calorimetry is provided by barrel and endcap high-granularity lead/liquid-argon (LAr) calorimeters, with an additional thin LAr presampler covering $|\eta| < 1.8$ to correct for energy loss in material upstream of the calorimeters. Hadronic calorimetry is provided by the steel/scintillator-tile calorimeter, segmented into three barrel structures in $|\eta| < 1.7$, and two copper/LAr hadronic endcap calorimeters. The solid angle coverage is completed with copper/LAr and tungsten/LAr calorimeter modules (FCal), covering the forward regions of $3.1 < |\eta| < 4.9$. Minimum-bias trigger scintillators detect charged particles over $2.1 < |\eta| < 3.9$ using two hodoscopes of 12 counters, positioned at $z = \pm 3.6$ m along the beamline from the center of the ATLAS detector, which are used for the minimum bias triggers and data samples. The zero-degree calorimeters (ZDC) consist of layers of alternating quartz rods and tungsten plates and are located symmetrically at $z = \pm 140$ m and cover $|\eta| \geq 8.3$. In Pb+Pb collisions, the ZDCs primarily measure "spectator" neutrons: neutrons that do not interact hadronically when the incident nuclei collide.

An extensive software suite [29] is used in simulation, in reconstruction and analysis of real and simulated events, in detector operations, and in the trigger and data acquisition systems of the experiment. Events of interest are selected for recording and offline analysis by the first-level (L1) trigger system implemented in custom hardware, followed by selections made by algorithms implemented in software in the high-level trigger (HLT) [30–32]. The L1 trigger identifies jet candidates by applying a sliding-window algorithm and selecting events above an E_{T} threshold of 30 GeV. These events are then passed to the HLT trigger, which uses a jet reconstruction and background subtraction procedure similar to that used in the offline analysis and requires a minimum p_{T} of 100 GeV for anti-k_t $R = 0.4$ jets. The jet trigger efficiencies are evaluated separately for each of the jet radii considered here. The p_{T} thresholds are set such that the triggers were fully efficient for each R value over the p_{T} range considered in this measurement, with the highest threshold trigger sampling the full luminosity. In addition to the jet triggers, a minimum-bias sample was constructed using three different triggers, each one corresponding to one of the following conditions: total E_{T} in the calorimeter less than 50 GeV at L1 and at least one track reconstructed at HLT; total E_{T} in the calorimeter between 50 and 600 GeV at L1; total E_{T} greater than 600 GeV at L1. More details about the triggering used in ATLAS heavy-ion collisions can be found in Refs. [30–32].

3 Data and Monte Carlo selection

The Pb+Pb data used in these measurements were collected in 2018, and the pp data used were collected in 2017, both at a per-nucleon-pair center-of-mass energy $\sqrt{s_{\mathrm{NN}}} = 5.02$ TeV. Events were selected by the minimum-bias and jet triggers [30, 33] described in Section 2. Although only a small fraction of the Pb+Pb events ($< 0.5\%$) contain multiple collisions, these were suppressed utilizing the observed anti-correlation, expected from the nuclear geometry, between the total transverse energy deposited in both of the forward calorimeters, $\Sigma E_{\mathrm{T}}^{\mathrm{FCal}}$, and the energy in both ZDCs, which is proportional to the number of observed spectator neutrons. Events with multiple collisions, called pileup, are not rejected in pp collisions.

The overlap area of the two colliding nuclei in Pb+Pb collisions is characterized by the event centrality, which is estimated from $\Sigma E_{\mathrm{T}}^{\mathrm{FCal}}$ [34]. This measurement considers five centrality intervals as defined according to successive percentiles of the $\Sigma E_{\mathrm{T}}^{\mathrm{FCal}}$ distribution obtained from minimum-bias collisions. The centrality intervals considered in this measurement are 0–10% (largest $\Sigma E_{\mathrm{T}}^{\mathrm{FCal}}$, most central collisions), 10–20%, 20–40%, 40–60%, and 60–80% (smallest $\Sigma E_{\mathrm{T}}^{\mathrm{FCal}}$, peripheral collisions). The values of the mean nuclear thickness function, $\langle T_{\mathrm{AA}} \rangle$ [5], and their uncertainties [35] are determined using the TGlauberMC v3.2 package [36]. The $\langle T_{\mathrm{AA}} \rangle$ values and their uncertainties are listed in Table 1 for each centrality interval considered in this measurement.

The analysis uses three Monte Carlo (MC) samples to evaluate the detector performance and correct for detector effects. The pp MC sample includes 3.2×10^7 Pythia 8 [37] pp dijet events generated at center-of-mass energy $\sqrt{s} = 5.02$ TeV with the A14 set of tuned parameters [38] and the NNPDF23lo parton distribution functions (PDFs) [39]. Pileup due to additional inelastic pp interactions is similarly generated using Pythia 8 with the same PDFs and utilizing the A3 set of tuned parameters [40], tuned for inclusive QCD processes, matching the number of extra collisions in the pp data. The MC sample for Pb+Pb collisions uses the 2018 detector conditions and contains 3.2×10^7 pp Pythia 8 events with the same tune and PDFs as used for the generation of the pp MC samples. The underlying event (UE) contribution to the detector signal is accounted for by overlaying the simulated pp events with dedicated minimum-bias

Table 1: The $\langle T_{\mathrm{AA}} \rangle$ values and their uncertainties for the centrality selections used in this measurement, obtained from the TGlauberMC v3.2 modeling of the total transverse energy in the forward calorimeters, $\Sigma E_{\mathrm{T}}^{\mathrm{FCal}}$.

Centrality selection	$\langle T_{\mathrm{AA}} \rangle \pm \delta\langle T_{\mathrm{AA}} \rangle$ [mb^{-1}]
0–10%	23.35 ± 0.20
10–20%	14.33 ± 0.17
20–40%	6.79 ± 0.16
40–60%	1.96 ± 0.09
60–80%	0.39 ± 0.03

Pb+Pb data events. The minimum-bias data events from Pb+Pb collisions are combined with the signal from the Pythia 8 simulation of hard scattering events at the digitization stage, and then reconstructed as a combined event. This procedure enables the "data overlay" sample to accurately reproduce the effects of the UE on the jet response. This sample is reweighted on an event-by-event basis to ensure the same centrality distribution as is measured in the triggered data samples. Finally, pp Herwig7 [41, 42] events using the UEEE5 tune [43] and the CTEQ6L1 PDFs [44] are used for flavor uncertainty studies and comparisons with pp data. The detector response in all three MC samples is simulated utilizing Geant4 [45, 46].

4 Jet reconstruction and performance

The jet reconstruction procedures follow those used by ATLAS for previous jet measurements in Pb+Pb collisions [6, 17]. Jets are reconstructed using the anti-k_t algorithm [25] implemented in the FastJet software package [47]. In both the pp and Pb+Pb collisions, jets with $R = 0.2, 0.3, 0.4, 0.5$ and 0.6 are formed by clustering calorimetric towers of spatial size $\Delta\eta \times \Delta\phi = 0.1 \times \pi/32$. In Pb+Pb collisions, a background subtraction procedure is applied in each event to estimate the UE average transverse energy density, $\rho(\eta, \phi)$, where the ϕ dependence is due to global azimuthal correlations in the particle production from the hydrodynamic flow [48]. The modulation accounts for the contribution to the UE of the second-, third-, and fourth-order azimuthal anisotropy harmonics characterized by values of flow coefficients v_n^{UE} [48]. An iterative procedure is used to remove the impact of jets on the estimated ρ and v_n^{UE} values. Jet R-, η-, and p_{T}-dependent correction factors derived in simulations are applied to the measured jet energy to correct for the calorimeter energy response [49, 50]. An additional correction based on *in situ* studies of jets recoiling against photons and jets in other regions of the calorimeter is applied to account for differences between the data and MC [51]. This calibration is followed by a "cross-calibration" in which the jet energy scale (JES) of jets reconstructed by the procedure outlined in this section is related to the JES in 13 TeV pp collisions. The cross-calibration allows for the use of uncertainties obtained for the latter [50].

"Truth"-level jets are defined in the MC samples before detector simulation by applying the anti-k_t algorithm with $R = 0.2, 0.3, 0.4, 0.5$ and 0.6 to stable particles with a proper lifetime greater than 30 ps, but excluding muons and neutrinos, which do not leave significant energy deposits in the calorimeter. After the detector simulation the truth jets are matched to the nearest reconstructed jet in $\Delta R < 0.75R$. The performance of the jet reconstruction is characterized by the JES and jet energy resolution (JER), which correspond to the mean and variance, respectively, of the $p_{\mathrm{T}}^{\mathrm{reco}}/p_{\mathrm{T}}^{\mathrm{truth}}$ distribution, where $p_{\mathrm{T}}^{\mathrm{reco}}$ is the reconstructed jet p_{T} and $p_{\mathrm{T}}^{\mathrm{truth}}$ is the p_{T} of the matched truth-level jet. The JES and JER as a function of $p_{\mathrm{T}}^{\mathrm{truth}}$ can be seen in Figure 1 for $R = 0.2$ and $R = 0.6$ jets. The broadening of the JER with centrality is due to the UE

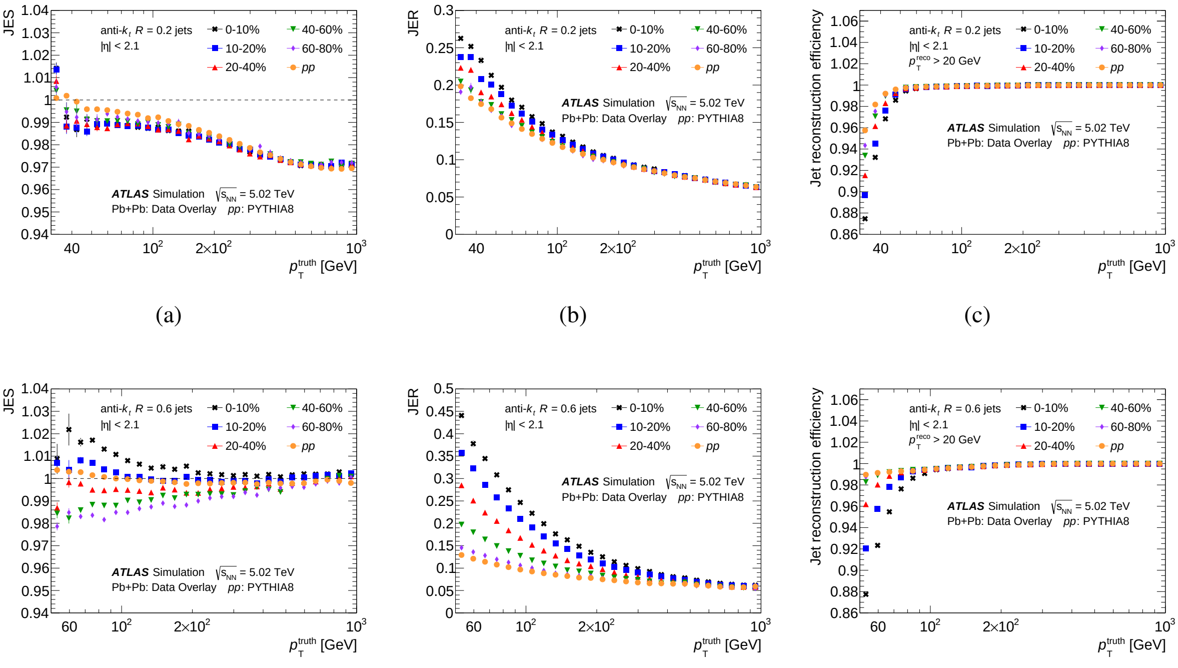

(a) (b) (c)

(d) (e) (f)

Figure 1: The (a,d) JES, (b,e) JER, and (c,f) jet reconstruction efficiency for (a,b,c) $R = 0.2$ and (d,e,f) $R = 0.6$ jets in pp collisions and the centrality selections in Pb+Pb collisions used in this analysis.

fluctuations, which are larger in more central collisions and cause the jet p_T to smear. Additionally, a larger jet radius allows for a larger contribution of the UE fluctuations, causing the larger R jets to have a larger JER. The deviation of the JES from unity for high-p_T $R = 0.2$ jets is due to the different requirements used in the determination of the jet calibration compared to this analysis. JES and JER effects are corrected for by the unfolding procedure described below. The efficiency of reconstructing a jet with $p_T > 20$ GeV, as evaluated from the probability of a truth-jet matching to a reconstructed jet, can also be seen as a function of p_T^{truth} in Figure 1. The lower p_T bounds in this figure are based on the p_T requirements used in the analysis, which are different for the various jet radii in order to minimize the effects from the UE.

5 Data analysis

The analysis and dijet selection used here closely follow those in Ref. [21]. In each data event, the reconstructed leading dijet is constructed from the two highest-p_T^{reco} jets in the event with reconstructed leading $p_{T,1}^{reco} > 79$ GeV, and reconstructed subleading $p_{T,2}^{reco} > 32$ GeV for $R = 0.2, 0.3$ and 0.4 jets, $p_{T,2}^{reco} > 41$ GeV for $R = 0.5$ jets, and $p_{T,2}^{reco} > 51$ GeV for $R = 0.6$ jets. The minimum $p_{T,1}^{reco}$ was based on the minimum p_T for which the trigger is fully efficient for the various jet radii. The minimum $p_{T,2}^{reco}$ was based on 0.32 of the minimum p_T for which the rate of jets created by UE fluctuations becomes negligible. For $R = 0.2, 0.3$ and 0.4 jets, the rate of jets created by UE fluctuations is negligible above approximately 100 GeV, so results are quoted for leading jet $p_{T,1}^{reco} > 100$ GeV. A minimum x_J of 0.32 implies $p_{T,2}^{reco} = 0.32 p_{T,1}^{reco}$, giving a corresponding minimum subleading jet $p_{T,1}^{reco} > 32$ GeV. The rate of jets created by the UE fluctuations depends on the jet radius, so an analogous minimum $p_{\mathrm{T},2}^{\mathrm{reco}}$ was selected for the other jet radii. Both jets are required to have $|y^{\mathrm{reco}}| < 2.1$. These selections provide an underflow region for the unfolding to enable inflow and outflow of jets from the measurement region. These dijets are required to be back-to-back with $|\phi_1 - \phi_2| > 7\pi/8$. Leading dijets meeting these criteria represent approximately 62% of inclusive $R = 0.2$ jets with $100 < p_{\mathrm{T}}^{\mathrm{reco}} < 562$ GeV, and approximately 72% of inclusive $R = 0.6$ jets with $158 < p_{\mathrm{T}}^{\mathrm{reco}} < 562$ GeV. Events in which the leading dijets do not meet these criteria are discarded. For dijets matching the selection criteria, two-dimensional $(p_{\mathrm{T},1}^{\mathrm{reco}}, p_{\mathrm{T},2}^{\mathrm{reco}})$ distributions are constructed symmetrically across $p_{\mathrm{T},1}^{\mathrm{reco}} = p_{\mathrm{T},2}^{\mathrm{reco}}$. The distributions are symmetrized to account for the possibility of swapping the leading and subleading jet definition due to the finite JER.

The measured $(p_{\mathrm{T},1}^{\mathrm{reco}}, p_{\mathrm{T},2}^{\mathrm{reco}})$ distributions are a combination of the dijet signal and pairs of uncorrelated jets. Since the UE subtraction accounts for azimuthal correlations in the particle production due to hydrodynamic flow, the contribution from uncorrelated dijets is largely independent of the $|\phi_1 - \phi_2|$ of the jets; therefore, a $|\phi_1 - \phi_2|$ sideband method is used to remove these pairs as a function of $(p_{\mathrm{T},1}^{\mathrm{reco}}, p_{\mathrm{T},2}^{\mathrm{reco}})$. The symmetrized two-dimensional $(p_{\mathrm{T},1}^{\mathrm{reco}}, p_{\mathrm{T},2}^{\mathrm{reco}})$ distribution of background combinatoric dijets is determined using dijets with $1 < |\phi_1 - \phi_2| < 1.4$ which, after normalizing to the $|\phi_1 - \phi_2|$ window of the signal band, is subtracted from the dijet yields. This effect is strongest for 0–10% centrality Pb+Pb events at low $p_{\mathrm{T},1}^{\mathrm{reco}}$. In the most central collisions, combinatoric dijets constitute 2% of the $R = 0.2$ dijets with $p_{\mathrm{T},1}^{\mathrm{reco}} > 100$ GeV and $p_{\mathrm{T},2}^{\mathrm{reco}} > 32$ GeV, and 1% of the $R = 0.6$ dijets with $p_{\mathrm{T},1}^{\mathrm{reco}} > 158$ GeV and $p_{\mathrm{T},2}^{\mathrm{reco}} > 51$ GeV. The combinatoric dijet rate drops off rapidly with increasing $p_{\mathrm{T},1}^{\mathrm{reco}}$ and more peripheral events. Because of how the leading dijet is defined, the presence of residual combinatoric dijets in the sample results in an inefficiency for genuine jet pairs, where one of the jets might be replaced by an uncorrelated third jet. This effect is corrected for using the measured inclusive jet spectrum from minimum-bias events, reweighted to match the centrality distribution in the triggered data, to determine the efficiency loss as a function of the measured jet p_{T}, following the method discussed in Ref. [20]. This efficiency correction is the largest in the 0–10% centrality interval, being at most 3% for $R = 0.2$ jets and 7% for $R = 0.6$ jets.

To correct for the effects of the JES and JER, the measured $(p_{\mathrm{T},1}^{\mathrm{reco}}, p_{\mathrm{T},2}^{\mathrm{reco}})$ distributions are unfolded using the iterative Bayesian unfolding procedure [52] as implemented in the RooUnfold [53] software package. A two-dimensional unfolding is used to account for bin migration of both the leading and the subleading jet p_{T} and to account for possible swapping of the leading and subleading jet. Separate response matrices are generated for pp collisions and for each centrality selection in Pb+Pb collisions, for each R value used. The response matrix used in the unfolding contains the relationship between $(p_{\mathrm{T},1}^{\mathrm{truth}}, p_{\mathrm{T},2}^{\mathrm{truth}})$ and $(p_{\mathrm{T},1}^{\mathrm{reco}}, p_{\mathrm{T},2}^{\mathrm{reco}})$. It is populated by identifying the leading and subleading truth-level jets in the MC sample, which are matched to the corresponding reconstructed jets with $\Delta R < 0.75R$. To account for migration from lower jet $p_{\mathrm{T}}^{\mathrm{reco}}$, the response matrices are populated with truth-level jets down to $p_{\mathrm{T},1}^{\mathrm{truth}}$ of 20 GeV and $p_{\mathrm{T},2}^{\mathrm{truth}}$ of 10 GeV. As with the reconstructed data, truth dijets are required to have $|\phi_1^{\mathrm{truth}} - \phi_2^{\mathrm{truth}}| > 7\pi/8$, with each jet having $|y^{\mathrm{truth}}| < 2.1$. The two selected reconstructed jets from the MC simulations are required to meet the same selection criteria as applied to dijets measured in data. Truth dijets that do not match to a reconstructed dijet meeting the selection criteria are accounted for by using an efficiency correction in the unfolding.

Similarly to the construction of the data distributions, the response matrix is populated symmetrically in $p_{\mathrm{T},1}$ and $p_{\mathrm{T},2}$. The symmetrization is done in order to regularize the response matrix [54]. The unfolding requires an assumed initial distribution, referred to here as the prior, which is similar to the measured distributions. To generate the prior, the response matrices are reweighted along the $p_{\mathrm{T},1}^{\mathrm{truth}}$ and $p_{\mathrm{T},2}^{\mathrm{truth}}$ axes by the ratio of the two-dimensional reconstructed yields in data to those from simulation. The number of iterations used in the unfolding is tuned separately for each centrality in Pb+Pb collisions and for pp collisions, for each jet radius. The number of iterations in each case is selected to optimize the balance between the accuracy of the final unfolded yield, and the increased statistical uncertainty that results from a larger number of iterations. In Pb+Pb collisions, the number of iterations is largest for central events and larger radii; two iterations were used for the $R = 0.2$ jets in 60–80% central Pb+Pb collisions, while seven iterations were used for the $R = 0.6$ jets in 0–10% central Pb+Pb collisions. In pp collisions, the number of iterations increased with the jet radii; seven iterations were used for the $R = 0.6$ jets and three iterations were used for the $R = 0.2$ jets.

To evaluate the statistical uncertainties of the data and the MC simulations, 100 bootstrap [55] variations following a Poisson distribution were used. The nominal data was unfolded with each of the response matrix variations to obtain the statistical uncertainties of the MC sample. Similarly, each variation of the data was unfolded with the nominal response matrix to obtain the statistical uncertainties of the data. The statistical uncertainties were obtained from the standard deviation of both the data and MC variations of the unfolded distributions. The data and MC components were added in quadrature to obtain the total statistical uncertainty.

To extract the measurements of the dijet momentum balance observable, x_{J}, the unfolded two-dimensional $(p_{\mathrm{T},1}, p_{\mathrm{T},2})$ distributions are first reflected about $p_{\mathrm{T},1} = p_{\mathrm{T},2}$ to restore the leading/subleading hierarchy. Then, following the procedure discussed in Refs. [20, 21, 56], the two-dimensional distributions are projected into bins of x_{J} for different $p_{\mathrm{T},1}$ slices. After projecting the resulting distributions over selections of $p_{\mathrm{T},1}$, the absolutely normalized x_{J} distributions are extracted by normalizing the x_{J} distributions either by the integrated luminosity in pp collisions or the number of events and the $\langle T_{\mathrm{AA}} \rangle$ in Pb+Pb collisions, as described in Eqs. (6) and (7).

6 Systematic uncertainties

Systematic uncertainties for this measurement are attributed to three categories of sources arising from: the analysis and unfolding procedure, the uncertainties in the JES and JER, and the global normalization. For each uncertainty component in the first two categories, the entire analysis procedure is repeated accounting for the change in the analysis procedure or the response matrix and the result is compared with the nominal one. The third category applies only to the absolutely normalized x_{J} distributions, J_{AA} distributions, and $R_{\mathrm{AA}}^{\mathrm{pair}}(p_{\mathrm{T},1})$ and $R_{\mathrm{AA}}^{\mathrm{pair}}(p_{\mathrm{T},2})$ distributions; it contains the uncertainty in the determination of the mean nuclear thickness function $\langle T_{\mathrm{AA}} \rangle$, and the pp luminosity. The $\langle T_{\mathrm{AA}} \rangle$ uncertainties are shown in Table 1, while the relative luminosity uncertainty in pp collisions is $\delta L_{pp}/L_{pp} = 1\%$ [26]. These uncertainties are independent of the jet p_{T} and are noted on the figures.

The systematic uncertainty in the JES has five parts. Four parts are identical to those in Ref. [21], which correspond to the in situ studies, the cross-calibration, the flavor uncertainties, and the modification of parton showers due to quenching. The modifications to the parton shower can impact the detector response to jets in Pb+Pb collisions resulting in a small disagreement in the JES between data and simulations. The extent of this disagreement, and corresponding uncertainty contribution is evaluated by the method used in Ref. [50] for 2015 and 2011 data, which compares the jet p_{T} measured in the calorimeter with the sum of the transverse momenta of charged particles within the jet, in both the data and MC samples. This uncertainty is determined as a function of the event centrality and is found to be independent of the jet p_{T} and η. The selected charged-particle tracks have $p_{\mathrm{T}} > 4$ GeV in order to exclude particles from the UE. The sum of the charged-particle transverse momenta provides a data-driven estimate of the centrality dependence of the JES arising from the observed centrality-dependent modification of the jet fragmentation due to jet quenching in Pb+Pb collisions [57]. The size of this centrality-dependent uncertainty in the JES reaches 1.2% in the most central collisions and its value is applied independently of x_J. The systematic uncertainties from the JES discussed above are derived for $R = 0.4$ jets.

The fifth component accounts for the potential difference in uncertainties between $R = 0.4$ and the other jet radii. It does not depend on the collision centrality for $R = 0.2$ and $R = 0.3$ jets, but contains a centrality dependent contribution for $R = 0.5$ and $R = 0.6$ jets to account for data and MC differences of the jet response due to the larger area. The centrality-independent component is assessed by comparing the p_T for matched $R = 0.2$, $R = 0.3$, $R = 0.5$, and $R = 0.6$ jets with $R = 0.4$ jets measured in the data and the MC samples. For each individual component, the JES in the MC simulation is modified as a function of p_T and η by one standard deviation, and the response matrix is recomputed.

The uncertainty due to the JER is evaluated by repeating the unfolding procedure with modified response matrices, where an additional contribution is added to the resolution of the reconstructed p_T in the MC sample using a Gaussian smearing procedure. The smearing factor is evaluated using an in situ technique in 13 TeV pp data that involves studies of dijet p_T balance [58]. Furthermore, an uncertainty is included to account for differences between the tower-based jet reconstruction and the jet reconstruction used in analyses of 13 TeV pp data, as well as differences in the calibration procedures. Similarly to the JES, an additional uncertainty is assigned to the JER to account for differences between the $R = 0.4$ jets and the other jet radii. The changes in the response are propagated through the unfolding and the resulting uncertainty is symmetrized.

Two sources of systematic uncertainty are included to account for uncertainties in the removal of the combinatoric background. The first contribution stems from the combinatoric subtraction method, and is determined by extracting the two-dimensional $(p_{T,1}, p_{T,2})$ distribution of combinatoric jets from an alternative sideband of $1.1 < |\phi_1 - \phi_2| < 1.5$ as was done in Refs. [20, 21]. The second contribution stems from the sensitivity of the analysis to the efficiency correction for combinatoric jets, and is evaluated by repeating the analysis without the inclusion of this efficiency correction. The deviation from the nominal result is symmetrized and taken as the uncertainty contribution. Both these contributions are found to be negligible compared with the other sources of systematic uncertainties.

Additional sources of systematic uncertainty that account for the unfolding procedure are considered. The sensitivity to the Bayesian prior is evaluated by modifying the weights applied when producing the response matrix in a centrality-dependent manner in order to enclose the data $(p_{T,1}^{\text{reco}}, p_{T,2}^{\text{reco}})$ distributions between the corresponding MC distributions based on the nominal and alternative priors. There is a sensitivity to the minimum p_T^{jet} in the analysis at small x_J and small $p_{T,1}$ due to the efficiency correction made as part of the unfolding. The sensitivity of the result to this effect is evaluated by varying the minimum reconstructed p_T^{jet}, motivated by the magnitude of the JER, from 32 to 39 GeV for $R = 0.2, 0.3$ and 0.4 jets, from 41 to 51 GeV for $R = 0.5$ jets, and from 51 to 63 GeV for $R = 0.6$ jets, for both the data and simulation. This results in a significant contribution to the systematic uncertainties at low x_J in low $p_{T,1}$ bins. For each of these contributions the deviation of the unfolded result from the nominal is symmetrized and taken as a contribution to the systematic uncertainties.

The systematic uncertainties in the absolutely normalized x_J distributions can be seen in Figure 2, for 0–10% central Pb+Pb and pp collisions, and for $R = 0.2$ and $R = 0.6$ jets. In central Pb+Pb collisions for $R = 0.2$ jets, the total uncertainties are driven by the JES and JER uncertainties; for $R = 0.6$ jets in these collisions, the total systematic uncertainties are driven by the unfolding's sensitivity to the choice of prior and its closure. In pp collisions, the total uncertainties are largely driven by the JES and JER uncertainties for both the $R = 0.2$ and $R = 0.6$ jets. The relative uncertainties are largest at low x_J in both collision systems; however, the yield in these x_J regions is small. Similar trends were obtained for the systematic uncertainties of $R = 0.3$, $R = 0.4$, and $R = 0.5$ jets, with similar values of the relative uncertainties.

The systematic uncertainty contributions are similarly propagated to the calculation of $R_\mathrm{AA}^\mathrm{pair}$ and J_AA. The centrality-independent components of the JES and JER, and the centrality-independent part of the jet radius dependent uncertainty are treated as correlated between Pb+Pb and pp collisions. The rest of the contributions to the systematic uncertainty are treated as uncorrelated between Pb+Pb and pp. The resulting uncertainties in $R_\mathrm{AA}^\mathrm{pair}(p_\mathrm{T,1})$ and $R_\mathrm{AA}^\mathrm{pair}(p_\mathrm{T,2})$ are shown for 0–10% central Pb+Pb collisions in Figure 3 for $R = 0.2$ and $R = 0.6$ jets; these uncertainties are dominated by the JES and JER. Similar trends were obtained for the systematic uncertainties of $R = 0.3$, $R = 0.4$, and $R = 0.5$ jets, with similar values of the relative uncertainties. In the ratio $R_\mathrm{AA}^\mathrm{pair}(p_\mathrm{T,2})/R_\mathrm{AA}^\mathrm{pair}(p_\mathrm{T,1})$ each source of systematic uncertainty is treated as fully correlated between $R_\mathrm{AA}^\mathrm{pair}(p_\mathrm{T,2})$ and $R_\mathrm{AA}^\mathrm{pair}(p_\mathrm{T,1})$, including the global systematic uncertainties. The ratios allow the cancellation of systematic uncertainties and improve the precision of the measurements.

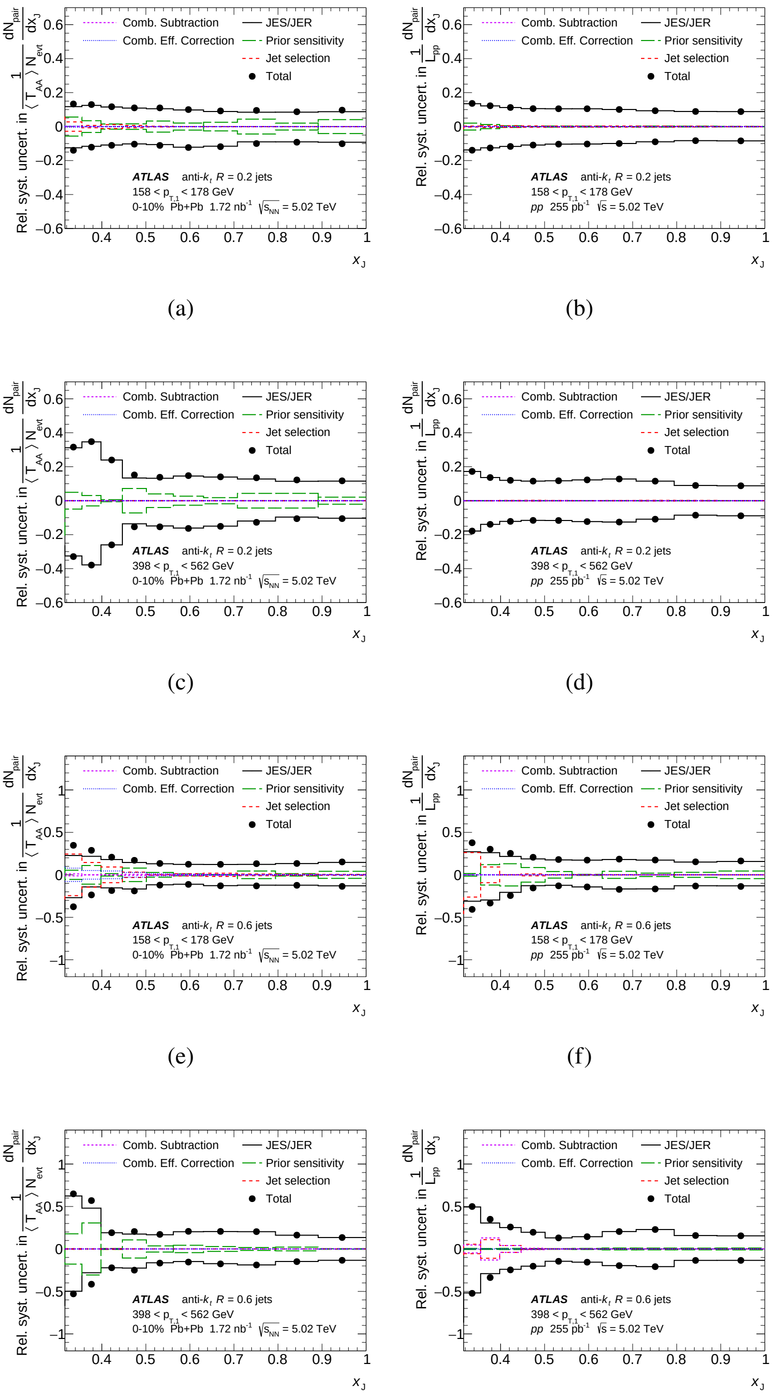

(a) (b)

(c) (d)

(e) (f)

(g) (h)

Figure 2: Relative systematic uncertainties in the absolutely normalized x_J distributions in (a,c,e,g) 0–10% central Pb+Pb collisions and (b,d,f,h) pp collisions for (a,b,c,d) $R = 0.2$ and (e,f,g,h) $R = 0.6$ jets for leading jets with (a,b,e,f) $158 < p_{T,1} < 178$ GeV and (c,d,g,h) $398 < p_{T,1} < 562$ GeV. Jets are selected with $|y| < 2.1$ and $|\phi_1 - \phi_2| > 7\pi/8$. The normalization uncertainties (not shown) are $\delta\langle T_{AA}\rangle/\langle T_{AA}\rangle = 0.9\%$ in 0–10% Pb+Pb collisions and $\delta L_{pp}/L_{pp} = 1\%$ in pp collisions.

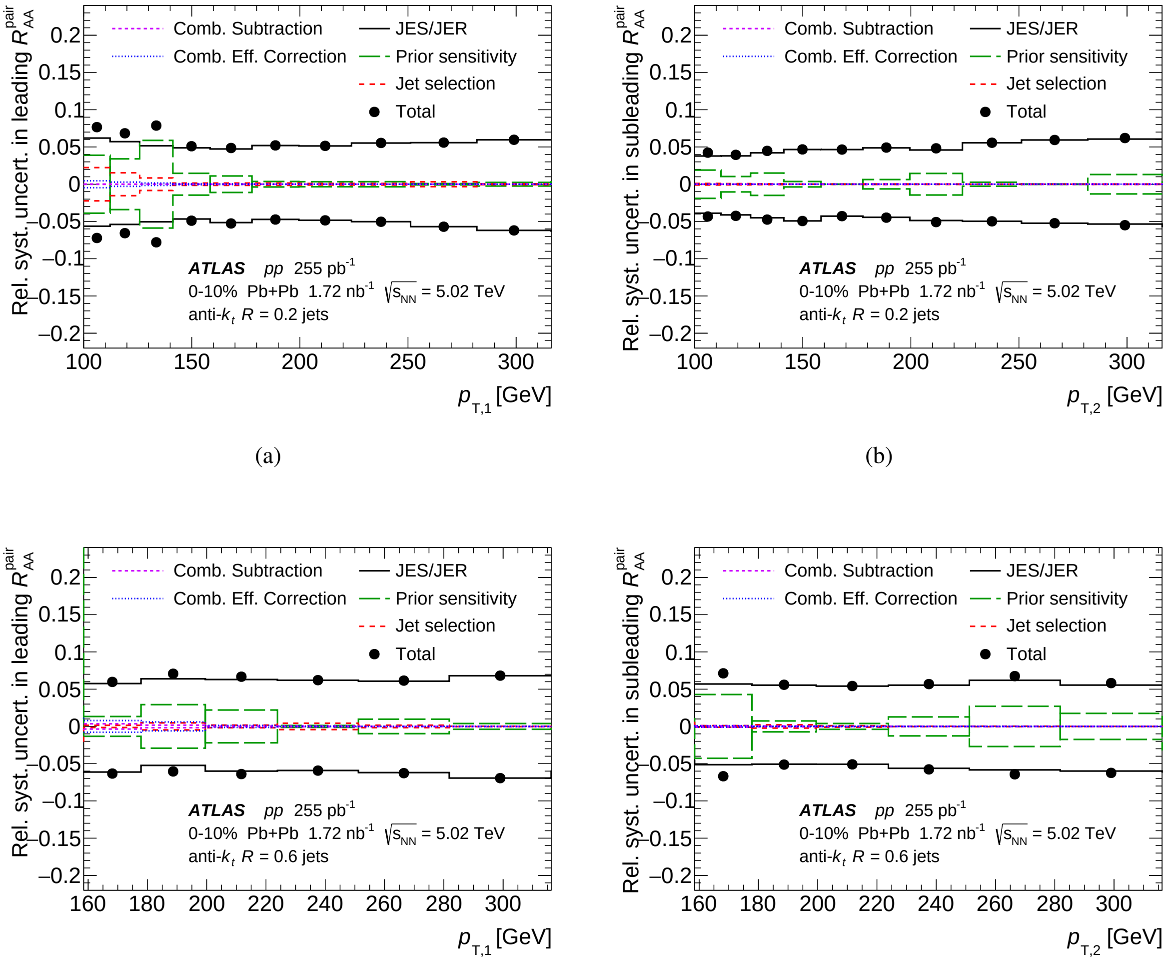

(a) (b)

(c) (d)

Figure 3: Relative systematic uncertainties in the R_{AA}^{pair} for (a,c) leading and (b,d) subleading (a,b) $R = 0.2$ and (c,d) $R = 0.6$ jets. Jets are selected with $|y| < 2.1$ and $|\phi_1 - \phi_2| > 7\pi/8$. The normalization uncertainties (not shown) are $\delta\langle T_{AA}\rangle/\langle T_{AA}\rangle = 0.9\%$ in 0–10% Pb+Pb collisions and $\delta L_{pp}/L_{pp} = 1\%$ in pp collisions.

7 Results

7.1 $R_{\mathrm{AA}}^{\mathrm{pair}}$ distributions

The leading and subleading dijet yields in 0–10% central Pb+Pb collisions and the dijet cross sections in pp collisions are shown in Figure 4 for the various jet radii. These distributions correspond to the numerators and denominators in Eqs. (4) and (5). Figure 5 shows the dijet cross-section ratios of $R = 0.3, 0.4, 0.5, 0.6$ jets with respect to $R = 0.2$ jets in central Pb+Pb and pp collisions. The dijet yields increase with increasing jet radius for both the leading and subleading jets in both collision systems. Additionally, the dijet cross-section ratios in pp data, for R jets with respect to $R = 0.2$ jets, are compared with PYTHIA 8 and HERWIG7 simulations in Figure 5. Generally the PYTHIA 8 results are closer to the data than the HERWIG7 results. HERWIG7 consistently underpredicts the cross-section ratios.

The $R_{\mathrm{AA}}^{\mathrm{pair}}$ distributions are shown in Figure 6 for $R = 0.2$ and $R = 0.6$ jets. For both jet radii, the leading jet $R_{\mathrm{AA}}^{\mathrm{pair}}(p_{\mathrm{T},1})$ is larger than the subleading jet $R_{\mathrm{AA}}^{\mathrm{pair}}(p_{\mathrm{T},2})$ for all p_{T} considered here. It is also observed that $R_{\mathrm{AA}}^{\mathrm{pair}}(p_{\mathrm{T},1})$ and $R_{\mathrm{AA}}^{\mathrm{pair}}(p_{\mathrm{T},2})$ generally increase with increasing p_{T}, except for the leading $R_{\mathrm{AA}}^{\mathrm{pair}}(p_{\mathrm{T},1})$ of the $R = 0.6$ jets, which is flatter as a function of p_{T}. This behavior had also been previously observed with $R = 0.4$ jets in Ref. [21].

To understand the differences between the $R_{\mathrm{AA}}^{\mathrm{pair}}$ of leading and subleading jets, the $R_{\mathrm{AA}}^{\mathrm{pair}}(p_{\mathrm{T},2})/R_{\mathrm{AA}}^{\mathrm{pair}}(p_{\mathrm{T},1})$ ratio is considered. Figure 7 shows $R_{\mathrm{AA}}^{\mathrm{pair}}(p_{\mathrm{T},2})/R_{\mathrm{AA}}^{\mathrm{pair}}(p_{\mathrm{T},1})$ as a function of centrality, jet radius, and p_{T} for jets with $158 < p_{\mathrm{T}} < 316$ GeV. The overall trend as a function of centrality is as expected; for all jet radii, the most central collisions show the most suppression of the subleading jet relative to the leading jet in the dijet, and the most peripheral collisions show the least. This can be explained in terms of a path length dependent jet energy loss, which causes the subleading jets to experience an additional amount of quenching by traversing a longer distance within the QGP medium compared to the leading jets. The R dependence of this ratio is shown for both the most central and most peripheral Pb+Pb collisions; no significant R dependence is observed for either. For central Pb+Pb collisions the value of this ratio is approximately 0.7–0.8, whereas for peripheral collisions the value is higher, it is approximately 0.9–1.1. Additionally, the $R_{\mathrm{AA}}^{\mathrm{pair}}(p_{\mathrm{T},2})/R_{\mathrm{AA}}^{\mathrm{pair}}(p_{\mathrm{T},1})$ ratio shows no significant dependence on p_{T}, for both central and peripheral collisions

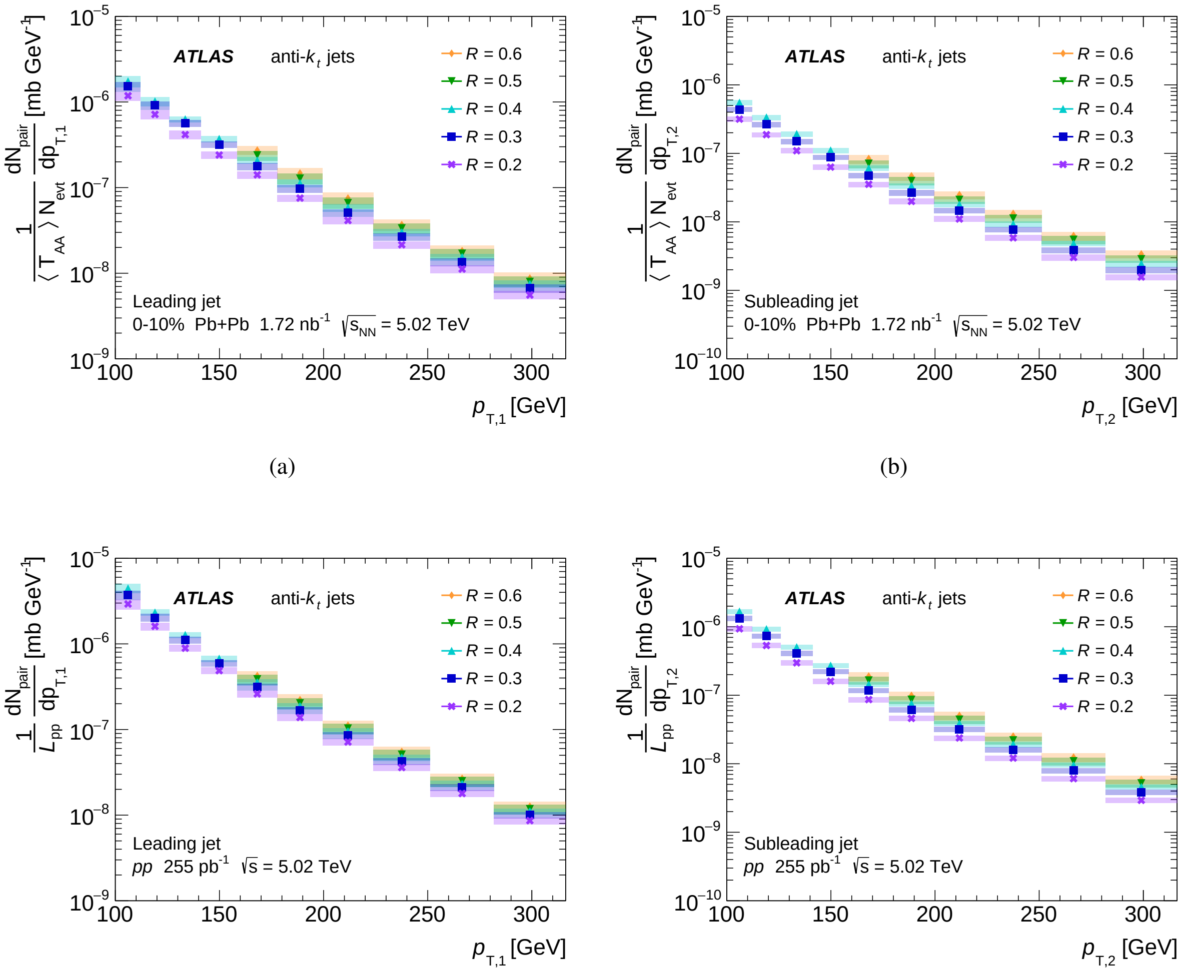

(a)

(b)

(c)

(d)

Figure 4: The (a,c) leading and (b,d) subleading dijet yields in (a,b) 0–10% central Pb+Pb collisions and the dijet cross sections in (c,d) pp collisions as a function of p_{T} for the various jet radii. Jets are selected with $|y| < 2.1$ and $|\phi_1 - \phi_2| > 7\pi/8$. The normalization uncertainties (not shown) are $\delta\langle T_{\mathrm{AA}}\rangle/\langle T_{\mathrm{AA}}\rangle = 0.9\%$ in 0–10% Pb+Pb collisions and $\delta L_{pp}/L_{pp} = 1\%$ in pp collisions. The boxes correspond to systematic uncertainties and the bars to statistical uncertainties.

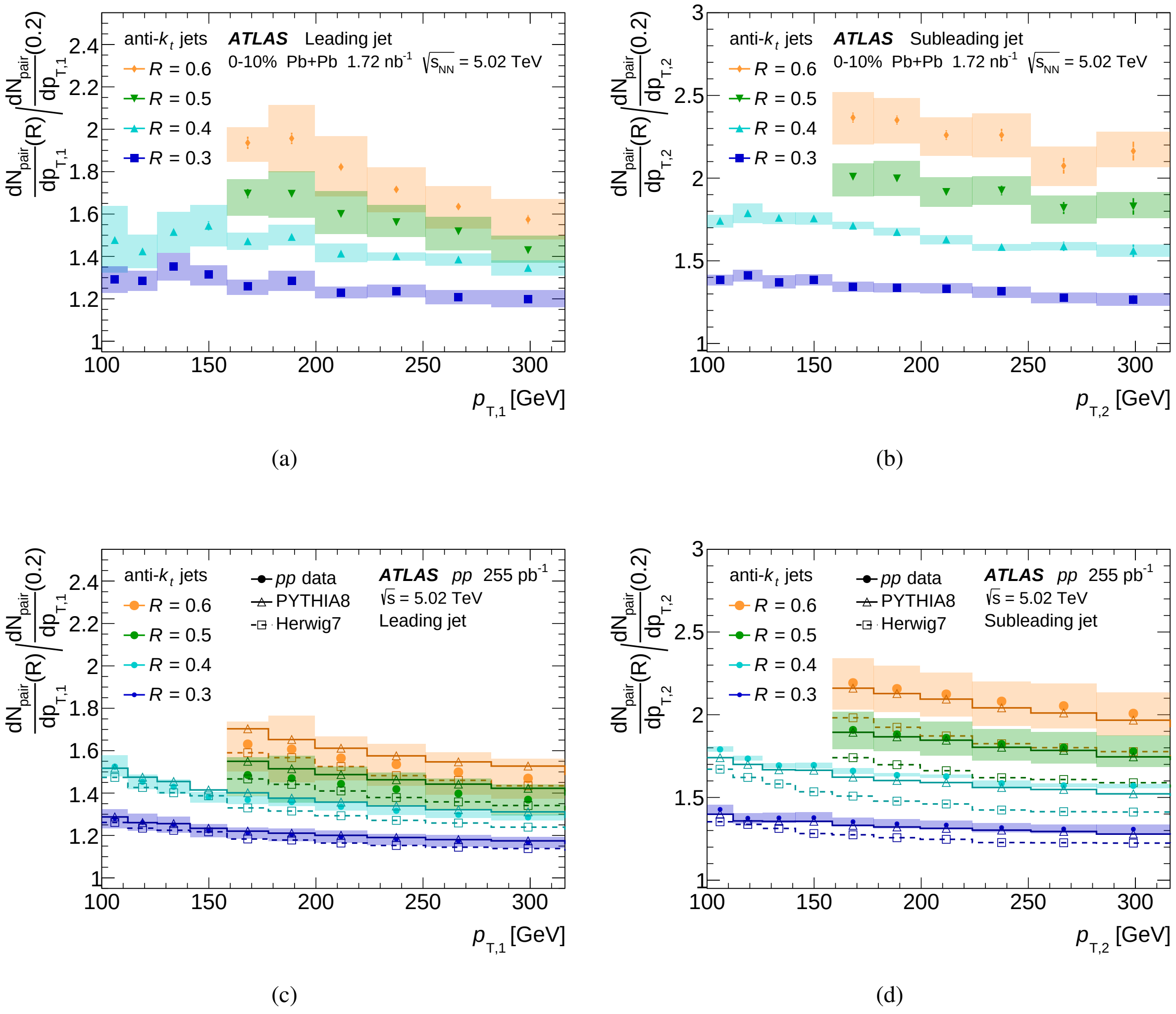

(a)

(b)

(c)

(d)

Figure 5: The (a,c) leading and (b,d) subleading dijet cross-section ratios for R jets with respect to $R = 0.2$ jets as a function of p_T for the various jet radii in (a,b) 0–10% central Pb+Pb and (c,d) pp collisions. The pp data is compared with Pythia 8 and Herwig7 simulations. Jets are selected with $|y| < 2.1$ and $|\phi_1 - \phi_2| > 7\pi/8$. The boxes correspond to systematic uncertainties and the bars to statistical uncertainties.

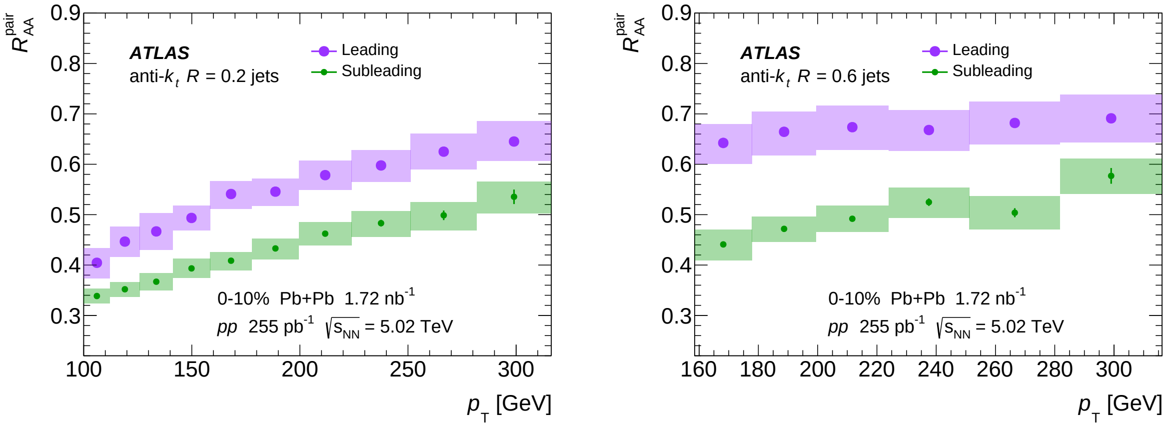

(a)

(b)

Figure 6: The leading and subleading jet $R_{\mathrm{AA}}^{\mathrm{pair}}$ distributions in dijets as a function of jet p_{T} for (a) $R = 0.2$ and (b) $R = 0.6$ jets in 0–10% Pb+Pb collisions. Jets are selected with $|y| < 2.1$ and $|\phi_1 - \phi_2| > 7\pi/8$. The normalization uncertainties (not shown) are $\delta\langle T_{\mathrm{AA}}\rangle/\langle T_{\mathrm{AA}}\rangle = 0.9\%$ in 0–10% Pb+Pb collisions and $\delta L_{pp}/L_{pp} = 1\%$ in pp collisions. The boxes correspond to systematic uncertainties and the bars to statistical uncertainties.

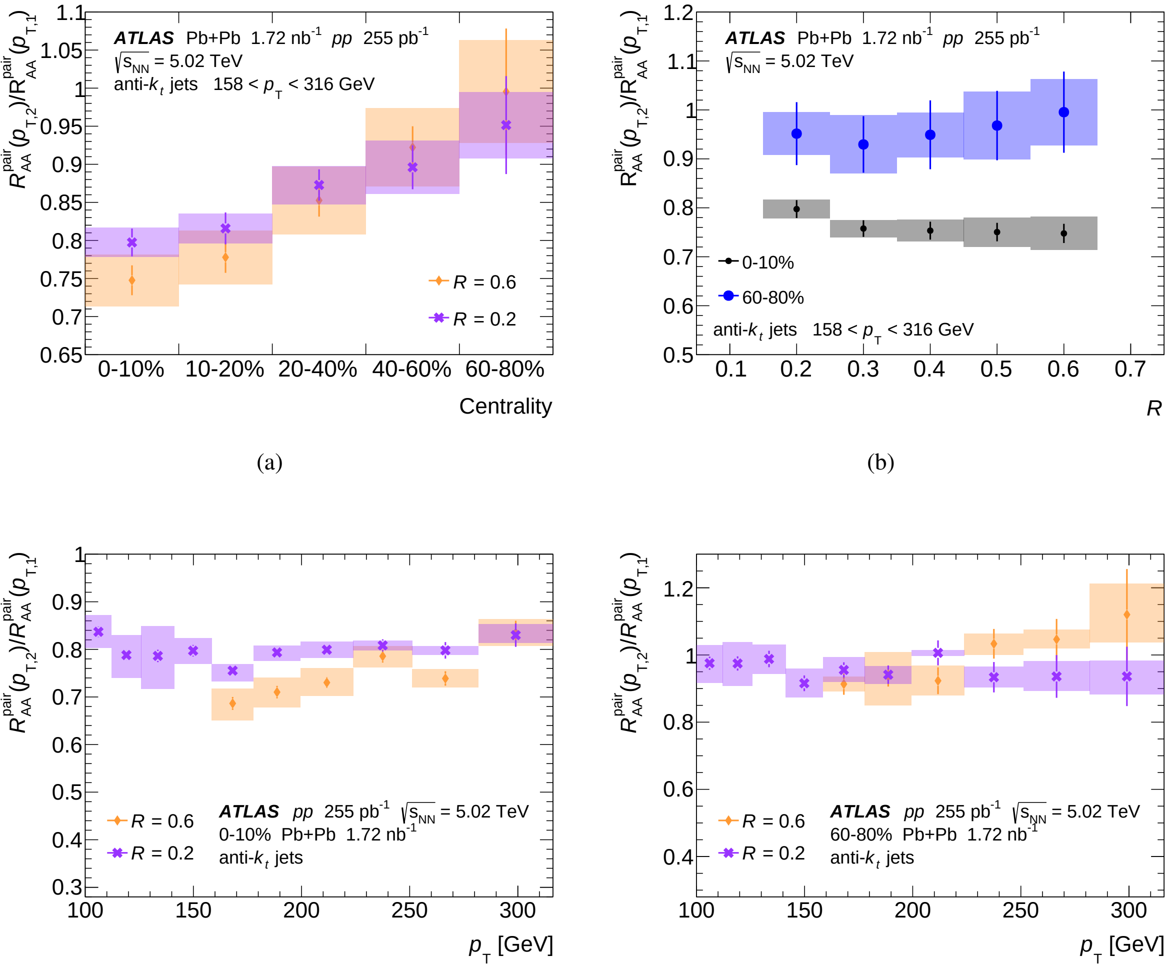

(a) (b)

(c) (d)

Figure 7: The double ratio $R_{\mathrm{AA}}^{\mathrm{pair}}(p_{\mathrm{T},2})/R_{\mathrm{AA}}^{\mathrm{pair}}(p_{\mathrm{T},1})$ of the subleading to leading jet $R_{\mathrm{AA}}^{\mathrm{pair}}$ distributions in dijets as a function of (a) centrality and (b) jet radius for $158 < p_{\mathrm{T}} < 316$ GeV, and as a function of jet p_{T} for (c) 0–10% and (d) 60–80% central Pb+Pb collisions. Jets are selected with $|y| < 2.1$ and $|\phi_1 - \phi_2| > 7\pi/8$. The boxes correspond to systematic uncertainties and the bars to statistical uncertainties.

7.1.1 Discussion of the $R_{\mathrm{AA}}^{\mathrm{pair}}$ distributions

To evaluate the R dependence of the $R_{\mathrm{AA}}^{\mathrm{pair}}$ distributions, the leading and subleading jet R_{AA}, along with the corresponding $R_{\mathrm{AA}}^{\mathrm{pair}}(R)/R_{\mathrm{AA}}^{\mathrm{pair}}(0.2)$ ratios, are shown in Figure 8 for the various jet radii for the 0–10% centrality selection. Some R dependence is observed for the leading jets, with $R_{\mathrm{AA}}^{\mathrm{pair}}(p_{\mathrm{T},1})$ increasing with the jet radius. In the most central collisions at a p_{T} of approximately 200 GeV, the $R_{\mathrm{AA}}^{\mathrm{pair}}(p_{\mathrm{T},1})$ of $R = 0.2$ jets is approximately 0.55, whereas for $R = 0.6$ it is closer to 0.65. This R dependence is consistent with larger R jets being less suppressed than smaller R jets. A similar R dependence was observed in Ref. [59]. An R dependence is also observed for subleading jets, but the $R_{\mathrm{AA}}^{\mathrm{pair}}(p_{\mathrm{T},2})$ values and the deviations from unity in the $R_{\mathrm{AA}}^{\mathrm{pair}}(R)/R_{\mathrm{AA}}^{\mathrm{pair}}(0.2)$ ratio is smaller than for the leading jets. Since the $R_{\mathrm{AA}}^{\mathrm{pair}}(p_{\mathrm{T},2})/R_{\mathrm{AA}}^{\mathrm{pair}}(p_{\mathrm{T},1})$ ratio shows no significant dependence on R or p_{T} (as seen in Figure 7), the $R_{\mathrm{AA}}^{\mathrm{pair}}(p_{\mathrm{T},2})$ of subleading jets can be seen, approximately, as a scaled down version of the $R_{\mathrm{AA}}^{\mathrm{pair}}(p_{\mathrm{T},1})$ of leading jets, by a factor only dependent on centrality.

Additionally, the $R_{\mathrm{AA}}^{\mathrm{pair}}$ distribution as a function of the jet radius is shown in Figure 9 for two p_{T} selections in 0–10% central collisions, $158 < p_{\mathrm{T}} < 178$ GeV and $282 < p_{\mathrm{T}} < 316$ GeV. Some R dependence of $R_{\mathrm{AA}}^{\mathrm{pair}}$ is observed, with $R_{\mathrm{AA}}^{\mathrm{pair}}$ increasing with the jet radius, a dependence that is stronger at lower p_{T}.

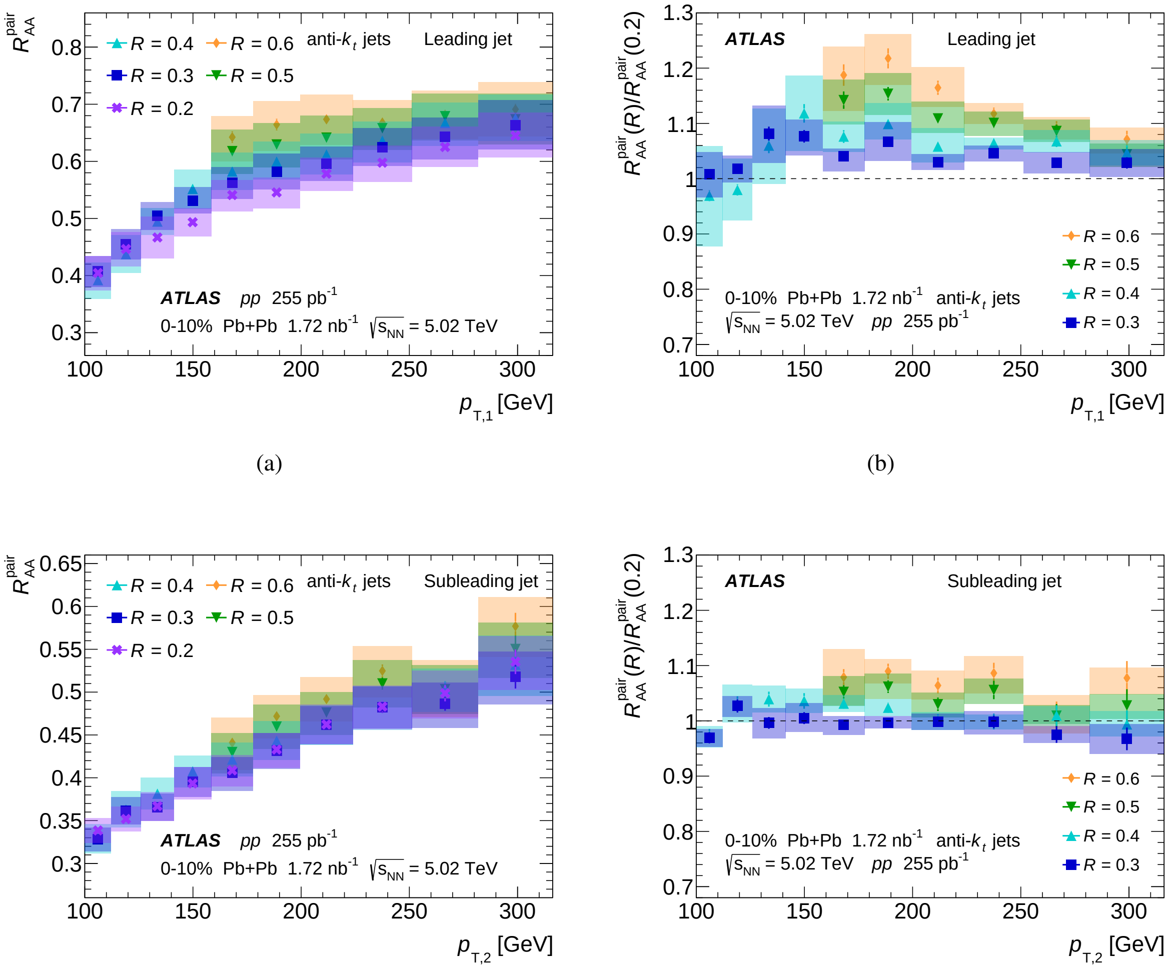

(a)

(b)

(c)

(d)

Figure 8: The (a,b) leading and (c,d) subleading jet (a,c) $R_{\mathrm{AA}}^{\mathrm{pair}}$ distributions in dijets and the corresponding (b,d) $R_{\mathrm{AA}}^{\mathrm{pair}}(R)/R_{\mathrm{AA}}^{\mathrm{pair}}(0.2)$ ratios as a function of jet p_{T} in 0–10% central Pb+Pb collisions. Jets are selected with $|y| < 2.1$ and $|\phi_1 - \phi_2| > 7\pi/8$. The normalization uncertainties (not shown) are $\delta\langle T_{\mathrm{AA}}\rangle/\langle T_{\mathrm{AA}}\rangle = 0.9\%$ in 0–10% Pb+Pb collisions and $\delta L_{pp}/L_{pp} = 1\%$ in pp collisions. The boxes correspond to systematic uncertainties and the bars to statistical uncertainties.

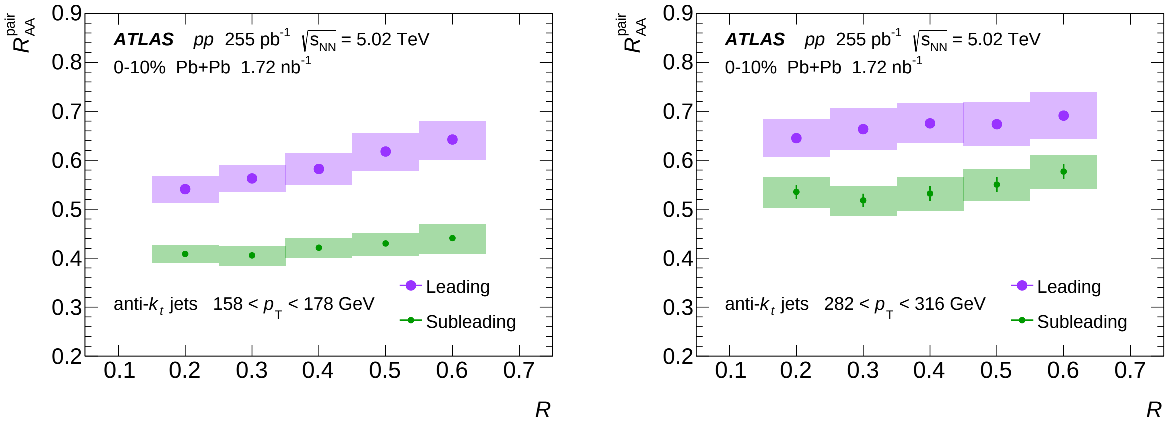

(a)

(b)

Figure 9: The leading and subleading jet $R_{\mathrm{AA}}^{\mathrm{pair}}$ distributions in dijets as a function of jet radius in 0–10% central Pb+Pb collisions, for (a) $158 < p_{\mathrm{T}} < 178$ GeV and (b) $282 < p_{\mathrm{T}} < 316$ GeV. Jets are selected with $|y| < 2.1$ and $|\phi_1 - \phi_2| > 7\pi/8$. The normalization uncertainties (not shown) are $\delta\langle T_{\mathrm{AA}}\rangle/\langle T_{\mathrm{AA}}\rangle = 0.9\%$ in 0–10% Pb+Pb collisions and $\delta L_{pp}/L_{pp} = 1\%$ in pp collisions. The boxes correspond to systematic uncertainties and the bars to statistical uncertainties.

7.2 x_J distributions

The absolutely normalized x_J distributions in pp collisions, as defined in Eq. (6), are shown in Figure 10, for leading jets with $158 < p_{\mathrm{T},1} < 178$ GeV and $398 < p_{\mathrm{T},1} < 562$ GeV for all jet radii considered here. The shapes of the distributions are similar for the two $p_{\mathrm{T},1}$ selections shown. In both cases, the distributions are peaked toward balanced dijets as expected. The distributions are more sharply peaked at $x_\mathrm{J} \approx 1$ for larger radius jets. This is expected if the larger radius jets cluster together radiation that could be reconstructed as separate jets for the smaller radii. For higher $p_{\mathrm{T},1}$, the distributions for the various jet radii are closer together than for lower $p_{\mathrm{T},1}$, presumably because higher p_T jets are more collimated.

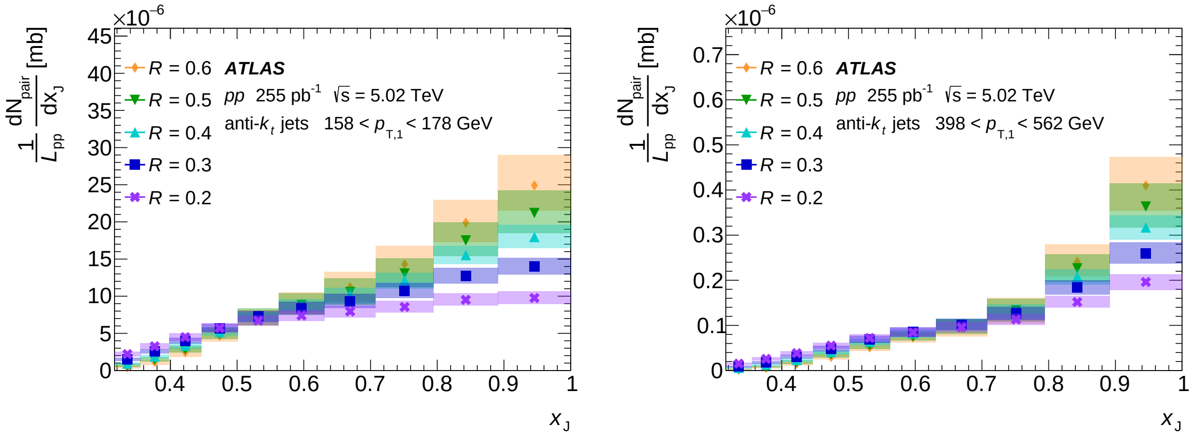

(a)

(b)

Figure 10: The absolutely normalized x_J distributions in pp collisions for leading jets with (a) $158 < p_{\mathrm{T},1} < 178$ GeV and (b) $398 < p_{\mathrm{T},1} < 562$ GeV. Jets are selected with $|y| < 2.1$ and $|\phi_1 - \phi_2| > 7\pi/8$. The normalization uncertainty (not shown) is $\delta L_{pp}/L_{pp} = 1\%$. The boxes correspond to systematic uncertainties and the bars to statistical uncertainties.

A comparison of the pp data to Pythia 8 and Herwig7 simulations is shown in Figure 11. Here the dijet-yield-normalized x_J distributions are plotted for $R = 0.2$ and $R = 0.6$ jets with $158 < p_{\mathrm{T},1} < 178$ GeV and $398 < p_{\mathrm{T},1} < 562$ GeV. The dijet-yield-normalized x_J distributions are considered in order to take out any overall cross-section difference between the models and data. The pp data is well described by the simulations for the various jet radii.

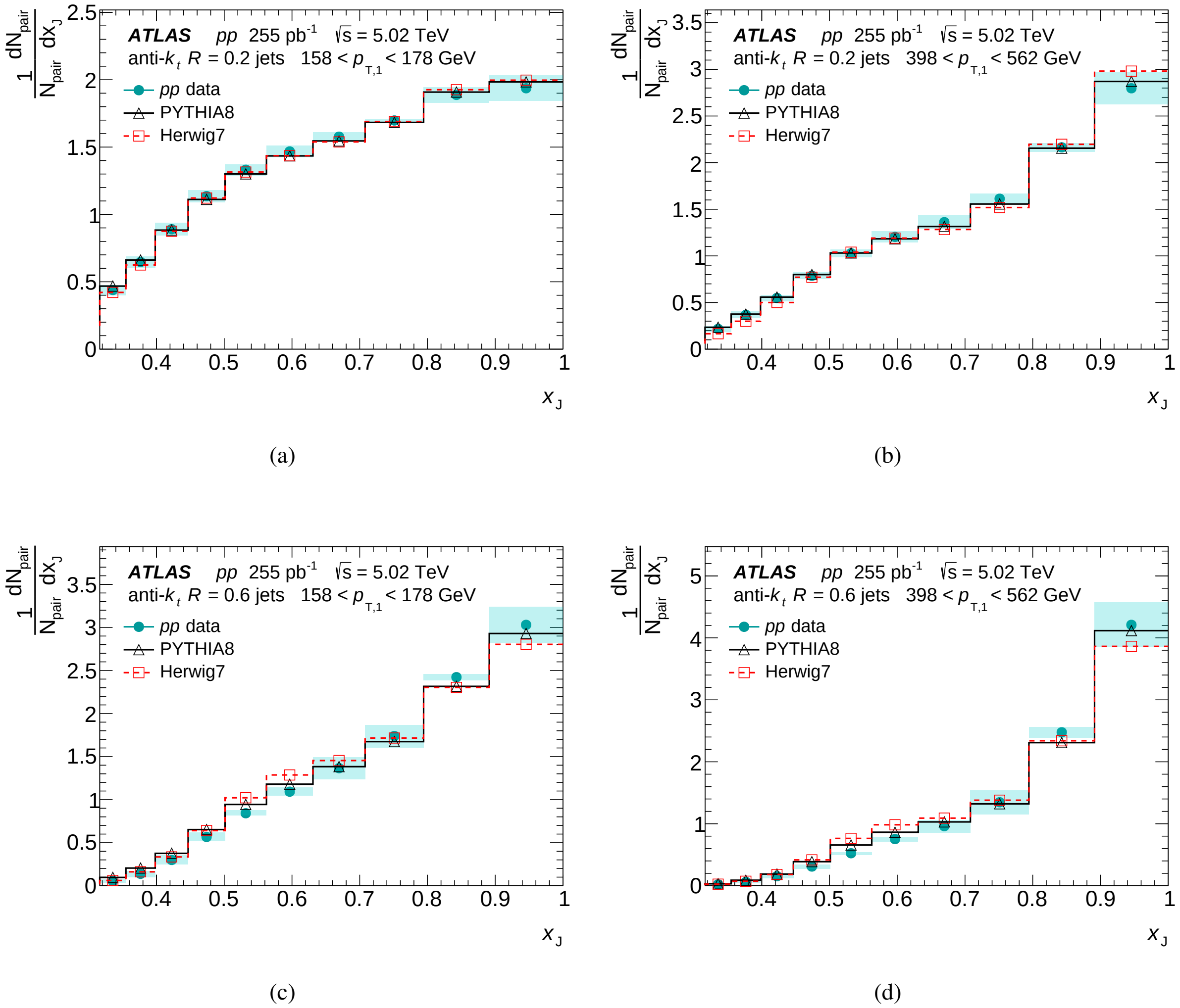

(a)

(b)

(c)

(d)

Figure 11: The dijet-yield-normalized x_J distributions in pp collisions, and in Pythia 8 and Herwig7 simulations, for (a,b) $R = 0.2$ and (c,d) $R = 0.6$ jets with (a,c) $158 < p_{T,1} < 178$ GeV and (b,d) $398 < p_{T,1} < 562$ GeV. Jets are selected with $|y| < 2.1$ and $|\phi_1 - \phi_2| > 7\pi/8$. The boxes correspond to systematic uncertainties and the bars to statistical uncertainties.

7.2.1 Discussion of the x_J distributions

Figure 12 shows the R dependence of the absolutely normalized x_J distributions in Pb+Pb collisions, as defined in Eq. (7), for the centrality selections 0–10% and 20–40%, and the same $p_{T,1}$ selections as shown for pp collisions. The x_J distributions in Pb+Pb collisions are broadened compared to those in pp collisions in Figure 10. The magnitude of the modification is larger for lower $p_{T,1}$ values and for more central collisions. For the $158 < p_{T,1} < 178$ GeV selection in mid-central collisions, the peak at balanced dijets remains compared to pp collisions, but becomes weaker as the jet radius decreases. For this $p_{T,1}$ selection in 0–10% central collisions, the distributions are nearly flat for $x_J > 0.5$. For the $398 < p_{T,1} < 562$ GeV selection, the x_J distributions in both central and mid-central Pb+Pb collisions remain peaked at $x_J \approx 1$ for the jet radii considered here.

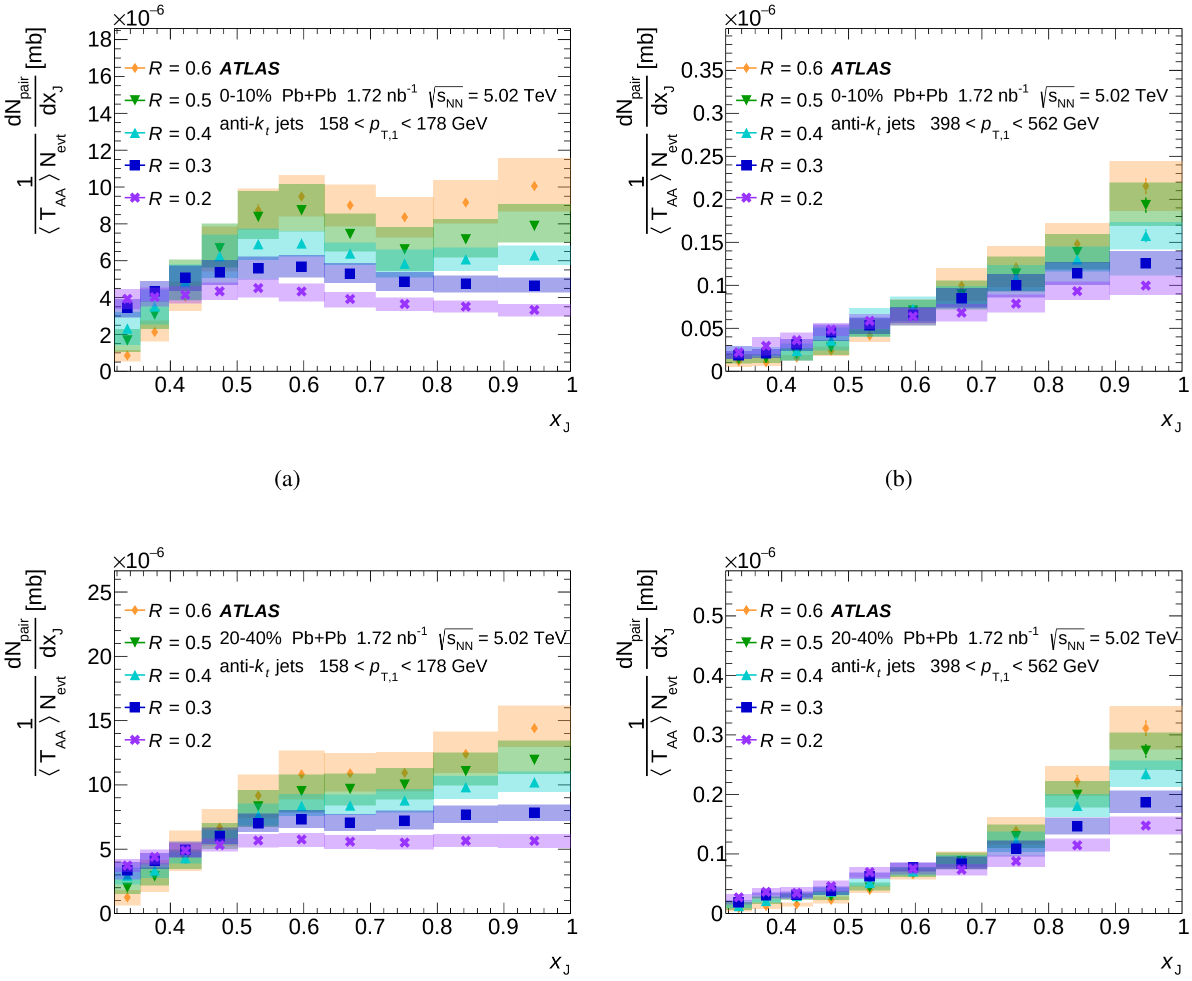

(a)

(b)

(c)

(d)

Figure 12: The absolutely normalized x_J distributions in (a,b) 0–10% and (c,d) 20–40% central Pb+Pb collisions, for leading jets with (a,c) $158 < p_{\mathrm{T},1} < 178$ GeV and (b,d) $398 < p_{\mathrm{T},1} < 562$ GeV. Jets are selected with $|y| < 2.1$ and $|\phi_1 - \phi_2| > 7\pi/8$. The normalization uncertainties (not shown) are $\delta\langle T_{\mathrm{AA}}\rangle/\langle T_{\mathrm{AA}}\rangle = 0.9\%$ and 2% for Pb+Pb centrality selections 0–10% and 20–40%, respectively. The boxes correspond to systematic uncertainties and the bars to statistical uncertainties.

To look more closely at the centrality dependent modification from the distributions in pp collisions, Figure 13 shows the overlaid x_J distributions for 0–10%, 20–40%, and 40–60% central Pb+Pb collisions. Two $p_{\mathrm{T},1}$ selections, $158 < p_{\mathrm{T},1} < 178$ GeV and $398 < p_{\mathrm{T},1} < 562$ GeV, for $R = 0.2$ and $R = 0.6$ jets are shown. As expected, x_J distributions in the most central Pb+Pb collisions are the most modified compared to those in pp collisions, with the rate of balanced dijets being strongly suppressed.

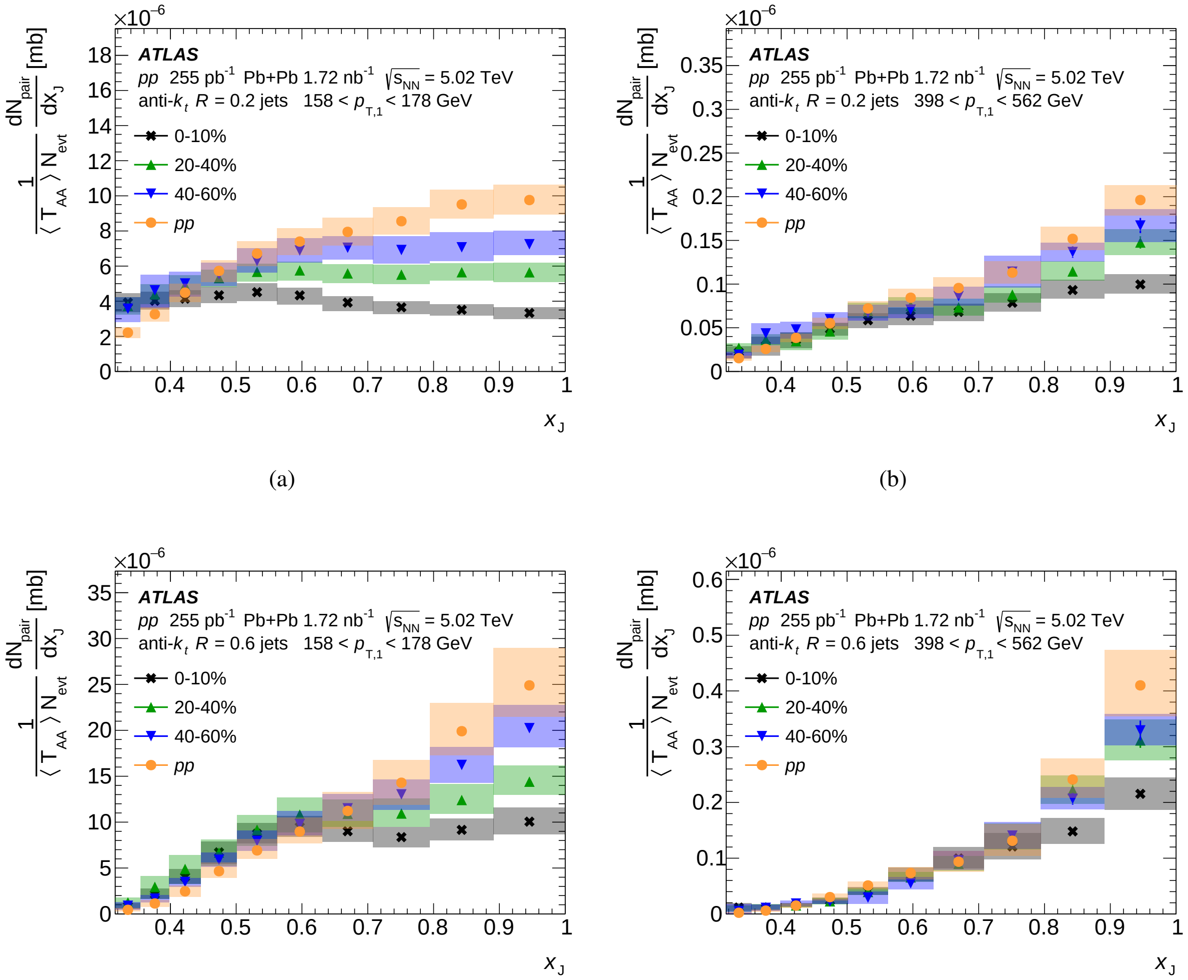

(a)

(b)

(c)

(d)

Figure 13: The absolutely normalized x_J distributions for (a,b) $R = 0.2$ and (c,d) $R = 0.6$ jets for three centrality selections in Pb+Pb collisions and pp collisions. Leading jets with (a,c) $158 < p_{\mathrm{T},1} < 178$ GeV and (b,d) $398 < p_{\mathrm{T},1} < 562$ GeV are shown. Jets are selected with $|y| < 2.1$ and $|\phi_1 - \phi_2| > 7\pi/8$. The normalization uncertainties (not shown) are $\delta\langle T_\mathrm{AA}\rangle/\langle T_\mathrm{AA}\rangle = 0.9\%$, 2%, and 5% in 0–10%, 20–40%, and 40–60% Pb+Pb collisions, respectively, and $\delta L_{pp}/L_{pp} = 1\%$ in pp collisions. The boxes correspond to systematic uncertainties and the bars to statistical uncertainties.

7.3 J_AA distributions

The ratio of the dijet yields in Pb+Pb collisions to pp collisions, J_AA, is defined in Eq. (9). The J_AA distributions for 0–10%, 20–40%, and 40–60%, are shown in Figure 14 for $R = 0.2$, $R = 0.4$, and $R = 0.6$ jets. The p_T selection of $200 < p_{\mathrm{T},1} < 224$ GeV was chosen because it is representative of the overall trends in the results. For the various centralities, there is a suppression in the number of balanced (high x_J) dijets and an enhancement in the number of imbalanced (low x_J) dijets, with the modifications being larger towards more central collisions. While the enhancement at low x_J can be large in terms of J_AA, it is worth recalling that the corresponding absolute dijet yields are small at low x_J, especially for the larger R jets, as was previously seen in Figure 12. The larger uncertainties in J_{AA} for the $R = 0.6$ jets in the most central collisions are driven by the sensitivity to the unfolding prior weights as well as the JES and JER, which affect the bins at low x_{J} and low p_{T}.

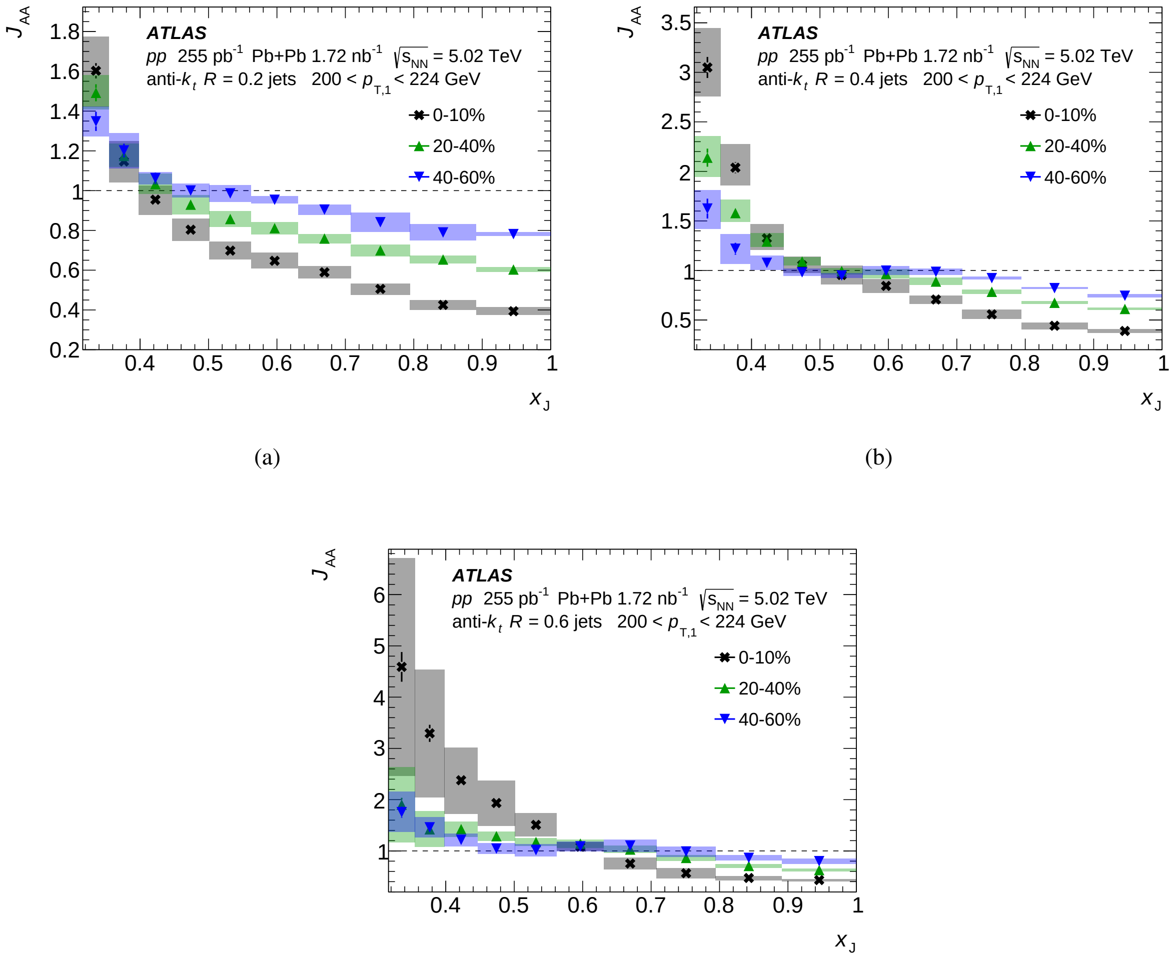

(a)

(b)

(c)

Figure 14: The J_{AA} distributions for (a) $R = 0.2$, (b) $R = 0.4$, and (c) $R = 0.6$ jets for three centrality selections in Pb+Pb collisions and pp collisions. Leading jets with $200 < p_{\mathrm{T},1} < 224$ GeV are shown. Jets are selected with $|y| < 2.1$ and $|\phi_1 - \phi_2| > 7\pi/8$. The normalization uncertainties (not shown) are $\delta\langle T_{\mathrm{AA}}\rangle/\langle T_{\mathrm{AA}}\rangle = 0.9\%$, 2%, and 5% in 0–10%, 20–40%, and 40–60% Pb+Pb collisions, respectively, and $\delta L_{pp}/L_{pp} = 1\%$ in pp collisions. The boxes correspond to systematic uncertainties and the bars to statistical uncertainties.

7.3.1 Discussion of the J_{AA} distributions

The J_{AA} distributions are overlaid for the various jet radii in Figure 15, along with their corresponding $J_{\mathrm{AA}}(R)/J_{\mathrm{AA}}(0.2)$ ratios. In the most central collisions, 0–10%, a larger J_{AA} is observed for larger jet radius, a trend more noticeable towards lower x_{J}. In 20–40% central collisions, the same quantitative trend is observed but the magnitude of the deviation from unity is smaller. Similarly, in terms of the

$J_{\mathrm{AA}}(R)/J_{\mathrm{AA}}(0.2)$ ratios, at low x_{J} there is a spread of the central values of J_{AA} for the various jet radii and the uncertainties are larger. At high-x_{J}, the J_{AA} values show an R dependence of smaller magnitude.

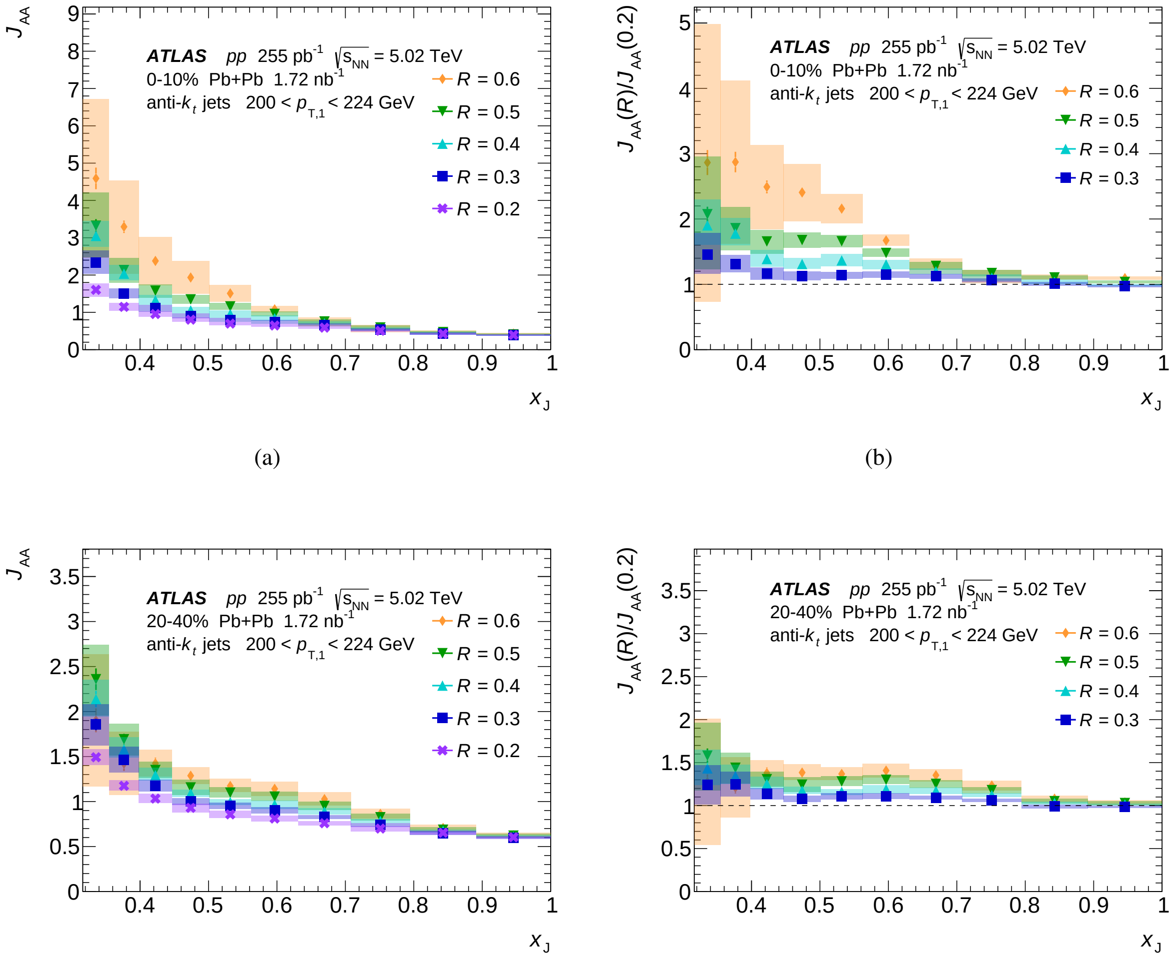

(a)

(b)

(c)

(d)

Figure 15: The (a,c) J_{AA} distributions and its corresponding (b,d) $J_{\mathrm{AA}}(R)/J_{\mathrm{AA}}(0.2)$ ratios in (a,b) 0–10% and (c,d) 20–40% central Pb+Pb collisions, for $200 < p_{\mathrm{T},1} < 224$ GeV. Jets are selected with $|y| < 2.1$ and $|\phi_1 - \phi_2| > 7\pi/8$. The normalization uncertainties in J_{AA} (not shown) are $\delta\langle T_{\mathrm{AA}}\rangle/\langle T_{\mathrm{AA}}\rangle = 0.9\%$ and 2% in 0–10% and 20–40% Pb+Pb collisions, respectively, and $\delta L_{pp}/L_{pp} = 1\%$ in pp collisions. The boxes correspond to systematic uncertainties and the bars to statistical uncertainties.

To evaluate the R dependence of these distributions, the J_{AA} is plotted as a function of the jet radius in Figure 16, for several $p_{\mathrm{T},1}$ selections at x_{J} values of $0.89 < x_{\mathrm{J}} < 1.0$ and $0.50 < x_{\mathrm{J}} < 0.56$ in the most central collisions. The corresponding $J_{\mathrm{AA}}(R)/J_{\mathrm{AA}}(0.2)$ ratios are shown in Figure 17. For nearly balanced dijets ($0.89 < x_{\mathrm{J}} < 1.0$), a small R dependence to J_{AA} is observed (more noticeable in the $J_{\mathrm{AA}}(R)/J_{\mathrm{AA}}(0.2)$ ratios), with J_{AA} increasing with the jet radius, and dependent on $p_{\mathrm{T},1}$. As the dijets become more imbalanced ($0.50 < x_{\mathrm{J}} < 0.56$), this R dependence becomes stronger. For both balanced and imbalanced dijets, the R dependence is observed to be larger for lower $p_{\mathrm{T},1}$ values. This R-dependent behavior can be explained by considering that the subleading jets, which have lost energy and thus caused the dijets to become imbalanced, recover some of the lost energy as the jet radius increases. Another contribution comes from the medium response, which can add energy to the jets.

To assess the p_{T} dependence of the $J_{\mathrm{AA}}(R)/J_{\mathrm{AA}}(0.2)$ ratios, Figure 18 shows the $J_{\mathrm{AA}}(R)/J_{\mathrm{AA}}(0.2)$ ratios as a function of $p_{\mathrm{T,1}}$, for $R = 0.4$ and $R = 0.6$ jets, and two x_{J} selections, $0.50 < x_{\mathrm{J}} < 0.56$ and $0.89 < x_{\mathrm{J}} < 1.0$. The $J_{\mathrm{AA}}(R)/J_{\mathrm{AA}}(0.2)$ ratios come closer to unity with increasing $p_{\mathrm{T,1}}$, with the modification being larger for larger R jets. The deviations from unity are much smaller for balanced dijets than for imbalanced dijets.

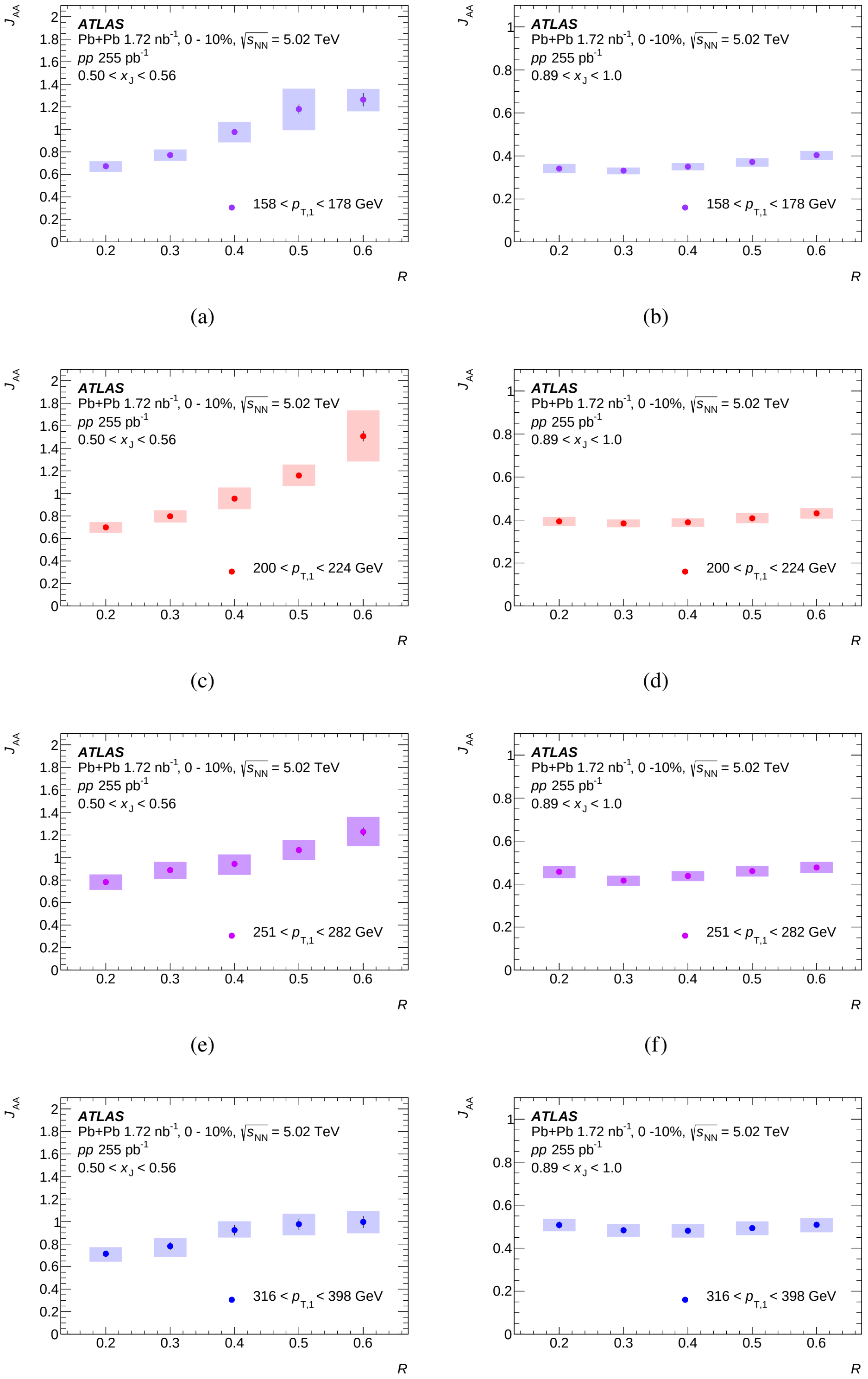

(a) (b)

(c) (d)

(e) (f)

(g) (h)

Figure 16: The J_{AA} values as a function of R for jets with (a,b) $158 < p_{T,1} < 178$ GeV, (c,d) $200 < p_{T,1} < 224$ GeV, (e,f) $251 < p_{T,1} < 282$ GeV, and (g,h) $316 < p_{T,1} < 398$ GeV in 0–10% central Pb+Pb collisions, for (a,c,e,g) $0.50 < x_J < 0.56$ and (b,d,f,h) $0.89 < x_J < 1.0$. Jets are selected with $|y| < 2.1$ and $|\phi_1 - \phi_2| > 7\pi/8$. The normalization uncertainties (not shown) are $\delta\langle T_{AA}\rangle/\langle T_{AA}\rangle = 0.9\%$ and 2% in 0–10% and 20–40% Pb+Pb collisions, respectively, and $\delta L_{pp}/L_{pp} = 1\%$ in pp collisions. The boxes correspond to systematic uncertainties and the bars to statistical uncertainties.

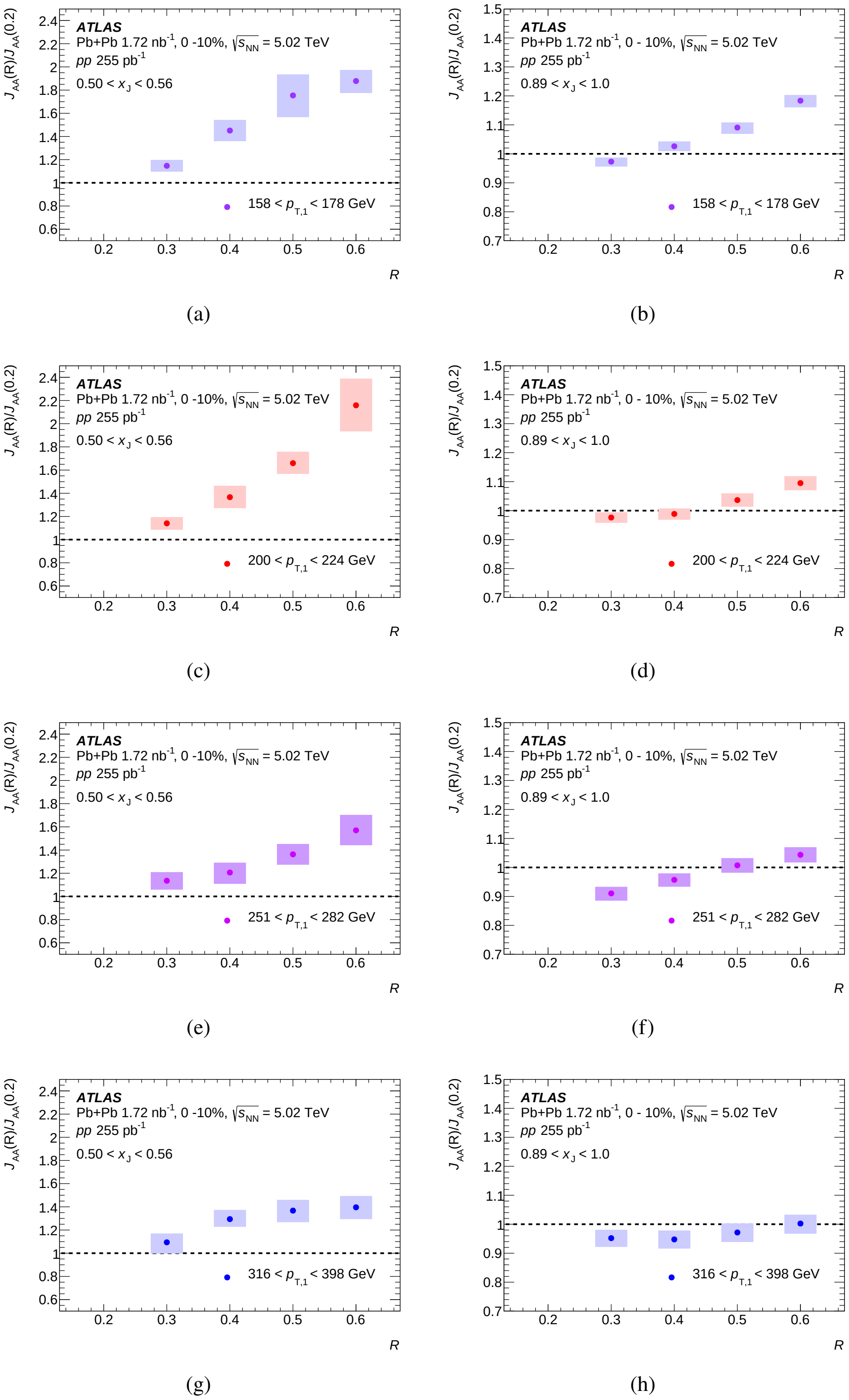

(a) (b)

(c) (d)

(e) (f)

(g) (h)

Figure 17: The $J_{AA}(R)/J_{AA}(0.2)$ ratios as a function of R for jets with (a,b) $158 < p_{T,1} < 178$ GeV, (c,d) $200 < p_{T,1} < 224$ GeV, (e,f) $251 < p_{T,1} < 282$ GeV, (g,h) $316 < p_{T,1} < 398$ GeV in 0–10% central Pb+Pb collisions, for (a,c,e,g) $0.50 < x_J < 0.56$ and (b,d,f,h) $0.89 < x_J < 1.0$. Jets are selected with $|y| < 2.1$ and $|\phi_1 - \phi_2| > 7\pi/8$. The boxes correspond to systematic uncertainties and the bars to statistical uncertainties.

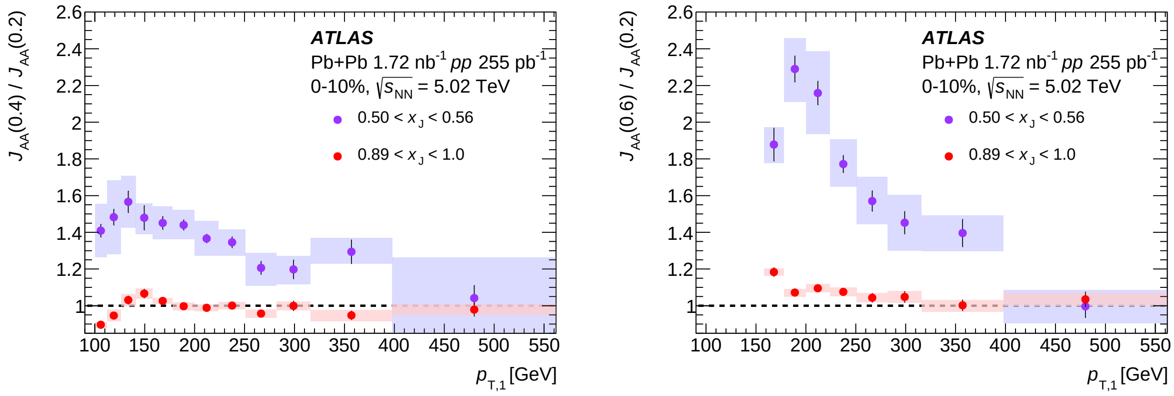

(a) (b)

Figure 18: The $J_{\mathrm{AA}}(R)/J_{\mathrm{AA}}(0.2)$ ratios as a function of $p_{\mathrm{T},1}$ for (a) $R = 0.4$ and (b) $R = 0.6$ jets in 0–10% central Pb+Pb collisions, for $0.50 < x_{\mathrm{J}} < 0.56$ and $0.89 < x_{\mathrm{J}} < 1.0$. Jets are selected with $|y| < 2.1$ and $|\phi_1 - \phi_2| > 7\pi/8$. The boxes correspond to systematic uncertainties and the bars to statistical uncertainties.

7.4 Comparison to theory

Results are compared with the Linear Boltzmann Transport (LBT) [60] and JETSCAPE [61] models. Both of these models use Pythia 8 pp as the baseline for the hard processes, but with a different evolution of the parton showers. The LBT model uses Boltzmann transport equations to describe the propagation of jet and medium partons as they traverse a QGP, including elastic and inelastic perturbative QCD processes. The JETSCAPE model combines [62], in tune v3.5 AA22, the LBT model at low parton virtuality with a MATTER [63] medium-modified parton shower at high parton virtuality.

Figure 19 shows the absolutely normalized x_{J} distributions in data compared with the JETSCAPE model for the various jet radii in 0–10% central Pb+Pb and in pp collisions. At high x_{J} values ($x_{\mathrm{J}} > 0.65$), the model describes the pp data well, while at lower x_{J} values it overestimates the data. In the case of the Pb+Pb data, the model describes the data at high x_{J} values. For $0.45 < x_{\mathrm{J}} < 0.65$, the model underestimates the Pb+Pb data. For lower x_{J} values, the model overestimates the Pb+Pb data.

Figure 20 shows the $R^{\mathrm{pair}}_{\mathrm{AA}}$ distributions of the leading and subleading jets in dijets compared with the LBT and JETSCAPE models, for $R = 0.2$ and $R = 0.6$ jets in 0–10% central collisions. For both the large and small-R jets, the models predict that the subleading jets are more suppressed than the leading jets in dijets in terms of the $R^{\mathrm{pair}}_{\mathrm{AA}}$. However, they have varying degrees of success in describing the measured $R^{\mathrm{pair}}_{\mathrm{AA}}$ values. For $R = 0.2$ jets, the LBT model underestimates the data for both the leading and subleading jets; the JETSCAPE model describes the leading jet $R^{\mathrm{pair}}_{\mathrm{AA}}$ distribution well, but overestimates the subleading jet distribution. For $R = 0.6$ jets, the LBT model fully describes the leading jet $R^{\mathrm{pair}}_{\mathrm{AA}}$ distribution, but overestimates the subleading jet distribution; the JETSCAPE model describes the subleading jet $R^{\mathrm{pair}}_{\mathrm{AA}}$ distribution, but underestimates the leading jet distribution.

The $R^{\mathrm{pair}}_{\mathrm{AA}}(R = 0.6)/R^{\mathrm{pair}}_{\mathrm{AA}}(R = 0.2)$ ratio is shown in Figure 21 for both the leading and subleading jets in 0–10% central collisions. For both the leading and subleading jet $R^{\mathrm{pair}}_{\mathrm{AA}}$, the data lies between the models for the full p_{T} range, with the LBT model above the data and the JETSCAPE model below the data. Additionally, the data shows larger values of the $R^{\mathrm{pair}}_{\mathrm{AA}}(R = 0.6)/R^{\mathrm{pair}}_{\mathrm{AA}}(R = 0.2)$ ratio for the leading jets

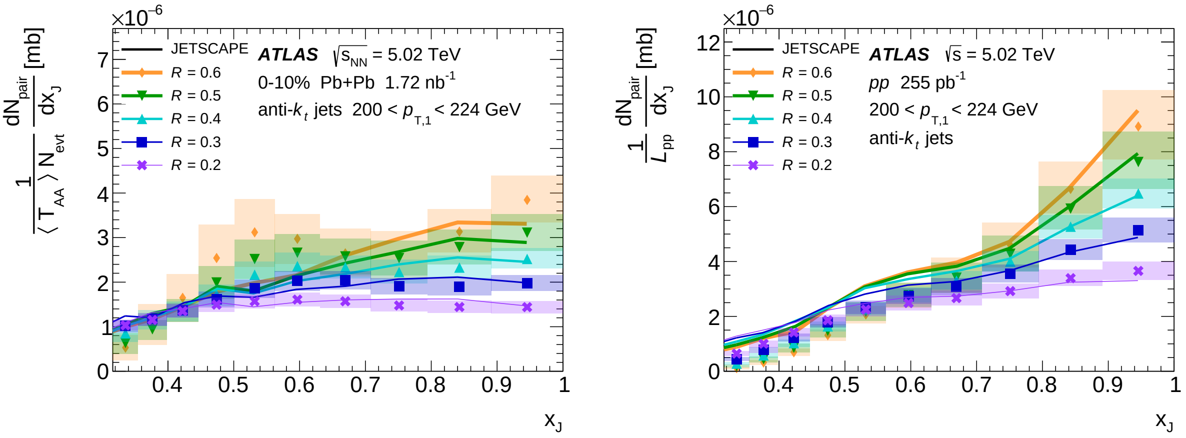

(a) (b)

Figure 19: The x_J distributions in data compared with the JETSCAPE (LBT+MATTER) model, for $R = 0.2, 0.3, 0.4, 0.5$ and 0.6 jets in (a) 0–10% central Pb+Pb collisions and (b) pp collisions, for $200 < p_{\mathrm{T},1} < 224$ GeV. Jets are selected with $|y| < 2.1$ and $|\phi_1 - \phi_2| > 7\pi/8$. The normalization uncertainties in the data (not shown) are $\delta\langle T_\mathrm{AA}\rangle/\langle T_\mathrm{AA}\rangle = 0.9\%$ in 0–10% Pb+Pb collisions and $\delta L_{pp}/L_{pp} = 1\%$ in pp collisions. The boxes correspond to systematic uncertainties and the bars to statistical uncertainties.

than for the subleading jets. The JETSCAPE model predicts this order while the LBT model predicts the opposite order.

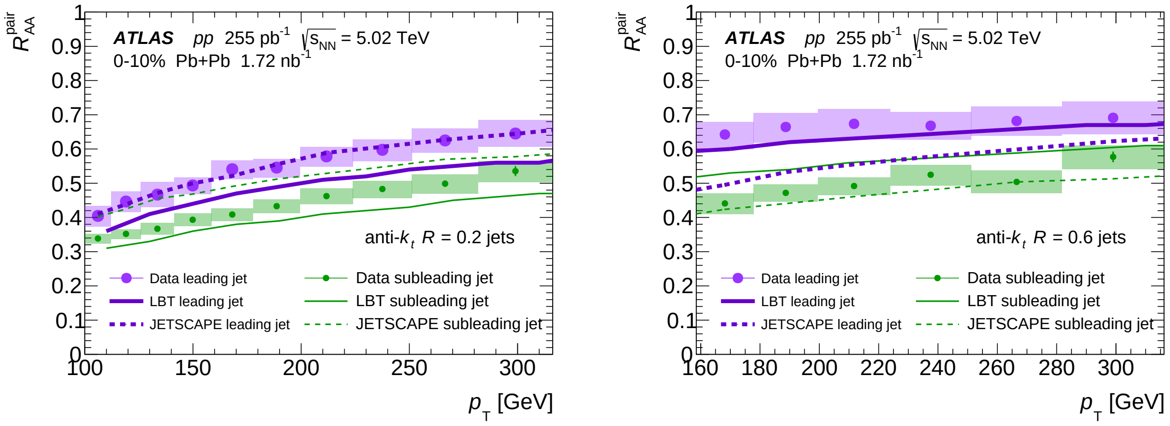

(a) (b)

Figure 20: The leading and subleading jet $R_{\mathrm{AA}}^{\mathrm{pair}}$ distributions in dijets in data, compared with the LBT and JETSCAPE (LBT+MATTER) models. (a) $R = 0.2$ and (b) $R = 0.6$ jets are shown for 0–10% central collisions. Jets are selected with $|y| < 2.1$ and $|\phi_1 - \phi_2| > 7\pi/8$. The normalization uncertainties in the data (not shown) are $\delta\langle T_{\mathrm{AA}}\rangle/\langle T_{\mathrm{AA}}\rangle = 0.9\%$ in 0–10% Pb+Pb collisions and $\delta L_{pp}/L_{pp} = 1\%$ in pp collisions. The boxes correspond to systematic uncertainties and the bars to statistical uncertainties.

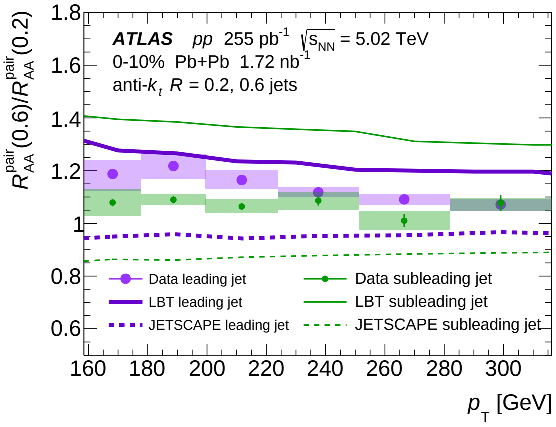

Figure 21: The leading and subleading jet $R_{\mathrm{AA}}^{\mathrm{pair}}(R = 0.6)/R_{\mathrm{AA}}^{\mathrm{pair}}(R = 0.2)$ in dijets in data, compared with the LBT and JETSCAPE (LBT+MATTER) models, for 0–10% central collisions. Jets are selected with $|y| < 2.1$ and $|\phi_1 - \phi_2| > 7\pi/8$. The boxes correspond to systematic uncertainties and the bars to statistical uncertainties.

8 Conclusion

This paper presents a measurement of the dependence of the dijet momentum balance on the jet radius, in Pb+Pb and pp collisions at $\sqrt{s_{\mathrm{NN}}} = 5.02$ TeV. Dijets were studied for jet radii $R = 0.2, 0.3, 0.4, 0.5$ and 0.6 by measuring the absolutely normalized x_{J}, J_{AA}, and $R_{\mathrm{AA}}^{\mathrm{pair}}$ distributions. The measurement covers a broad transverse momentum range, with leading jet $p_{\mathrm{T},1}$ ranging from 100 to 562 GeV for $R = 0.2, 0.3$ and 0.4 jets and from 158 to 562 GeV for $R = 0.5$ and 0.6 jets.

The results show that larger jet radii give x_J distributions peaked at higher x_J values, whereas smaller jet radii give flatter distributions. This is true in both the Pb+Pb and pp collisions, but the Pb+Pb collisions lead to broader and more modified distributions compared to pp, with the modifications being larger for more central collisions.

The J_AA results for more imbalanced dijets, primarily at low leading jet transverse momentum, show that jet suppression decreases (J_AA increases) with increasing jet radius. For more balanced dijets, the suppression is also present and dependent on the jet radius, but smaller in magnitude than for imbalanced dijets.

The $R_\mathrm{AA}^\mathrm{pair}$ results show that subleading jets in dijets are more suppressed than leading jets, for the various jet radii considered. Significant jet radius dependence of the $R_\mathrm{AA}^\mathrm{pair}$ is observed, with jet suppression decreasing ($R_\mathrm{AA}^\mathrm{pair}$ increasing) with increasing jet radius. This jet radius dependence is observed in both the leading jet $R_\mathrm{AA}^\mathrm{pair}(p_\mathrm{T,1})$ and subleading jet $R_\mathrm{AA}^\mathrm{pair}(p_\mathrm{T,2})$, though not in the $R_\mathrm{AA}^\mathrm{pair}(p_\mathrm{T,2})/R_\mathrm{AA}^\mathrm{pair}(p_\mathrm{T,1})$ ratio, which is dependent on centrality only.

These results present a comprehensive look at the modification of dijet rates in Pb+Pb collisions compared to pp collisions. These results are complementary to existing measurements of the jet radius dependence of jet suppression, and will provide important new constraints to theoretical models of jet energy loss.

Acknowledgments

We thank CERN for the very successful operation of the LHC and its injectors, as well as the support staff at CERN and at our institutions worldwide without whom ATLAS could not be operated efficiently.

The crucial computing support from all WLCG partners is acknowledged gratefully, in particular from CERN, the ATLAS Tier-1 facilities at TRIUMF/SFU (Canada), NDGF (Denmark, Norway, Sweden), CC-IN2P3 (France), KIT/GridKA (Germany), INFN-CNAF (Italy), NL-T1 (Netherlands), PIC (Spain), RAL (UK) and BNL (USA), the Tier-2 facilities worldwide and large non-WLCG resource providers. Major contributors of computing resources are listed in Ref. [64].

We gratefully acknowledge the support of ANPCyT, Argentina; YerPhI, Armenia; ARC, Australia; BMWFW and FWF, Austria; ANAS, Azerbaijan; CNPq and FAPESP, Brazil; NSERC, NRC and CFI, Canada; CERN; ANID, Chile; CAS, MOST and NSFC, China; Minciencias, Colombia; MEYS CR, Czech Republic; DNRF and DNSRC, Denmark; IN2P3-CNRS and CEA-DRF/IRFU, France; SRNSFG, Georgia; BMBF, HGF and MPG, Germany; GSRI, Greece; RGC and Hong Kong SAR, China; ISF and Benoziyo Center, Israel; INFN, Italy; MEXT and JSPS, Japan; CNRST, Morocco; NWO, Netherlands; RCN, Norway; MNiSW, Poland; FCT, Portugal; MNE/IFA, Romania; MESTD, Serbia; MSSR, Slovakia; ARIS and MVZI, Slovenia; DSI/NRF, South Africa; MICIU/AEI, Spain; SRC and Wallenberg Foundation, Sweden; SERI, SNSF and Cantons of Bern and Geneva, Switzerland; NSTC, Taipei; TENMAK, Türkiye; STFC/UKRI, United Kingdom; DOE and NSF, United States of America.

Individual groups and members have received support from BCKDF, CANARIE, CRC and DRAC, Canada; CERN-CZ, FORTE and PRIMUS, Czech Republic; COST, ERC, ERDF, Horizon 2020, ICSC-NextGenerationEU and Marie Skłodowska-Curie Actions, European Union; Investissements d'Avenir Labex, Investissements d'Avenir Idex and ANR, France; DFG and AvH Foundation, Germany; Herakleitos, Thales and Aristeia programmes co-financed by EU-ESF and the Greek NSRF, Greece; BSF-NSF and MINERVA, Israel; NCN and NAWA, Poland; La Caixa Banking Foundation, CERCA Programme Generalitat de

Catalunya and PROMETEO and GenT Programmes Generalitat Valenciana, Spain; Göran Gustafssons Stiftelse, Sweden; The Royal Society and Leverhulme Trust, United Kingdom.

In addition, individual members wish to acknowledge support from Armenia: Yerevan Physics Institute (FAPERJ); CERN: European Organization for Nuclear Research (CERN PJAS); Chile: Agencia Nacional de Investigación y Desarrollo (FONDECYT 1230812, FONDECYT 1230987, FONDECYT 1240864); China: Chinese Ministry of Science and Technology (MOST-2023YFA1605700), National Natural Science Foundation of China (NSFC - 12175119, NSFC 12275265, NSFC-12075060); Czech Republic: Czech Science Foundation (GACR - 24-11373S), Ministry of Education Youth and Sports (FORTE CZ.02.01.01/00/22_008/0004632), PRIMUS Research Programme (PRIMUS/21/SCI/017); EU: H2020 European Research Council (ERC - 101002463); European Union: European Research Council (ERC - 948254, ERC 101089007), Horizon 2020 Framework Programme (MUCCA - CHIST-ERA-19-XAI-00), European Union, Future Artificial Intelligence Research (FAIR-NextGenerationEU PE00000013), Italian Center for High Performance Computing, Big Data and Quantum Computing (ICSC, NextGenerationEU); France: Agence Nationale de la Recherche (ANR-20-CE31-0013, ANR-21-CE31-0013, ANR-21-CE31-0022, ANR-22-EDIR-0002), Investissements d'Avenir Labex (ANR-11-LABX-0012); Germany: Baden-Württemberg Stiftung (BW Stiftung-Postdoc Eliteprogramme), Deutsche Forschungsgemeinschaft (DFG - 469666862, DFG - CR 312/5-2); Italy: Istituto Nazionale di Fisica Nucleare (ICSC, NextGenerationEU), Ministero dell'Università e della Ricerca (PRIN - 20223N7F8K - PNRR M4.C2.1.1); Japan: Japan Society for the Promotion of Science (JSPS KAKENHI JP22H01227, JSPS KAKENHI JP22H04944, JSPS KAKENHI JP22KK0227, JSPS KAKENHI JP23KK0245); Netherlands: Netherlands Organisation for Scientific Research (NWO Veni 2020 - VI.Veni.202.179); Norway: Research Council of Norway (RCN-314472); Poland: Ministry of Science and Higher Education (IDUB AGH, POB8, D4 no 9722), Polish National Agency for Academic Exchange (PPN/PPO/2020/1/00002/U/00001), Polish National Science Centre (NCN 2021/42/E/ST2/00350, NCN OPUS nr 2022/47/B/ST2/03059, NCN UMO-2019/34/E/ST2/00393, UMO-2020/37/B/ST2/01043, UMO-2021/40/C/ST2/00187, UMO-2022/47/O/ST2/00148, UMO-2023/49/B/ST2/04085); Slovenia: Slovenian Research Agency (ARIS grant J1-3010); Spain: Generalitat Valenciana (Artemisa, FEDER, IDIFEDER/2018/048), Ministry of Science and Innovation (MCIN & NextGenEU PCI2022-135018-2, MICIN & FEDER PID2021-125273NB, RYC2019-028510-I, RYC2020-030254-I, RYC2021-031273-I, RYC2022-038164-I), PROMETEO and GenT Programmes Generalitat Valenciana (CIDEGENT/2019/027); Sweden: Swedish Research Council (Swedish Research Council 2023-04654, VR 2018-00482, VR 2022-03845, VR 2022-04683, VR 2023-03403, VR grant 2021-03651), Knut and Alice Wallenberg Foundation (KAW 2018.0157, KAW 2018.0458, KAW 2019.0447, KAW 2022.0358); Switzerland: Swiss National Science Foundation (SNSF - PCEFP2_194658); United Kingdom: Leverhulme Trust (Leverhulme Trust RPG-2020-004), Royal Society (NIF-R1-231091); United States of America: U.S. Department of Energy (ECA DE-AC02-76SF00515), Neubauer Family Foundation.

References

[1] L. Evans and P. Bryant, *LHC Machine*, JINST **3** (2008) S08001.

[2] W. Busza, K. Rajagopal, and W. van der Schee, *Heavy Ion Collisions: The Big Picture, and the Big Questions*, Ann. Rev. Nucl. Part. Sci. **68** (2018) 339, arXiv: `1802.04801 [hep-ph]`.

[3] L. Cunqueiro and A. M. Sickles, *Studying the QGP with Jets at the LHC and RHIC*, Prog. Part. Nucl. Phys. **124** (2022) 103940, arXiv: `2110.14490 [nucl-ex]`.

[4] I. Vitev, S. Wicks, and B.-W. Zhang, *A theory of jet shapes and cross sections: from hadrons to nuclei*, JHEP **11** (2008) 093, arXiv: `0810.2807 [hep-ph]`.

[5] M. L. Miller, K. Reygers, S. J. Sanders, and P. Steinberg, *Glauber Modeling in High Energy Nuclear Collisions*, Ann. Rev. Nucl. Part. Sci. **57** (2007) 205, arXiv: `nucl-ex/0701025`.

[6] ATLAS Collaboration, *Measurement of the nuclear modification factor for inclusive jets in Pb+Pb collisions at* $\sqrt{s_{\text{NN}}} = 5.02$ *TeV with the ATLAS detector*, Phys. Lett. B **790** (2019) 108, arXiv: `1805.05635 [nucl-ex]`.

[7] CMS Collaboration, *First measurement of large area jet transverse momentum spectra in heavy-ion collisions*, JHEP **05** (2021) 284, arXiv: `2102.13080 [hep-ex]`.

[8] ALICE Collaboration, *Measurements of inclusive jet spectra in pp and central Pb-Pb collisions at* $\sqrt{s_{\text{NN}}} = 5.02$ *TeV*, Phys. Rev. C **101** (2020) 034911, arXiv: `1909.09718 [nucl-ex]`.

[9] ATLAS Collaboration, *Measurement of suppression of large-radius jets and its dependence on substructure in Pb+Pb collisions at* $\sqrt{s_{\text{NN}}} = 5.02$ *TeV with the ATLAS detector*, Phys. Rev. Lett. **131** (2023) 172301, arXiv: `2301.05606 [nucl-ex]`.

[10] D. Pablos, *Jet Suppression From a Small to Intermediate to Large Radius*, Phys. Rev. Lett. **124** (2020) 052301, arXiv: `1907.12301 [hep-ph]`.

[11] Y. Mehtar-Tani, D. Pablos, and K. Tywoniuk, *Jet Suppression and Azimuthal Anisotropy from RHIC to LHC*, 2024, arXiv: `2402.07869 [hep-ph]`.

[12] CMS Collaboration, *First measurement of large area jet transverse momentum spectra in heavy-ion collisions*, JHEP **05** (2021) 284, arXiv: `2102.13080 [hep-ex]`.

[13] ATLAS Collaboration, *Measurement of the jet radius and transverse momentum dependence of inclusive jet suppression in lead-lead collisions at* $\sqrt{s_{NN}}$= *2.76 TeV with the ATLAS detector*, Phys. Lett. B **719** (2013) 220, arXiv: `1208.1967 [hep-ex]`.

[14] ALICE Collaboration, *Measurement of the radius dependence of charged-particle jet suppression in Pb–Pb collisions at sNN=5.02TeV*, Phys. Lett. B **849** (2024) 138412, arXiv: `2303.00592 [nucl-ex]`.

[15] S. Cao and X.-N. Wang, *Jet quenching and medium response in high-energy heavy-ion collisions: a review*, Rept. Prog. Phys. **84** (2021) 024301, arXiv: `2002.04028 [hep-ph]`.

[16] G.-Y. Qin and B. Müller,
Explanation of Dijet Asymmetry in Pb-Pb Collisions at the Large Hadron Collider,
Phys. Rev. Lett. **106** (2011) 162302, arXiv: `1012.5280 [hep-ph]`,
Erratum: Phys. Rev. Lett. **106** (2011) 162302.

[17] ATLAS Collaboration, *Measurements of azimuthal anisotropies of jet production in Pb+Pb collisions at* $\sqrt{s_{NN}} = 5.02$ *TeV with the ATLAS detector*, Phys. Rev. C **105** (2022) 064903, arXiv: `2111.06606 [nucl-ex]`.

[18] J. G. Milhano and K. C. Zapp, *Origins of the di-jet asymmetry in heavy-ion collisions*, Eur. Phys. J. C **76** (2016) 288, arXiv: `1512.08107 [hep-ph]`.

[19] CMS Collaboration, *In-medium modification of dijets in PbPb collisions at* $\sqrt{s_{\mathrm{NN}}} = 5.02$ *TeV*, JHEP **05** (2021) 116, arXiv: `2101.04720 [hep-ex]`.

[20] ATLAS Collaboration, *Measurement of jet* p_{T} *correlations in Pb+Pb and* pp *collisions at* $\sqrt{s_{\mathrm{NN}}} =$ *2.76 TeV with the ATLAS detector*, Phys. Lett. B **774** (2017) 379, arXiv: `1706.09363 [hep-ex]`.

[21] ATLAS Collaboration,
Measurements of the suppression and correlations of dijets in Pb+Pb collisions at $\sqrt{s_{NN}} = 5.02$ *TeV*,
Phys. Rev. C **107** (2023) 054908, arXiv: `2205.00682 [nucl-ex]`.

[22] ATLAS Collaboration, *Observation of a Centrality-Dependent Dijet Asymmetry in Lead-Lead Collisions at* $\sqrt{s_{NN}} = 2.76$ *TeV with the ATLAS Detector at the LHC*,
Phys. Rev. Lett. **105** (2010) 252303, arXiv: `1011.6182 [hep-ex]`.

[23] CMS Collaboration,
Observation and studies of jet quenching in PbPb collisions at $\sqrt{s_{\mathrm{NN}}} = 2.76$ *TeV*,
Phys. Rev. C **84** (2011) 024906, arXiv: `1102.1957 [nucl-ex]`.

[24] ATLAS Collaboration, *The ATLAS Experiment at the CERN Large Hadron Collider*,
JINST **3** (2008) S08003.

[25] M. Cacciari, G. P. Salam, and G. Soyez, *The anti-*k_t *jet clustering algorithm*, JHEP **04** (2008) 063, arXiv: `0802.1189 [hep-ph]`.

[26] ATLAS Collaboration,
Luminosity determination in pp *collisions at* $\sqrt{s} = 13$ *TeV using the ATLAS detector at the LHC*,
Eur. Phys. J. C **83** (2023) 982, arXiv: `2212.09379 [hep-ex]`.

[27] ATLAS Collaboration, *ATLAS Insertable B-Layer Technical Design Report*,
ATLAS-TDR-19; CERN-LHCC-2010-013, 2010,
URL: `https://cds.cern.ch/record/1291633`, Addendum: ATLAS-TDR-19-ADD-1;
CERN-LHCC-2012-009, 2012, URL: `https://cds.cern.ch/record/1451888`.

[28] B. Abbott et al., *Production and integration of the ATLAS Insertable B-Layer*,
JINST **13** (2018) T05008, arXiv: `1803.00844 [physics.ins-det]`.

[29] ATLAS Collaboration, *Software and computing for Run 3 of the ATLAS experiment at the LHC*, (2024), arXiv: `2404.06335 [hep-ex]`.

[30] ATLAS Collaboration, *Operation of the ATLAS trigger system in Run 2*, JINST **15** (2020) P10004, arXiv: `2007.12539 [hep-ex]`.

[31] ATLAS Collaboration, *Trigger Menu in 2017*, ATL-DAQ-PUB-2018-002, 2018,
URL: `https://cds.cern.ch/record/2625986`.

[32] ATLAS Collaboration, *Trigger Menu in 2018*, ATL-DAQ-PUB-2019-001, 2019, URL: `https://cds.cern.ch/record/2693402`.

[33] ATLAS Collaboration, *Performance of the ATLAS trigger system in 2015*, Eur. Phys. J. C **77** (2017) 317, arXiv: `1611.09661 [hep-ex]`.

[34] ATLAS Collaboration, *Measurement of longitudinal flow decorrelations in Pb+Pb collisions at* $\sqrt{s_{NN}} = 2.76$ *and 5.02 TeV with the ATLAS detector*, Eur. Phys. J. C **78** (2018) 142, arXiv: `1709.02301 [nucl-ex]`.

[35] ATLAS Collaboration, *Measurement of* $W^{\pm}$ *boson production in Pb+Pb collisions at* $\sqrt{s_{\mathrm{NN}}} = 5.02$ *TeV with the ATLAS detector*, Eur. Phys. J. C **79** (2019) 935, arXiv: `1907.10414 [nucl-ex]`.

[36] C. Loizides, J. Kamin, and D. d'Enterria, *Improved Monte Carlo Glauber predictions at present and future nuclear colliders*, Phys. Rev. C **97** (2018) 054910, arXiv: `1710.07098 [nucl-ex]`, Erratum: Phys. Rev. C **99** (2018) 019901.

[37] T. Sjöstrand et al., *An introduction to PYTHIA 8.2*, Comput. Phys. Commun. **191** (2015) 159, arXiv: `1410.3012 [hep-ph]`.

[38] ATLAS Collaboration, *ATLAS Pythia 8 tunes to* 7 *TeV data*, ATL-PHYS-PUB-2014-021, 2014, URL: `https://cds.cern.ch/record/1966419`.

[39] NNPDF Collaboration, *Parton distributions with LHC data*, Nucl. Phys. B **867** (2013) 244, arXiv: `1207.1303 [hep-ph]`.

[40] ATLAS Collaboration, *The Pythia 8 A3 tune description of ATLAS minimum bias and inelastic measurements incorporating the Donnachie–Landshoff diffractive model*, ATL-PHYS-PUB-2016-017, 2016, URL: `https://cds.cern.ch/record/2206965`.

[41] M. Bähr et al., *Herwig++ physics and manual*, Eur. Phys. J. C **58** (2008) 639, arXiv: `0803.0883 [hep-ph]`.

[42] J. Bellm et al., *Herwig 7.0/Herwig++ 3.0 release note*, Eur. Phys. J. C **76** (2016) 196, arXiv: `1512.01178 [hep-ph]`.

[43] S. Gieseke, C. Röhr, and A. Siódmok, *Colour reconnections in Herwig++*, Eur. Phys. J. C **72** (2012) 2225, arXiv: `1206.0041 [hep-ph]`.

[44] J. Pumplin et al., *New generation of Parton Distributions with Uncertainties from Global QCD Analysis*, JHEP **07** (2002) 012, arXiv: `hep-ph/0201195`.

[45] S. Agostinelli et al., *GEANT4–a simulation toolkit*, Nucl. Instrum. Meth. A **506** (2003) 250.

[46] ATLAS Collaboration, *The ATLAS Simulation Infrastructure*, Eur. Phys. J. C **70** (2010) 823, arXiv: `1005.4568 [physics.ins-det]`.

[47] M. Cacciari, G. P. Salam, and G. Soyez, *FastJet User Manual*, Eur. Phys. J. C **72** (2012) 1896, arXiv: `1111.6097 [hep-ph]`.

[48] ATLAS Collaboration, *Measurement of the azimuthal anisotropy of charged particles produced in* $\sqrt{s_{NN}} = 5.02$ *TeV Pb+Pb collisions with the ATLAS detector*, Eur. Phys. J. C **78** (2018) 997, arXiv: `1808.03951 [hep-ex]`.

[49] ATLAS Collaboration, *Jet energy measurement and its systematic uncertainty in proton-proton collisions at* $\sqrt{s}$ = 7 *TeV with the ATLAS detector*, Eur. Phys. J. C **75** (2015) 17, arXiv: `1406.0076 [hep-ex]`.

[50] ATLAS Collaboration, *Jet energy scale and its uncertainty for jets reconstructed using the ATLAS heavy ion jet algorithm*, ATLAS-CONF-2015-016, 2015, URL: `https://cds.cern.ch/record/2008677`.

[51] ATLAS Collaboration, *Measurement of photon-jet transverse momentum correlations in* 5.02 *TeV Pb+Pb and* pp *collisions with ATLAS*, Phys. Lett. B **789** (2019) 167, arXiv: `1809.07280 [hep-ex]`.

[52] G. D'Agostini, *A Multidimensional unfolding method based on Bayes' theorem*, Nucl. Instrum. Meth. A **362** (1995) 487.

[53] T. Adye, *Unfolding algorithms and tests using RooUnfold*, 2011, arXiv: `1105.1160 [physics.data-an]`.

[54] ATLAS Collaboration, *Measurement of jet* p_T *correlations in Pb+Pb and* pp *collisions at* $\sqrt{s_{NN}}$ = 2.76 *TeV with the ATLAS detector*, Phys. Lett. B **774** (2017) 379, arXiv: `1706.09363 [hep-ex]`.

[55] ATLAS Collaboration, *Evaluating statistical uncertainties and correlations using the bootstrap method*, ATL-PHYS-PUB-2021-011, 2021, URL: `https://cds.cern.ch/record/2759945`.

[56] ATLAS Collaboration, *Measurements of the suppression and correlations of dijets in Xe+Xe collisions at* $\sqrt{s_{\mathrm{NN}}} = 5.44$ *TeV*, Phys. Rev. C **108** (2023) 024906, arXiv: `2302.03967 [nucl-ex]`.

[57] ATLAS Collaboration, *Measurement of jet fragmentation in Pb+Pb and* pp *collisions at* $\sqrt{s_{NN}}$ = 5.02 *TeV with the ATLAS detector*, Phys. Rev. C **98** (2018) 024908, arXiv: `1805.05424 [nucl-ex]`.

[58] ATLAS Collaboration, *Jet energy scale and resolution measured in proton–proton collisions at* $\sqrt{s}$ = 13 *TeV with the ATLAS detector*, Eur. Phys. J. C **81** (2021) 689, arXiv: `2007.02645 [hep-ex]`.

[59] ATLAS Collaboration, *Measurement of the jet radius and transverse momentum dependence of inclusive jet suppression in lead–lead collisions at* $\sqrt{s_{NN}}$ = 2.76 *TeV with the ATLAS detector*, Phys. Lett. B **719** (2013) 220, arXiv: `1208.1967 [hep-ex]`.

[60] Y. He et al., *Interplaying mechanisms behind single inclusive jet suppression in heavy-ion collisions*, Phys. Rev. C **99** (2019) 054911, arXiv: `1809.02525`.

[61] J. H. Putschke et al., *The JETSCAPE framework*, 2019, arXiv: `1903.07706 [nucl-th]`.

[62] JETSCAPE Collaboration, *Multistage Monte Carlo simulation of jet modification in a static medium*, Phys. Rev. C **96** (2017) 024909, arXiv: `1705.00050`.

[63] S. Cao and A. Majumder, *Nuclear modification of leading hadrons and jets within a virtuality ordered parton shower*, Physical Review C **101** (2020), arXiv: `1712.10055`.

[64] ATLAS Collaboration, *ATLAS Computing Acknowledgements*, ATL-SOFT-PUB-2023-001, 2023, URL: `https://cds.cern.ch/record/2869272`.

The ATLAS Collaboration

G. Aad[104], E. Aakvaag[17], B. Abbott[123], S. Abdelhameed[119a], K. Abeling[56], N.J. Abicht[50], S.H. Abidi[30], M. Aboelela[45], A. Aboulhorma[36e], H. Abramowicz[154], H. Abreu[153], Y. Abulaiti[120], B.S. Acharya[70a,70b,k], A. Ackermann[64a], C. Adam Bourdarios[4], L. Adamczyk[87a], S.V. Addepalli[27], M.J. Addison[103], J. Adelman[118], A. Adiguzel[22c], T. Adye[137], A.A. Affolder[139], Y. Afik[40], M.N. Agaras[13], J. Agarwala[74a,74b], A. Aggarwal[102], C. Agheorghiesei[28c], F. Ahmadov[39,x], W.S. Ahmed[106], S. Ahuja[97], X. Ai[63e], G. Aielli[77a,77b], A. Aikot[166], M. Ait Tamlihat[36e], B. Aitbenchikh[36a], M. Akbiyik[102], T.P.A. Åkesson[100], A.V. Akimov[38], D. Akiyama[171], N.N. Akolkar[25], S. Aktas[22a], K. Al Khoury[42], G.L. Alberghi[24b], J. Albert[168], P. Albicocco[54], G.L. Albouy[61], S. Alderweireldt[53], Z.L. Alegria[124], M. Aleksa[37], I.N. Aleksandrov[39], C. Alexa[28b], T. Alexopoulos[10], F. Alfonsi[24b], M. Algren[57], M. Alhroob[170], B. Ali[135], H.M.J. Ali[93,r], S. Ali[32], S.W. Alibocus[94], M. Aliev[34c], G. Alimonti[72a], W. Alkakhi[56], C. Allaire[67], B.M.M. Allbrooke[149], J.F. Allen[53], C.A. Allendes Flores[140f], P.P. Allport[21], A. Aloisio[73a,73b], F. Alonso[92], C. Alpigiani[141], Z.M.K. Alsolami[93], M. Alvarez Estevez[101], A. Alvarez Fernandez[102], M. Alves Cardoso[57], M.G. Alviggi[73a,73b], M. Aly[103], Y. Amaral Coutinho[84b], A. Ambler[106], C. Amelung[37], M. Amerl[103], C.G. Ames[111], D. Amidei[108], B. Amini[55], K.J. Amirie[158], S.P. Amor Dos Santos[133a], K.R. Amos[166], D. Amperiadou[155], S. An[85], V. Ananiev[128], C. Anastopoulos[142], T. Andeen[11], J.K. Anders[37], A.C. Anderson[60], S.Y. Andrean[48a,48b], A. Andreazza[72a,72b], S. Angelidakis[9], A. Angerami[42], A.V. Anisenkov[38], A. Annovi[75a], C. Antel[57], E. Antipov[148], M. Antonelli[54], F. Anulli[76a], M. Aoki[85], T. Aoki[156], M.A. Aparo[149], L. Aperio Bella[49], C. Appelt[19], A. Apyan[27], S.J. Arbiol Val[88], C. Arcangeletti[54], A.T.H. Arce[52], J-F. Arguin[110], S. Argyropoulos[55], J.-H. Arling[49], O. Arnaez[4], H. Arnold[148], G. Artoni[76a,76b], H. Asada[113], K. Asai[121], S. Asai[156], N.A. Asbah[37], R.A. Ashby Pickering[170], K. Assamagan[30], R. Astalos[29a], K.S.V. Astrand[100], S. Atashi[162], R.J. Atkin[34a], M. Atkinson[165], H. Atmani[36f], P.A. Atmasiddha[131], K. Augsten[135], S. Auricchio[73a,73b], A.D. Auriol[21], V.A. Austrup[103], G. Avolio[37], K. Axiotis[57], G. Azuelos[110,ac], D. Babal[29b], H. Bachacou[138], K. Bachas[155,o], A. Bachiu[35], F. Backman[48a,48b], A. Badea[40], T.M. Baer[108], P. Bagnaia[76a,76b], M. Bahmani[19], D. Bahner[55], K. Bai[126], J.T. Baines[137], L. Baines[96], O.K. Baker[175], E. Bakos[16], D. Bakshi Gupta[8], L.E. Balabram Filho[84b], V. Balakrishnan[123], R. Balasubramanian[4], E.M. Baldin[38], P. Balek[87a], E. Ballabene[24b,24a], F. Balli[138], L.M. Baltes[64a], W.K. Balunas[33], J. Balz[102], I. Bamwidhi[119b], E. Banas[88], M. Bandieramonte[132], A. Bandyopadhyay[25], S. Bansal[25], L. Barak[154], M. Barakat[49], E.L. Barberio[107], D. Barberis[58b,58a], M. Barbero[104], M.Z. Barel[117], T. Barillari[112], M-S. Barisits[37], T. Barklow[146], P. Baron[125], D.A. Baron Moreno[103], A. Baroncelli[63a], A.J. Barr[129], J.D. Barr[98], F. Barreiro[101], J. Barreiro Guimarães da Costa[14], U. Barron[154], M.G. Barros Teixeira[133a], S. Barsov[38], F. Bartels[64a], R. Bartoldus[146], A.E. Barton[93], P. Bartos[29a], A. Basan[102], M. Baselga[50], A. Bassalat[67,b], M.J. Basso[159a], S. Bataju[45], R. Bate[167], R.L. Bates[60], S. Batlamous[101], B. Batool[144], M. Battaglia[139], D. Battulga[19], M. Bauce[76a,76b], M. Bauer[80], P. Bauer[25], L.T. Bazzano Hurrell[31], J.B. Beacham[52], T. Beau[130], J.Y. Beaucamp[92], P.H. Beauchemin[161], P. Bechtle[25], H.P. Beck[20,n], K. Becker[170], A.J. Beddall[83], V.A. Bednyakov[39], C.P. Bee[148], L.J. Beemster[16], T.A. Beermann[37], M. Begalli[84d], M. Begel[30], A. Behera[148], J.K. Behr[49], J.F. Beirer[37], F. Beisiegel[25], M. Belfkir[119b], G. Bella[154], L. Bellagamba[24b], A. Bellerive[35], P. Bellos[21], K. Beloborodov[38], D. Benchekroun[36a], F. Bendebba[36a], Y. Benhammou[154], K.C. Benkendorfer[62], L. Beresford[49], M. Beretta[54], E. Bergeaas Kuutmann[164], N. Berger[4], B. Bergmann[135], J. Beringer[18a], G. Bernardi[5], C. Bernius[146], F.U. Bernlochner[25], F. Bernon[37,104], A. Berrocal Guardia[13], T. Berry[97], P. Berta[136], A. Berthold[51], S. Bethke[112], A. Betti[76a,76b], A.J. Bevan[96], N.K. Bhalla[55], S. Bhatta[148], D.S. Bhattacharya[169], P. Bhattarai[146], K.D. Bhide[55], V.S. Bhopatkar[124], R.M. Bianchi[132], G. Bianco[24b,24a], O. Biebel[111], R. Bielski[126], M. Biglietti[78a], C.S. Billingsley[45], Y. Bimgdi[36f], M. Bindi[56], A. Bingul[22b], C. Bini[76a,76b], G.A. Bird[33], M. Birman[172], M. Biros[136], S. Biryukov[149], T. Bisanz[50], E. Bisceglie[44b,44a], J.P. Biswal[137], D. Biswas[144], I. Bloch[49], A. Blue[60], U. Blumenschein[96], J. Blumenthal[102], V.S. Bobrovnikov[38], M. Boehler[55], B. Boehm[169], D. Bogavac[37], A.G. Bogdanchikov[38], L.S. Boggia[130], C. Bohm[48a], V. Boisvert[97], P. Bokan[37], T. Bold[87a], M. Bomben[5], M. Bona[96], M. Boonekamp[138], C.D. Booth[97], A.G. Borbély[60], I.S. Bordulev[38], G. Borissov[93], D. Bortoletto[129], D. Boscherini[24b], M. Bosman[13], J.D. Bossio Sola[37], K. Bouaouda[36a], N. Bouchhar[166], L. Boudet[4], J. Boudreau[132], E.V. Bouhova-Thacker[93], D. Boumediene[41], R. Bouquet[58b,58a], A. Boveia[122], J. Boyd[37], D. Boye[30], I.R. Boyko[39], L. Bozianu[57], J. Bracinik[21], N. Brahimi[4], G. Brandt[174], O. Brandt[33], F. Braren[49], B. Brau[105], J.E. Brau[126], R. Brener[172], L. Brenner[117], R. Brenner[164], S. Bressler[172], G. Brianti[79a,79b], D. Britton[60], D. Britzger[112], I. Brock[25], G. Brooijmans[42], E.M. Brooks[159b], E. Brost[30], L.M. Brown[168], L.E. Bruce[62], T.L. Bruckler[129], P.A. Bruckman de Renstrom[88], B. Brüers[49], A. Bruni[24b], G. Bruni[24b], M. Bruschi[24b], N. Bruscino[76a,76b], T. Buanes[17], Q. Buat[141], D. Buchin[112], A.G. Buckley[60], O. Bulekov[38], B.A. Bullard[146], S. Burdin[94], C.D. Burgard[50], A.M. Burger[37], B. Burghgrave[8], O. Burlayenko[55], J. Burleson[165], J.T.P. Burr[33], J.C. Burzynski[145], E.L. Busch[42], V. Büscher[102], P.J. Bussey[60], J.M. Butler[26], C.M. Buttar[60], J.M. Butterworth[98], W. Buttinger[137], C.J. Buxo Vazquez[109], A.R. Buzykaev[38], S. Cabrera Urbán[166], L. Cadamuro[67], D. Caforio[59], H. Cai[132], Y. Cai[14,114c], Y. Cai[114a], V.M.M. Cairo[37], O. Cakir[3a], N. Calace[37], P. Calafiura[18a], G. Calderini[130], P. Calfayan[69], G. Callea[60], L.P. Caloba[84b], D. Calvet[41], S. Calvet[41], M. Calvetti[75a,75b], R. Camacho Toro[130], S. Camarda[37], D. Camarero Munoz[27], P. Camarri[77a,77b], M.T. Camerlingo[73a,73b], D. Cameron[37], C. Camincher[168], M. Campanelli[98], A. Camplani[43], V. Canale[73a,73b], A.C. Canbay[3a], E. Canonero[97], J. Cantero[166], Y. Cao[165], F. Capocasa[27], M. Capua[44b,44a], A. Carbone[72a,72b], R. Cardarelli[77a], J.C.J. Cardenas[8], G. Carducci[44b,44a], T. Carli[37], G. Carlino[73a], J.I. Carlotto[13], B.T. Carlson[132,p], E.M. Carlson[168,159a], J. Carmignani[94], L. Carminati[72a,72b], A. Carnelli[138], M. Carnesale[76a,76b], S. Caron[116], E. Carquin[140f], I.B. Carr[107], S. Carrá[72a], G. Carratta[24b,24a], A.M. Carroll[126], T.M. Carter[53], M.P. Casado[13,h], M. Caspar[49], F.L. Castillo[4], L. Castillo Garcia[13], V. Castillo Gimenez[166], N.F. Castro[133a,133e], A. Catinaccio[37], J.R. Catmore[128], T. Cavaliere[4], V. Cavaliere[30], N. Cavalli[24b,24a], L.J. Caviedes Betancourt[23b], Y.C. Cekmecelioglu[49], E. Celebi[83], S. Cella[37], F. Celli[129], M.S. Centonze[71a,71b], V. Cepaitis[57], K. Cerny[125], A.S. Cerqueira[84a], A. Cerri[149], L. Cerrito[77a,77b], F. Cerutti[18a], B. Cervato[144], A. Cervelli[24b], G. Cesarini[54], S.A. Cetin[83], D. Chakraborty[118], J. Chan[18a], W.Y. Chan[156], J.D. Chapman[33], E. Chapon[138], B. Chargeishvili[152b], D.G. Charlton[21], M. Chatterjee[20], C. Chauhan[136], Y. Che[114a], S. Chekanov[6], S.V. Chekulaev[159a], G.A. Chelkov[39,a], A. Chen[108], B. Chen[154], B. Chen[168], H. Chen[114a], H. Chen[30], J. Chen[63c], J. Chen[145], M. Chen[129], S. Chen[89], S.J. Chen[114a], X. Chen[63c], X. Chen[15,ab], Y. Chen[63a], C.L. Cheng[173], H.C. Cheng[65a], S. Cheong[146], A. Cheplakov[39], E. Cheremushkina[49], E. Cherepanova[117], R. Cherkaoui El Moursli[36e], E. Cheu[7], K. Cheung[66], L. Chevalier[138], V. Chiarella[54], G. Chiarelli[75a], N. Chiedde[104], G. Chiodini[71a], A.S. Chisholm[21], A. Chitan[28b], M. Chitishvili[166], M.V. Chizhov[39],

K. Choi[11], Y. Chou[141], E.Y.S. Chow[116], K.L. Chu[172], M.C. Chu[65a], X. Chu[14,114c],
Z. Chubinidze[54], J. Chudoba[134], J.J. Chwastowski[88], D. Cieri[112], K.M. Ciesla[87a],
V. Cindro[95], A. Ciocio[18a], F. Cirotto[73a,73b], Z.H. Citron[172], M. Citterio[72a], D.A. Ciubotaru[28b],
A. Clark[57], P.J. Clark[53], N. Clarke Hall[98], C. Clarry[158], J.M. Clavijo Columbie[49],
S.E. Clawson[49], C. Clement[48a,48b], Y. Coadou[104], M. Cobal[70a,70c], A. Coccaro[58b],
R.F. Coelho Barrue[133a], R. Coelho Lopes De Sa[105], S. Coelli[72a], B. Cole[42], J. Collot[61],
P. Conde Muiño[133a,133g], M.P. Connell[34c], S.H. Connell[34c], E.I. Conroy[129], F. Conventi[73a,ad],
H.G. Cooke[21], A.M. Cooper-Sarkar[129], F.A. Corchia[24b,24a], A. Cordeiro Oudot Choi[130],
L.D. Corpe[41], M. Corradi[76a,76b], F. Corriveau[106,w], A. Cortes-Gonzalez[19], M.J. Costa[166],
F. Costanza[4], D. Costanzo[142], B.M. Cote[122], J. Couthures[4], G. Cowan[97], K. Cranmer[173],
L. Cremer[50], D. Cremonini[24b,24a], S. Crépé-Renaudin[61], F. Crescioli[130], M. Cristinziani[144],
M. Cristoforetti[79a,79b], V. Croft[117], J.E. Crosby[124], G. Crosetti[44b,44a], A. Cueto[101], H. Cui[98],
Z. Cui[7], W.R. Cunningham[60], F. Curcio[166], J.R. Curran[53], P. Czodrowski[37],
M.J. Da Cunha Sargedas De Sousa[58b,58a], J.V. Da Fonseca Pinto[84b], C. Da Via[103],
W. Dabrowski[87a], T. Dado[37], S. Dahbi[151], T. Dai[108], D. Dal Santo[20], C. Dallapiccola[105],
M. Dam[43], G. D'amen[30], V. D'Amico[111], J. Damp[102], J.R. Dandoy[35], D. Dannheim[37],
M. Danninger[145], V. Dao[148], G. Darbo[58b], S.J. Das[30,ae], F. Dattola[49], S. D'Auria[72a,72b],
A. D'avanzo[73a,73b], C. David[34a], T. Davidek[136], I. Dawson[96], H.A. Day-hall[135], K. De[8],
R. De Asmundis[73a], N. De Biase[49], S. De Castro[24b,24a], N. De Groot[116], P. de Jong[117],
H. De la Torre[118], A. De Maria[114a], A. De Salvo[76a], U. De Sanctis[77a,77b], F. De Santis[71a,71b],
A. De Santo[149], J.B. De Vivie De Regie[61], J. Debevc[95], D.V. Dedovich[39], J. Degens[94],
A.M. Deiana[45], F. Del Corso[24b,24a], J. Del Peso[101], L. Delagrange[130], F. Deliot[138],
C.M. Delitzsch[50], M. Della Pietra[73a,73b], D. Della Volpe[57], A. Dell'Acqua[37],
L. Dell'Asta[72a,72b], M. Delmastro[4], P.A. Delsart[61], S. Demers[175], M. Demichev[39],
S.P. Denisov[38], L. D'Eramo[41], D. Derendarz[88], F. Derue[130], P. Dervan[94], K. Desch[25],
C. Deutsch[25], F.A. Di Bello[58b,58a], A. Di Ciaccio[77a,77b], L. Di Ciaccio[4],
A. Di Domenico[76a,76b], C. Di Donato[73a,73b], A. Di Girolamo[37], G. Di Gregorio[37],
A. Di Luca[79a,79b], B. Di Micco[78a,78b], R. Di Nardo[78a,78b], K.F. Di Petrillo[40],
M. Diamantopoulou[35], F.A. Dias[117], T. Dias Do Vale[145], M.A. Diaz[140a,140b],
F.G. Diaz Capriles[25], A.R. Didenko[39], M. Didenko[166], E.B. Diehl[108], S. Díez Cornell[49],
C. Diez Pardos[144], C. Dimitriadi[164], A. Dimitrievska[21], J. Dingfelder[25], T. Dingley[129],
I-M. Dinu[28b], S.J. Dittmeier[64b], F. Dittus[37], M. Divisek[136], B. Dixit[94], F. Djama[104],
T. Djobava[152b], C. Doglioni[103,100], A. Dohnalova[29a], J. Dolejsi[136], Z. Dolezal[136],
K. Domijan[87a], K.M. Dona[40], M. Donadelli[84d], B. Dong[109], J. Donini[41],
A. D'Onofrio[73a,73b], M. D'Onofrio[94], J. Dopke[137], A. Doria[73a], N. Dos Santos Fernandes[133a],
P. Dougan[103], M.T. Dova[92], A.T. Doyle[60], M.A. Draguet[129], E. Dreyer[172],
I. Drivas-koulouris[10], M. Drnevich[120], M. Drozdova[57], D. Du[63a], T.A. du Pree[117],
F. Dubinin[38], M. Dubovsky[29a], E. Duchovni[172], G. Duckeck[111], O.A. Ducu[28b], D. Duda[53],
A. Dudarev[37], E.R. Duden[27], M. D'uffizi[103], L. Duflot[67], M. Dührssen[37], I. Duminica[28g],
A.E. Dumitriu[28b], M. Dunford[64a], S. Dungs[50], K. Dunne[48a,48b], A. Duperrin[104],
H. Duran Yildiz[3a], M. Düren[59], A. Durglishvili[152b], B.L. Dwyer[118], G.I. Dyckes[18a],
M. Dyndal[87a], B.S. Dziedzic[37], Z.O. Earnshaw[149], G.H. Eberwein[129], B. Eckerova[29a],
S. Eggebrecht[56], E. Egidio Purcino De Souza[84e], L.F. Ehrke[57], G. Eigen[17], K. Einsweiler[18a],
T. Ekelof[164], P.A. Ekman[100], S. El Farkh[36b], Y. El Ghazali[63a], H. El Jarrari[37],
A. El Moussaouy[36a], V. Ellajosyula[164], M. Ellert[164], F. Ellinghaus[174], N. Ellis[37],
J. Elmsheuser[30], M. Elsawy[119a], M. Elsing[37], D. Emeliyanov[137], Y. Enari[85], I. Ene[18a],
S. Epari[13], P.A. Erland[88], D. Ernani Martins Neto[88], M. Errenst[174], M. Escalier[67],

C. Escobar[166], E. Etzion[154], G. Evans[133a], H. Evans[69], L.S. Evans[97], A. Ezhilov[38], S. Ezzarqtouni[36a], F. Fabbri[24b,24a], L. Fabbri[24b,24a], G. Facini[98], V. Fadeyev[139], R.M. Fakhrutdinov[38], D. Fakoudis[102], S. Falciano[76a], L.F. Falda Ulhoa Coelho[37], F. Fallavollita[112], G. Falsetti[44b,44a], J. Faltova[136], C. Fan[165], K.Y. Fan[65b], Y. Fan[14], Y. Fang[14,114c], M. Fanti[72a,72b], M. Faraj[70a,70b], Z. Farazpay[99], A. Farbin[8], A. Farilla[78a], T. Farooque[109], S.M. Farrington[53], F. Fassi[36e], D. Fassouliotis[9], M. Faucci Giannelli[77a,77b], W.J. Fawcett[33], L. Fayard[67], P. Federic[136], P. Federicova[134], O.L. Fedin[38,a], M. Feickert[173], L. Feligioni[104], D.E. Fellers[126], C. Feng[63b], Z. Feng[117], M.J. Fenton[162], L. Ferencz[49], R.A.M. Ferguson[93], S.I. Fernandez Luengo[140f], P. Fernandez Martinez[13], M.J.V. Fernoux[104], J. Ferrando[93], A. Ferrari[164], P. Ferrari[117,116], R. Ferrari[74a], D. Ferrere[57], C. Ferretti[108], D. Fiacco[76a,76b], F. Fiedler[102], P. Fiedler[135], S. Filimonov[38], A. Filipčič[95], E.K. Filmer[1], F. Filthaut[116], M.C.N. Fiolhais[133a,133c,c], L. Fiorini[166], W.C. Fisher[109], T. Fitschen[103], P.M. Fitzhugh[138], I. Fleck[144], P. Fleischmann[108], T. Flick[174], M. Flores[34d,z], L.R. Flores Castillo[65a], L. Flores Sanz De Acedo[37], F.M. Follega[79a,79b], N. Fomin[33], J.H. Foo[158], A. Formica[138], A.C. Forti[103], E. Fortin[37], A.W. Fortman[18a], M.G. Foti[18a], L. Fountas[9,i], D. Fournier[67], H. Fox[93], P. Francavilla[75a,75b], S. Francescato[62], S. Franchellucci[57], M. Franchini[24b,24a], S. Franchino[64a], D. Francis[37], L. Franco[116], V. Franco Lima[37], L. Franconi[49], M. Franklin[62], G. Frattari[27], Y.Y. Frid[154], J. Friend[60], N. Fritzsche[37], A. Froch[55], D. Froidevaux[37], J.A. Frost[129], Y. Fu[63a], S. Fuenzalida Garrido[140f], M. Fujimoto[104], K.Y. Fung[65a], E. Furtado De Simas Filho[84e], M. Furukawa[156], J. Fuster[166], A. Gaa[56], A. Gabrielli[24b,24a], A. Gabrielli[158], P. Gadow[37], G. Gagliardi[58b,58a], L.G. Gagnon[18a], S. Gaid[163], S. Galantzan[154], J. Gallagher[1], E.J. Gallas[129], B.J. Gallop[137], K.K. Gan[122], S. Ganguly[156], Y. Gao[53], F.M. Garay Walls[140a,140b], B. Garcia[30], C. García[166], A. Garcia Alonso[117], A.G. Garcia Caffaro[175], J.E. García Navarro[166], M. Garcia-Sciveres[18a], G.L. Gardner[131], R.W. Gardner[40], N. Garelli[161], D. Garg[81], R.B. Garg[146], J.M. Gargan[53], C.A. Garner[158], C.M. Garvey[34a], V.K. Gassmann[161], G. Gaudio[74a], V. Gautam[13], P. Gauzzi[76a,76b], J. Gavranovic[95], I.L. Gavrilenko[38], A. Gavrilyuk[38], C. Gay[167], G. Gaycken[126], E.N. Gazis[10], A.A. Geanta[28b], C.M. Gee[139], A. Gekow[122], C. Gemme[58b], M.H. Genest[61], A.D. Gentry[115], S. George[97], W.F. George[21], T. Geralis[47], P. Gessinger-Befurt[37], M.E. Geyik[174], M. Ghani[170], K. Ghorbanian[96], A. Ghosal[144], A. Ghosh[162], A. Ghosh[7], B. Giacobbe[24b], S. Giagu[76a,76b], T. Giani[117], A. Giannini[63a], S.M. Gibson[97], M. Gignac[139], D.T. Gil[87b], A.K. Gilbert[87a], B.J. Gilbert[42], D. Gillberg[35], G. Gilles[117], L. Ginabat[130], D.M. Gingrich[2,ac], M.P. Giordani[70a,70c], P.F. Giraud[138], G. Giugliarelli[70a,70c], D. Giugni[72a], F. Giuli[37], I. Gkialas[9,i], L.K. Gladilin[38], C. Glasman[101], G.R. Gledhill[126], G. Glemža[49], M. Glisic[126], I. Gnesi[44b], Y. Go[30], M. Goblirsch-Kolb[37], B. Gocke[50], D. Godin[110], B. Gokturk[22a], S. Goldfarb[107], T. Golling[57], M.G.D. Gololo[34g], D. Golubkov[38], J.P. Gombas[109], A. Gomes[133a,133b], G. Gomes Da Silva[144], A.J. Gomez Delegido[166], R. Gonçalo[133a], L. Gonella[21], A. Gongadze[152c], F. Gonnella[21], J.L. Gonski[146], R.Y. González Andana[53], S. González de la Hoz[166], R. Gonzalez Lopez[94], C. Gonzalez Renteria[18a], M.V. Gonzalez Rodrigues[49], R. Gonzalez Suarez[164], S. Gonzalez-Sevilla[57], L. Goossens[37], B. Gorini[37], E. Gorini[71a,71b], A. Gorišek[95], T.C. Gosart[131], A.T. Goshaw[52], M.I. Gostkin[39], S. Goswami[124], C.A. Gottardo[37], S.A. Gotz[111], M. Gouighri[36b], V. Goumarre[49], A.G. Goussiou[141], N. Govender[34c], R.P. Grabarczyk[129], I. Grabowska-Bold[87a], K. Graham[35], E. Gramstad[128], S. Grancagnolo[71a,71b], C.M. Grant[1,138], P.M. Gravila[28f], F.G. Gravili[71a,71b], H.M. Gray[18a], M. Greco[71a,71b], M.J. Green[1], C. Grefe[25], A.S. Grefsrud[17], I.M. Gregor[49], K.T. Greif[162],

P. Grenier[146], S.G. Grewe[112], A.A. Grillo[139], K. Grimm[32], S. Grinstein[13,s], J.-F. Grivaz[67], E. Gross[172], J. Grosse-Knetter[56], L. Guan[108], J.G.R. Guerrero Rojas[166], G. Guerrieri[37], R. Gugel[102], J.A.M. Guhit[108], A. Guida[19], E. Guilloton[170], S. Guindon[37], F. Guo[14,114c], J. Guo[63c], L. Guo[49], Y. Guo[108], A. Gupta[50], R. Gupta[132], S. Gurbuz[25], S.S. Gurdasani[55], G. Gustavino[76a,76b], P. Gutierrez[123], L.F. Gutierrez Zagazeta[131], M. Gutsche[51], C. Gutschow[98], C. Gwenlan[129], C.B. Gwilliam[94], E.S. Haaland[128], A. Haas[120], M. Habedank[49], C. Haber[18a], H.K. Hadavand[8], A. Hadef[51], S. Hadzic[112], A.I. Hagan[93], J.J. Hahn[144], E.H. Haines[98], M. Haleem[169], J. Haley[124], J.J. Hall[142], G.D. Hallewell[104], L. Halser[20], K. Hamano[168], M. Hamer[25], G.N. Hamity[53], E.J. Hampshire[97], J. Han[63b], K. Han[63a], L. Han[114a], L. Han[63a], S. Han[18a], Y.F. Han[158], K. Hanagaki[85], M. Hance[139], D.A. Hangal[42], H. Hanif[145], M.D. Hank[131], J.B. Hansen[43], P.H. Hansen[43], D. Harada[57], T. Harenberg[174], S. Harkusha[38], M.L. Harris[105], Y.T. Harris[25], J. Harrison[13], N.M. Harrison[122], P.F. Harrison[170], N.M. Hartman[112], N.M. Hartmann[111], R.Z. Hasan[97,137], Y. Hasegawa[143], F. Haslbeck[129], S. Hassan[17], R. Hauser[109], C.M. Hawkes[21], R.J. Hawkings[37], Y. Hayashi[156], D. Hayden[109], C. Hayes[108], R.L. Hayes[117], C.P. Hays[129], J.M. Hays[96], H.S. Hayward[94], F. He[63a], M. He[14,114c], Y. He[49], Y. He[98], N.B. Heatley[96], V. Hedberg[100], A.L. Heggelund[128], N.D. Hehir[96,*], C. Heidegger[55], K.K. Heidegger[55], J. Heilman[35], S. Heim[49], T. Heim[18a], J.G. Heinlein[131], J.J. Heinrich[126], L. Heinrich[112,aa], J. Hejbal[134], A. Held[173], S. Hellesund[17], C.M. Helling[167], S. Hellman[48a,48b], R.C.W. Henderson[93], L. Henkelmann[33], A.M. Henriques Correia[37], H. Herde[100], Y. Hernández Jiménez[148], L.M. Herrmann[25], T. Herrmann[51], G. Herten[55], R. Hertenberger[111], L. Hervas[37], M.E. Hesping[102], N.P. Hessey[159a], J. Hessler[112], M. Hidaoui[36b], N. Hidic[136], E. Hill[158], S.J. Hillier[21], J.R. Hinds[109], F. Hinterkeuser[25], M. Hirose[127], S. Hirose[160], D. Hirschbuehl[174], T.G. Hitchings[103], B. Hiti[95], J. Hobbs[148], R. Hobincu[28e], N. Hod[172], M.C. Hodgkinson[142], B.H. Hodkinson[129], A. Hoecker[37], D.D. Hofer[108], J. Hofer[166], T. Holm[25], M. Holzbock[37], L.B.A.H. Hommels[33], B.P. Honan[103], J.J. Hong[69], J. Hong[63c], T.M. Hong[132], B.H. Hooberman[165], W.H. Hopkins[6], M.C. Hoppesch[165], Y. Horii[113], M.E. Horstmann[112], S. Hou[151], A.S. Howard[95], J. Howarth[60], J. Hoya[6], M. Hrabovsky[125], A. Hrynevich[49], T. Hryn'ova[4], P.J. Hsu[66], S.-C. Hsu[141], T. Hsu[67], M. Hu[18a], Q. Hu[63a], S. Huang[65b], X. Huang[14,114c], Y. Huang[142], Y. Huang[102], Y. Huang[14], Z. Huang[103], Z. Hubacek[135], M. Huebner[25], F. Huegging[25], T.B. Huffman[129], C.A. Hugli[49], M. Huhtinen[37], S.K. Huiberts[17], R. Hulsken[106], N. Huseynov[12,f], J. Huston[109], J. Huth[62], R. Hyneman[146], G. Iacobucci[57], G. Iakovidis[30], L. Iconomidou-Fayard[67], J.P. Iddon[37], P. Iengo[73a,73b], R. Iguchi[156], Y. Iiyama[156], T. Iizawa[129], Y. Ikegami[85], N. Ilic[158], H. Imam[84c], G. Inacio Goncalves[84d], M. Ince Lezki[57], T. Ingebretsen Carlson[48a,48b], J.M. Inglis[96], G. Introzzi[74a,74b], M. Iodice[78a], V. Ippolito[76a,76b], R.K. Irwin[94], M. Ishino[156], W. Islam[173], C. Issever[19,49], S. Istin[22a,ag], H. Ito[171], R. Iuppa[79a,79b], A. Ivina[172], J.M. Izen[46], V. Izzo[73a], P. Jacka[134], P. Jackson[1], C.S. Jagfeld[111], G. Jain[159a], P. Jain[49], K. Jakobs[55], T. Jakoubek[172], J. Jamieson[60], W. Jang[156], M. Javurkova[105], P. Jawahar[103], L. Jeanty[126], J. Jejelava[152a,y], P. Jenni[55,e], C.E. Jessiman[35], C. Jia[63b], H. Jia[167], J. Jia[148], X. Jia[14,114c], Z. Jia[114a], C. Jiang[53], S. Jiggins[49], J. Jimenez Pena[13], S. Jin[114a], A. Jinaru[28b], O. Jinnouchi[157], P. Johansson[142], K.A. Johns[7], J.W. Johnson[139], F.A. Jolly[49], D.M. Jones[149], E. Jones[49], K.S. Jones[8], P. Jones[33], R.W.L. Jones[93], T.J. Jones[94], H.L. Joos[56,37], R. Joshi[122], J. Jovicevic[16], X. Ju[18a], J.J. Junggeburth[105], T. Junkermann[64a], A. Juste Rozas[13,s], M.K. Juzek[88], S. Kabana[140e], A. Kaczmarska[88], M. Kado[112], H. Kagan[122], M. Kagan[146], A. Kahn[131], C. Kahra[102], T. Kaji[156], E. Kajomovitz[153], N. Kakati[172], I. Kalaitzidou[55], C.W. Kalderon[30], N.J. Kang[139], D. Kar[34g], K. Karava[129], M.J. Kareem[159b], E. Karentzos[55], O. Karkout[117], S.N. Karpov[39], Z.M. Karpova[39], V. Kartvelishvili[93], A.N. Karyukhin[38], E. Kasimi[155], J. Katzy[49], S. Kaur[35], K. Kawade[143], M.P. Kawale[123], C. Kawamoto[89], T. Kawamoto[63a], E.F. Kay[37], F.I. Kaya[161], S. Kazakos[109], V.F. Kazanin[38], Y. Ke[148], J.M. Keaveney[34a], R. Keeler[168], G.V. Kehris[62], J.S. Keller[35], A.S. Kelly[98], J.J. Kempster[149], P.D. Kennedy[102], O. Kepka[134], B.P. Kerridge[137], S. Kersten[174], B.P. Kerševan[95], L. Keszeghova[29a], S. Ketabchi Haghighat[158], R.A. Khan[132], A. Khanov[124], A.G. Kharlamov[38], T. Kharlamova[38], E.E. Khoda[141], M. Kholodenko[133a], T.J. Khoo[19], G. Khoriauli[169], J. Khubua[152b,*], Y.A.R. Khwaira[130], B. Kibirige[34g], D. Kim[6], D.W. Kim[48a,48b], Y.K. Kim[40], N. Kimura[98], M.K. Kingston[56], A. Kirchhoff[56], C. Kirfel[25], F. Kirfel[25], J. Kirk[137], A.E. Kiryunin[112], S. Kita[160], C. Kitsaki[10], O. Kivernyk[25], M. Klassen[161], C. Klein[35], L. Klein[169], M.H. Klein[45], S.B. Klein[57], U. Klein[94], P. Klimek[37], A. Klimentov[30], T. Klioutchnikova[37], P. Kluit[117], S. Kluth[112], E. Kneringer[80], T.M. Knight[158], A. Knue[50], D. Kobylianskii[172], S.F. Koch[129], M. Kocian[146], P. Kodyš[136], D.M. Koeck[126], P.T. Koenig[25], T. Koffas[35], O. Kolay[51], I. Koletsou[4], T. Komarek[88], K. Köneke[55], A.X.Y. Kong[1], T. Kono[121], N. Konstantinidis[98], P. Kontaxakis[57], B. Konya[100], R. Kopeliansky[42], S. Koperny[87a], K. Korcyl[88], K. Kordas[155,d], A. Korn[98], S. Korn[56], I. Korolkov[13], N. Korotkova[38], B. Kortman[117], O. Kortner[112], S. Kortner[112], W.H. Kostecka[118], V.V. Kostyukhin[144], A. Kotsokechagia[37], A. Kotwal[52], A. Koulouris[37], A. Kourkoumeli-Charalampidi[74a,74b], C. Kourkoumelis[9], E. Kourlitis[112,aa], O. Kovanda[126], R. Kowalewski[168], W. Kozanecki[126], A.S. Kozhin[38], V.A. Kramarenko[38], G. Kramberger[95], P. Kramer[102], M.W. Krasny[130], A. Krasznahorkay[37], A.C. Kraus[118], J.W. Kraus[174], J.A. Kremer[49], T. Kresse[51], L. Kretschmann[174], J. Kretzschmar[94], K. Kreul[19], P. Krieger[158], M. Krivos[136], K. Krizka[21], K. Kroeninger[50], H. Kroha[112], J. Kroll[134], J. Kroll[131], K.S. Krowpman[109], U. Kruchonak[39], H. Krüger[25], N. Krumnack[82], M.C. Kruse[52], O. Kuchinskaia[38], S. Kuday[3a], S. Kuehn[37], R. Kuesters[55], T. Kuhl[49], V. Kukhtin[39], Y. Kulchitsky[38,a], S. Kuleshov[140d,140b], M. Kumar[34g], N. Kumari[49], P. Kumari[159b], A. Kupco[134], T. Kupfer[50], A. Kupich[38], O. Kuprash[55], H. Kurashige[86], L.L. Kurchaninov[159a], O. Kurdysh[67], Y.A. Kurochkin[38], A. Kurova[38], M. Kuze[157], A.K. Kvam[105], J. Kvita[125], T. Kwan[106], N.G. Kyriacou[108], L.A.O. Laatu[104], C. Lacasta[166], F. Lacava[76a,76b], H. Lacker[19], D. Lacour[130], N.N. Lad[98], E. Ladygin[39], A. Lafarge[41], B. Laforge[130], T. Lagouri[175], F.Z. Lahbabi[36a], S. Lai[56], J.E. Lambert[168], S. Lammers[69], W. Lampl[7], C. Lampoudis[155,d], G. Lamprinoudis[102], A.N. Lancaster[118], E. Lançon[30], U. Landgraf[55], M.P.J. Landon[96], V.S. Lang[55], O.K.B. Langrekken[128], A.J. Lankford[162], F. Lanni[37], K. Lantzsch[25], A. Lanza[74a], M. Lanzac Berrocal[166], J.F. Laporte[138], T. Lari[72a], F. Lasagni Manghi[24b], M. Lassnig[37], V. Latonova[134], A. Laurier[153], S.D. Lawlor[142], Z. Lawrence[103], R. Lazaridou[170], M. Lazzaroni[72a,72b], B. Le[103], H.D.M. Le[109], E.M. Le Boulicaut[175], L.T. Le Pottier[18a], B. Leban[24b,24a], A. Lebedev[82], M. LeBlanc[103], F. Ledroit-Guillon[61], S.C. Lee[151], S. Lee[48a,48b], T.F. Lee[94], L.L. Leeuw[34c], H.P. Lefebvre[97], M. Lefebvre[168], C. Leggett[18a], G. Lehmann Miotto[37], M. Leigh[57], W.A. Leight[105], W. Leinonen[116], A. Leisos[155,q], M.A.L. Leite[84c], C.E. Leitgeb[19], R. Leitner[136], K.J.C. Leney[45], T. Lenz[25], S. Leone[75a], C. Leonidopoulos[53], A. Leopold[147], R. Les[109], C.G. Lester[33], M. Levchenko[38], J. Levêque[4], L.J. Levinson[172], G. Levrini[24b,24a], M.P. Lewicki[88], C. Lewis[141], D.J. Lewis[4], L. Lewitt[142], A. Li[30], B. Li[63b], C. Li[63a], C-Q. Li[112], H. Li[63a], H. Li[63b], H. Li[114a], H. Li[15], H. Li[63b], J. Li[63c], K. Li[14], L. Li[63c], M. Li[14,114c], S. Li[14,114c], S. Li[63d,63c], T. Li[5], X. Li[106], Z. Li[129], Z. Li[156], Z. Li[14,114c], Z. Li[63a], S. Liang[14,114c], Z. Liang[14], M. Liberatore[138], B. Liberti[77a], K. Lie[65c], J. Lieber Marin[84e], H. Lien[69], H. Lin[108], K. Lin[109], R.E. Lindley[7], J.H. Lindon[2],

J. Ling[62], E. Lipeles[131], A. Lipniacka[17], A. Lister[167], J.D. Little[69], B. Liu[14], B.X. Liu[114b], D. Liu[63d,63c], E.H.L. Liu[21], J.B. Liu[63a], J.K.K. Liu[33], K. Liu[63d], K. Liu[63d,63c], M. Liu[63a], M.Y. Liu[63a], P. Liu[14], Q. Liu[63d,141,63c], X. Liu[63a], X. Liu[63b], Y. Liu[114b,114c], Y.L. Liu[63b], Y.W. Liu[63a], S.L. Lloyd[96], E.M. Lobodzinska[49], P. Loch[7], E. Lodhi[158], T. Lohse[19], K. Lohwasser[142], E. Loiacono[49], M. Lokajicek[134,*], J.D. Lomas[21], J.D. Long[42], I. Longarini[162], R. Longo[165], I. Lopez Paz[68], A. Lopez Solis[49], N.A. Lopez-canelas[7], N. Lorenzo Martinez[4], A.M. Lory[111], M. Losada[119a], G. Löschcke Centeno[149], O. Loseva[38], X. Lou[48a,48b], X. Lou[14,114c], A. Lounis[67], P.A. Love[93], G. Lu[14,114c], M. Lu[67], S. Lu[131], Y.J. Lu[66], H.J. Lubatti[141], C. Luci[76a,76b], F.L. Lucio Alves[114a], F. Luehring[69], O. Lukianchuk[67], B.S. Lunday[131], O. Lundberg[147], B. Lund-Jensen[147,*], N.A. Luongo[6], M.S. Lutz[37], A.B. Lux[26], D. Lynn[30], R. Lysak[134], E. Lytken[100], V. Lyubushkin[39], T. Lyubushkina[39], M.M. Lyukova[148], M.Firdaus M. Soberi[53], H. Ma[30], K. Ma[63a], L.L. Ma[63b], W. Ma[63a], Y. Ma[124], J.C. MacDonald[102], P.C. Machado De Abreu Farias[84e], R. Madar[41], T. Madula[98], J. Maeda[86], T. Maeno[30], H. Maguire[142], V. Maiboroda[138], A. Maio[133a,133b,133d], K. Maj[87a], O. Majersky[49], S. Majewski[126], N. Makovec[67], V. Maksimovic[16], B. Malaescu[130], Pa. Malecki[88], V.P. Maleev[38], F. Malek[61,m], M. Mali[95], D. Malito[97], U. Mallik[81], S. Maltezos[10], S. Malyukov[39], J. Mamuzic[13], G. Mancini[54], M.N. Mancini[27], G. Manco[74a,74b], J.P. Mandalia[96], S.S. Mandarry[149], I. Mandić[95], L. Manhaes de Andrade Filho[84a], I.M. Maniatis[172], J. Manjarres Ramos[91], D.C. Mankad[172], A. Mann[111], S. Manzoni[37], L. Mao[63c], X. Mapekula[34c], A. Marantis[155,q], G. Marchiori[5], M. Marcisovsky[134], C. Marcon[72a], M. Marinescu[21], S. Marium[49], M. Marjanovic[123], A. Markhoos[55], M. Markovitch[67], E.J. Marshall[93], Z. Marshall[18a], S. Marti-Garcia[166], J. Martin[98], T.A. Martin[137], V.J. Martin[53], B. Martin dit Latour[17], L. Martinelli[76a,76b], M. Martinez[13,s], P. Martinez Agullo[166], V.I. Martinez Outschoorn[105], P. Martinez Suarez[13], S. Martin-Haugh[137], G. Martinovicova[136], V.S. Martoiu[28b], A.C. Martyniuk[98], A. Marzin[37], D. Mascione[79a,79b], L. Masetti[102], J. Masik[103], A.L. Maslennikov[38], P. Massarotti[73a,73b], P. Mastrandrea[75a,75b], A. Mastroberardino[44b,44a], T. Masubuchi[127], T.T. Mathew[126], T. Mathisen[164], J. Matousek[136], J. Maurer[28b], T. Maurin[60], A.J. Maury[67], B. Maček[95], D.A. Maximov[38], A.E. May[103], R. Mazini[151], I. Maznas[118], M. Mazza[109], S.M. Mazza[139], E. Mazzeo[72a,72b], C. Mc Ginn[30], J.P. Mc Gowan[168], S.P. Mc Kee[108], C.C. McCracken[167], E.F. McDonald[107], A.E. McDougall[117], J.A. Mcfayden[149], R.P. McGovern[131], R.P. Mckenzie[34g], T.C. Mclachlan[49], D.J. Mclaughlin[98], S.J. McMahon[137], C.M. Mcpartland[94], R.A. McPherson[168,w], S. Mehlhase[111], A. Mehta[94], D. Melini[166], B.R. Mellado Garcia[34g], A.H. Melo[56], F. Meloni[49], A.M. Mendes Jacques Da Costa[103], H.Y. Meng[158], L. Meng[93], S. Menke[112], M. Mentink[37], E. Meoni[44b,44a], G. Mercado[118], S. Merianos[155], C. Merlassino[70a,70c], L. Merola[73a,73b], C. Meroni[72a,72b], J. Metcalfe[6], A.S. Mete[6], E. Meuser[102], C. Meyer[69], J-P. Meyer[138], R.P. Middleton[137], L. Mijović[53], G. Mikenberg[172], M. Mikestikova[134], M. Mikuž[95], H. Mildner[102], A. Milic[37], D.W. Miller[40], E.H. Miller[146], L.S. Miller[35], A. Milov[172], D.A. Milstead[48a,48b], T. Min[114a], A.A. Minaenko[38], I.A. Minashvili[152b], L. Mince[60], A.I. Mincer[120], B. Mindur[87a], M. Mineev[39], Y. Mino[89], L.M. Mir[13], M. Miralles Lopez[60], M. Mironova[18a], M.C. Missio[116], A. Mitra[170], V.A. Mitsou[166], Y. Mitsumori[113], O. Miu[158], P.S. Miyagawa[96], T. Mkrtchyan[64a], M. Mlinarevic[98], T. Mlinarevic[98], M. Mlynarikova[37], S. Mobius[20], P. Mogg[111], M.H. Mohamed Farook[115], A.F. Mohammed[14,114c], S. Mohapatra[42], G. Mokgatitswane[34g], L. Moleri[172], B. Mondal[144], S. Mondal[135], K. Mönig[49], E. Monnier[104], L. Monsonis Romero[166], J. Montejo Berlingen[13], A. Montella[48a,48b], M. Montella[122], F. Montereali[78a,78b], F. Monticelli[92], S. Monzani[70a,70c], A. Morancho Tarda[43],

N. Morange[67], A.L. Moreira De Carvalho[49], M. Moreno Llácer[166], C. Moreno Martinez[57], J.M. Moreno Perez[23b], P. Morettini[58b], S. Morgenstern[37], M. Morii[62], M. Morinaga[156], M. Moritsu[90], F. Morodei[76a,76b], L. Morvaj[37], P. Moschovakos[37], B. Moser[129], M. Mosidze[152b], T. Moskalets[45], P. Moskvitina[116], J. Moss[32,j], P. Moszkowicz[87a], A. Moussa[36d], E.J.W. Moyse[105], O. Mtintsilana[34g], S. Muanza[104], J. Mueller[132], D. Muenstermann[93], R. Müller[37], G.A. Mullier[164], A.J. Mullin[33], J.J. Mullin[131], A.E. Mulski[62], D.P. Mungo[158], D. Munoz Perez[166], F.J. Munoz Sanchez[103], M. Murin[103], W.J. Murray[170,137], M. Muškinja[95], C. Mwewa[30], A.G. Myagkov[38,a], A.J. Myers[8], G. Myers[108], M. Myska[135], B.P. Nachman[18a], O. Nackenhorst[50], K. Nagai[129], K. Nagano[85], J.L. Nagle[30,ae], E. Nagy[104], A.M. Nairz[37], Y. Nakahama[85], K. Nakamura[85], K. Nakkalil[5], H. Nanjo[127], E.A. Narayanan[115], I. Naryshkin[38], L. Nasella[72a,72b], M. Naseri[35], S. Nasri[119b], C. Nass[25], G. Navarro[23a], J. Navarro-Gonzalez[166], R. Nayak[154], A. Nayaz[19], P.Y. Nechaeva[38], S. Nechaeva[24b,24a], F. Nechansky[134], L. Nedic[129], T.J. Neep[21], A. Negri[74a,74b], M. Negrini[24b], C. Nellist[117], C. Nelson[106], K. Nelson[108], S. Nemecek[134], M. Nessi[37,g], M.S. Neubauer[165], F. Neuhaus[102], J. Neundorf[49], J. Newell[94], P.R. Newman[21], C.W. Ng[132], Y.W.Y. Ng[49], B. Ngair[119a], H.D.N. Nguyen[110], R.B. Nickerson[129], R. Nicolaidou[138], J. Nielsen[139], M. Niemeyer[56], J. Niermann[56], N. Nikiforou[37], V. Nikolaenko[38,a], I. Nikolic-Audit[130], K. Nikolopoulos[21], P. Nilsson[30], I. Ninca[49], G. Ninio[154], A. Nisati[76a], N. Nishu[2], R. Nisius[112], J-E. Nitschke[51], E.K. Nkadimeng[34g], T. Nobe[156], T. Nommensen[150], M.B. Norfolk[142], B.J. Norman[35], M. Noury[36a], J. Novak[95], T. Novak[95], L. Novotny[135], R. Novotny[115], L. Nozka[125], K. Ntekas[162], N.M.J. Nunes De Moura Junior[84b], J. Ocariz[130], A. Ochi[86], I. Ochoa[133a], S. Oerdek[49,t], J.T. Offermann[40], A. Ogrodnik[136], A. Oh[103], C.C. Ohm[147], H. Oide[85], R. Oishi[156], M.L. Ojeda[37], Y. Okumura[156], L.F. Oleiro Seabra[133a], I. Oleksiyuk[57], S.A. Olivares Pino[140d], G. Oliveira Correa[13], D. Oliveira Damazio[30], J.L. Oliver[162], Ö.O. Öncel[55], A.P. O'Neill[20], A. Onofre[133a,133e], P.U.E. Onyisi[11], M.J. Oreglia[40], G.E. Orellana[92], D. Orestano[78a,78b], N. Orlando[13], R.S. Orr[158], L.M. Osojnak[131], R. Ospanov[63a], G. Otero y Garzon[31], H. Otono[90], P.S. Ott[64a], G.J. Ottino[18a], M. Ouchrif[36d], F. Ould-Saada[128], T. Ovsiannikova[141], M. Owen[60], R.E. Owen[137], V.E. Ozcan[22a], F. Ozturk[88], N. Ozturk[8], S. Ozturk[83], H.A. Pacey[129], A. Pacheco Pages[13], C. Padilla Aranda[13], G. Padovano[76a,76b], S. Pagan Griso[18a], G. Palacino[69], A. Palazzo[71a,71b], J. Pampel[25], J. Pan[175], T. Pan[65a], D.K. Panchal[11], C.E. Pandini[117], J.G. Panduro Vazquez[137], H.D. Pandya[1], H. Pang[15], P. Pani[49], G. Panizzo[70a,70c], L. Panwar[130], L. Paolozzi[57], S. Parajuli[165], A. Paramonov[6], C. Paraskevopoulos[54], D. Paredes Hernandez[65b], A. Pareti[74a,74b], K.R. Park[42], T.H. Park[158], M.A. Parker[33], F. Parodi[58b,58a], E.W. Parrish[118], V.A. Parrish[53], J.A. Parsons[42], U. Parzefall[55], B. Pascual Dias[110], L. Pascual Dominguez[101], E. Pasqualucci[76a], S. Passaggio[58b], F. Pastore[97], P. Patel[88], U.M. Patel[52], J.R. Pater[103], T. Pauly[37], F. Pauwels[136], C.I. Pazos[161], J. Pearkes[146], M. Pedersen[128], R. Pedro[133a], S.V. Peleganchuk[38], O. Penc[37], E.A. Pender[53], S. Peng[15], G.D. Penn[175], K.E. Penski[111], M. Penzin[38], B.S. Peralva[84d], A.P. Pereira Peixoto[141], L. Pereira Sanchez[146], D.V. Perepelitsa[30,ae], G. Perera[105], E. Perez Codina[159a], M. Perganti[10], H. Pernegger[37], S. Perrella[76a,76b], O. Perrin[41], K. Peters[49], R.F.Y. Peters[103], B.A. Petersen[37], T.C. Petersen[43], E. Petit[104], V. Petousis[135], C. Petridou[155,d], T. Petru[136], A. Petrukhin[144], M. Pettee[18a], A. Petukhov[38], K. Petukhova[37], R. Pezoa[140f], L. Pezzotti[37], G. Pezzullo[175], A.J. Pfleger[37], T.M. Pham[173], T. Pham[107], P.W. Phillips[137], G. Piacquadio[148], E. Pianori[18a], F. Piazza[126], R. Piegaia[31], D. Pietreanu[28b], A.D. Pilkington[103], M. Pinamonti[70a,70c], J.L. Pinfold[2], B.C. Pinheiro Pereira[133a], J. Pinol Bel[13], A.E. Pinto Pinoargote[138,138], L. Pintucci[70a,70c], K.M. Piper[149], A. Pirttikoski[57], D.A. Pizzi[35], L. Pizzimento[65b], A. Pizzini[117], M.-A. Pleier[30], V. Pleskot[136], E. Plotnikova[39], G. Poddar[96], R. Poettgen[100], L. Poggioli[130], I. Pokharel[56], S. Polacek[136], G. Polesello[74a], A. Poley[145,159a], A. Polini[24b], C.S. Pollard[170], Z.B. Pollock[122], E. Pompa Pacchi[76a,76b], N.I. Pond[98], D. Ponomarenko[69], L. Pontecorvo[37], S. Popa[28a], G.A. Popeneciu[28d], A. Poreba[37], D.M. Portillo Quintero[159a], S. Pospisil[135], M.A. Postill[142], P. Postolache[28c], K. Potamianos[170], P.A. Potepa[87a], I.N. Potrap[39], C.J. Potter[33], H. Potti[150], J. Poveda[166], M.E. Pozo Astigarraga[37], A. Prades Ibanez[77a,77b], J. Pretel[168], D. Price[103], M. Primavera[71a], L. Primomo[70a,70c], M.A. Principe Martin[101], R. Privara[125], T. Procter[60], M.L. Proffitt[141], N. Proklova[131], K. Prokofiev[65c], G. Proto[112], J. Proudfoot[6], M. Przybycien[87a], W.W. Przygoda[87b], A. Psallidas[47], J.E. Puddefoot[142], D. Pudzha[55], D. Pyatiizbyantseva[38], J. Qian[108], D. Qichen[103], Y. Qin[13], T. Qiu[53], A. Quadt[56], M. Queitsch-Maitland[103], G. Quetant[57], R.P. Quinn[167], G. Rabanal Bolanos[62], D. Rafanoharana[55], F. Raffaeli[77a,77b], F. Ragusa[72a,72b], J.L. Rainbolt[40], J.A. Raine[57], S. Rajagopalan[30], E. Ramakoti[38], L. Rambelli[58b,58a], I.A. Ramirez-Berend[35], K. Ran[49,114c], D.S. Rankin[131], N.P. Rapheeha[34g], H. Rasheed[28b], V. Raskina[130], D.F. Rassloff[64a], A. Rastogi[18a], S. Rave[102], S. Ravera[58b,58a], B. Ravina[56], I. Ravinovich[172], M. Raymond[37], A.L. Read[128], N.P. Readioff[142], D.M. Rebuzzi[74a,74b], G. Redlinger[30], A.S. Reed[112], K. Reeves[27], J.A. Reidelsturz[174], D. Reikher[126], A. Rej[50], C. Rembser[37], M. Renda[28b], F. Renner[49], A.G. Rennie[162], A.L. Rescia[49], S. Resconi[72a], M. Ressegotti[58b,58a], S. Rettie[37], J.G. Reyes Rivera[109], E. Reynolds[18a], O.L. Rezanova[38], P. Reznicek[136], H. Riani[36d], N. Ribaric[52], E. Ricci[79a,79b], R. Richter[112], S. Richter[48a,48b], E. Richter-Was[87b], M. Ridel[130], S. Ridouani[36d], P. Rieck[120], P. Riedler[37], E.M. Riefel[48a,48b], J.O. Rieger[117], M. Rijssenbeek[148], M. Rimoldi[37], L. Rinaldi[24b,24a], P. Rincke[56,164], T.T. Rinn[30], M.P. Rinnagel[111], G. Ripellino[164], I. Riu[13], J.C. Rivera Vergara[168], F. Rizatdinova[124], E. Rizvi[96], B.R. Roberts[18a], S.S. Roberts[139], S.H. Robertson[106,w], D. Robinson[33], M. Robles Manzano[102], A. Robson[60], A. Rocchi[77a,77b], C. Roda[75a,75b], S. Rodriguez Bosca[37], Y. Rodriguez Garcia[23a], A. Rodriguez Rodriguez[55], A.M. Rodríguez Vera[118], S. Roe[37], J.T. Roemer[37], A.R. Roepe-Gier[139], O. Røhne[128], R.A. Rojas[105], C.P.A. Roland[130], J. Roloff[30], A. Romaniouk[38], E. Romano[74a,74b], M. Romano[24b], A.C. Romero Hernandez[165], N. Rompotis[94], L. Roos[130], S. Rosati[76a], B.J. Rosser[40], E. Rossi[129], E. Rossi[73a,73b], L.P. Rossi[62], L. Rossini[55], R. Rosten[122], M. Rotaru[28b], B. Rottler[55], C. Rougier[91], D. Rousseau[67], D. Rousso[49], A. Roy[165], S. Roy-Garand[158], A. Rozanov[104], Z.M.A. Rozario[60], Y. Rozen[153], A. Rubio Jimenez[166], A.J. Ruby[94], V.H. Ruelas Rivera[19], T.A. Ruggeri[1], A. Ruggiero[129], A. Ruiz-Martinez[166], A. Rummler[37], Z. Rurikova[55], N.A. Rusakovich[39], H.L. Russell[168], G. Russo[76a,76b], J.P. Rutherfoord[7], S. Rutherford Colmenares[33], M. Rybar[136], E.B. Rye[128], A. Ryzhov[45], J.A. Sabater Iglesias[57], H.F-W. Sadrozinski[139], F. Safai Tehrani[76a], B. Safarzadeh Samani[137], S. Saha[1], M. Sahinsoy[83], A. Saibel[166], M. Saimpert[138], M. Saito[156], T. Saito[156], A. Sala[72a,72b], D. Salamani[37], A. Salnikov[146], J. Salt[166], A. Salvador Salas[154], D. Salvatore[44b,44a], F. Salvatore[149], A. Salzburger[37], D. Sammel[55], E. Sampson[93], D. Sampsonidis[155,d], D. Sampsonidou[126], J. Sánchez[166], V. Sanchez Sebastian[166], H. Sandaker[128], C.O. Sander[49], J.A. Sandesara[105], M. Sandhoff[174], C. Sandoval[23b], L. Sanfilippo[64a], D.P.C. Sankey[137], T. Sano[89], A. Sansoni[54], L. Santi[37,76b], C. Santoni[41], H. Santos[133a,133b], A. Santra[172], E. Sanzani[24b,24a], K.A. Saoucha[163], J.G. Saraiva[133a,133d], J. Sardain[7], O. Sasaki[85], K. Sato[160], C. Sauer[64b], E. Sauvan[4], P. Savard[158,ac], R. Sawada[156], C. Sawyer[137], L. Sawyer[99], C. Sbarra[24b], A. Sbrizzi[24b,24a], T. Scanlon[98], J. Schaarschmidt[141], U. Schäfer[102], A.C. Schaffer[67,45], D. Schaile[111], R.D. Schamberger[148], C. Scharf[19], M.M. Schefer[20], V.A. Schegelsky[38], D. Scheirich[136], M. Schernau[162],

C. Scheulen[56], C. Schiavi[58b,58a], M. Schioppa[44b,44a], B. Schlag[146,l], K.E. Schleicher[55], S. Schlenker[37], J. Schmeing[174], M.A. Schmidt[174], K. Schmieden[102], C. Schmitt[102], N. Schmitt[102], S. Schmitt[49], L. Schoeffel[138], A. Schoening[64b], P.G. Scholer[35], E. Schopf[129], M. Schott[25], J. Schovancova[37], S. Schramm[57], T. Schroer[57], H-C. Schultz-Coulon[64a], M. Schumacher[55], B.A. Schumm[139], Ph. Schune[138], A.J. Schuy[141], H.R. Schwartz[139], A. Schwartzman[146], T.A. Schwarz[108], Ph. Schwemling[138], R. Schwienhorst[109], F.G. Sciacca[20], A. Sciandra[30], G. Sciolla[27], F. Scuri[75a], C.D. Sebastiani[94], K. Sedlaczek[118], S.C. Seidel[115], A. Seiden[139], B.D. Seidlitz[42], C. Seitz[49], J.M. Seixas[84b], G. Sekhniaidze[73a], L. Selem[61], N. Semprini-Cesari[24b,24a], D. Sengupta[57], V. Senthilkumar[166], L. Serin[67], M. Sessa[77a,77b], H. Severini[123], F. Sforza[58b,58a], A. Sfyrla[57], Q. Sha[14], E. Shabalina[56], A.H. Shah[33], R. Shaheen[147], J.D. Shahinian[131], D. Shaked Renous[172], L.Y. Shan[14], M. Shapiro[18a], A. Sharma[37], A.S. Sharma[167], P. Sharma[81], P.B. Shatalov[38], K. Shaw[149], S.M. Shaw[103], Q. Shen[63c], D.J. Sheppard[145], P. Sherwood[98], L. Shi[98], X. Shi[14], S. Shimizu[85], C.O. Shimmin[175], J.D. Shinner[97], I.P.J. Shipsey[129], S. Shirabe[90], M. Shiyakova[39,u], M.J. Shochet[40], D.R. Shope[128], B. Shrestha[123], S. Shrestha[122,af], I. Shreyber[38], M.J. Shroff[168], P. Sicho[134], A.M. Sickles[165], E. Sideras Haddad[34g], A.C. Sidley[117], A. Sidoti[24b], F. Siegert[51], Dj. Sijacki[16], F. Sili[92], J.M. Silva[53], I. Silva Ferreira[84b], M.V. Silva Oliveira[30], S.B. Silverstein[48a], S. Simion[67], R. Simoniello[37], E.L. Simpson[103], H. Simpson[149], L.R. Simpson[108], N.D. Simpson[100], S. Simsek[83], S. Sindhu[56], P. Sinervo[158], S. Singh[158], S. Sinha[49], S. Sinha[103], M. Sioli[24b,24a], I. Siral[37], E. Sitnikova[49], J. Sjölin[48a,48b], A. Skaf[56], E. Skorda[21], P. Skubic[123], M. Slawinska[88], V. Smakhtin[172], B.H. Smart[137], S.Yu. Smirnov[38], Y. Smirnov[38], L.N. Smirnova[38,a], O. Smirnova[100], A.C. Smith[42], D.R. Smith[162], E.A. Smith[40], J.L. Smith[103], R. Smith[146], M. Smizanska[93], K. Smolek[135], A.A. Snesarev[38], H.L. Snoek[117], S. Snyder[30], R. Sobie[168,w], A. Soffer[154], C.A. Solans Sanchez[37], E.Yu. Soldatov[38], U. Soldevila[166], A.A. Solodkov[38], S. Solomon[27], A. Soloshenko[39], K. Solovieva[55], O.V. Solovyanov[41], P. Sommer[51], A. Sonay[13], W.Y. Song[159b], A. Sopczak[135], A.L. Sopio[53], F. Sopkova[29b], J.D. Sorenson[115], I.R. Sotarriva Alvarez[157], V. Sothilingam[64a], O.J. Soto Sandoval[140c,140b], S. Sottocornola[69], R. Soualah[163], Z. Soumaimi[36e], D. South[49], N. Soybelman[172], S. Spagnolo[71a,71b], M. Spalla[112], D. Sperlich[55], G. Spigo[37], B. Spisso[73a,73b], D.P. Spiteri[60], M. Spousta[136], E.J. Staats[35], R. Stamen[64a], A. Stampekis[21], E. Stanecka[88], W. Stanek-Maslouska[49], M.V. Stange[51], B. Stanislaus[18a], M.M. Stanitzki[49], B. Stapf[49], E.A. Starchenko[38], G.H. Stark[139], J. Stark[91], P. Staroba[134], P. Starovoitov[64a], S. Stärz[106], R. Staszewski[88], G. Stavropoulos[47], P. Steinberg[30], B. Stelzer[145,159a], H.J. Stelzer[132], O. Stelzer-Chilton[159a], H. Stenzel[59], T.J. Stevenson[149], G.A. Stewart[37], J.R. Stewart[124], M.C. Stockton[37], G. Stoicea[28b], M. Stolarski[133a], S. Stonjek[112], A. Straessner[51], J. Strandberg[147], S. Strandberg[48a,48b], M. Stratmann[174], M. Strauss[123], T. Strebler[104], P. Strizenec[29b], R. Ströhmer[169], D.M. Strom[126], R. Stroynowski[45], A. Strubig[48a,48b], S.A. Stucci[30], B. Stugu[17], J. Stupak[123], N.A. Styles[49], D. Su[146], S. Su[63a], W. Su[63d], X. Su[63a], D. Suchy[29a], K. Sugizaki[156], V.V. Sulin[38], M.J. Sullivan[94], D.M.S. Sultan[129], L. Sultanaliyeva[38], S. Sultansoy[3b], T. Sumida[89], S. Sun[173], O. Sunneborn Gudnadottir[164], N. Sur[104], M.R. Sutton[149], H. Suzuki[160], M. Svatos[134], M. Swiatlowski[159a], T. Swirski[169], I. Sykora[29a], M. Sykora[136], T. Sykora[136], D. Ta[102], K. Tackmann[49,t], A. Taffard[162], R. Tafirout[159a], J.S. Tafoya Vargas[67], Y. Takubo[85], M. Talby[104], A.A. Talyshev[38], K.C. Tam[65b], N.M. Tamir[154], A. Tanaka[156], J. Tanaka[156], R. Tanaka[67], M. Tanasini[148], Z. Tao[167], S. Tapia Araya[140f], S. Tapprogge[102], A. Tarek Abouelfadl Mohamed[109], S. Tarem[153], K. Tariq[14], G. Tarna[28b], G.F. Tartarelli[72a], M.J. Tartarin[91], P. Tas[136],

M. Tasevsky[134], E. Tassi[44b,44a], A.C. Tate[165], G. Tateno[156], Y. Tayalati[36e,v], G.N. Taylor[107], W. Taylor[159b], R. Teixeira De Lima[146], P. Teixeira-Dias[97], J.J. Teoh[158], K. Terashi[156], J. Terron[101], S. Terzo[13], M. Testa[54], R.J. Teuscher[158,w], A. Thaler[80], O. Theiner[57], T. Theveneaux-Pelzer[104], O. Thielmann[174], D.W. Thomas[97], J.P. Thomas[21], E.A. Thompson[18a], P.D. Thompson[21], E. Thomson[131], R.E. Thornberry[45], C. Tian[63a], Y. Tian[56], V. Tikhomirov[38,a], Yu.A. Tikhonov[38], S. Timoshenko[38], D. Timoshyn[136], E.X.L. Ting[1], P. Tipton[175], A. Tishelman-Charny[30], S.H. Tlou[34g], K. Todome[157], S. Todorova-Nova[136], S. Todt[51], L. Toffolin[70a,70c], M. Togawa[85], J. Tojo[90], S. Tokár[29a], K. Tokushuku[85], O. Toldaiev[69], M. Tomoto[85,113], L. Tompkins[146,l], K.W. Topolnicki[87b], E. Torrence[126], H. Torres[91], E. Torró Pastor[166], M. Toscani[31], C. Tosciri[40], M. Tost[11], D.R. Tovey[142], I.S. Trandafir[28b], T. Trefzger[169], A. Tricoli[30], I.M. Trigger[159a], S. Trincaz-Duvoid[130], D.A. Trischuk[27], B. Trocmé[61], A. Tropina[39], L. Truong[34c], M. Trzebinski[88], A. Trzupek[88], F. Tsai[148], M. Tsai[108], A. Tsiamis[155], P.V. Tsiareshka[38], S. Tsigaridas[159a], A. Tsirigotis[155,q], V. Tsiskaridze[158], E.G. Tskhadadze[152a], M. Tsopoulou[155], Y. Tsujikawa[89], I.I. Tsukerman[38], V. Tsulaia[18a], S. Tsuno[85], K. Tsuri[121], D. Tsybychev[148], Y. Tu[65b], A. Tudorache[28b], V. Tudorache[28b], A.N. Tuna[62], S. Turchikhin[58b,58a], I. Turk Cakir[3a], R. Turra[72a], T. Turtuvshin[39], P.M. Tuts[42], S. Tzamarias[155,d], E. Tzovara[102], F. Ukegawa[160], P.A. Ulloa Poblete[140c,140b], E.N. Umaka[30], G. Unal[37], A. Undrus[30], G. Unel[162], J. Urban[29b], P. Urrejola[140a], G. Usai[8], R. Ushioda[157], M. Usman[110], F. Ustuner[53], Z. Uysal[83], V. Vacek[135], B. Vachon[106], T. Vafeiadis[37], A. Vaitkus[98], C. Valderanis[111], E. Valdes Santurio[48a,48b], M. Valente[159a], S. Valentinetti[24b,24a], A. Valero[166], E. Valiente Moreno[166], A. Vallier[91], J.A. Valls Ferrer[166], D.R. Van Arneman[117], T.R. Van Daalen[141], A. Van Der Graaf[50], P. Van Gemmeren[6], M. Van Rijnbach[37], S. Van Stroud[98], I. Van Vulpen[117], P. Vana[136], M. Vanadia[77a,77b], W. Vandelli[37], E.R. Vandewall[124], D. Vannicola[154], L. Vannoli[54], R. Vari[76a], E.W. Varnes[7], C. Varni[18b], T. Varol[151], D. Varouchas[67], L. Varriale[166], K.E. Varvell[150], M.E. Vasile[28b], L. Vaslin[85], G.A. Vasquez[168], A. Vasyukov[39], L.M. Vaughan[124], R. Vavricka[102], T. Vazquez Schroeder[37], J. Veatch[32], V. Vecchio[103], M.J. Veen[105], I. Veliscek[30], L.M. Veloce[158], F. Veloso[133a,133c], S. Veneziano[76a], A. Ventura[71a,71b], S. Ventura Gonzalez[138], A. Verbytskyi[112], M. Verducci[75a,75b], C. Vergis[96], M. Verissimo De Araujo[84b], W. Verkerke[117], J.C. Vermeulen[117], C. Vernieri[146], M. Vessella[105], M.C. Vetterli[145,ac], A. Vgenopoulos[102], N. Viaux Maira[140f], T. Vickey[142], O.E. Vickey Boeriu[142], G.H.A. Viehhauser[129], L. Vigani[64b], M. Vigl[112], M. Villa[24b,24a], M. Villaplana Perez[166], E.M. Villhauer[53], E. Vilucchi[54], M.G. Vincter[35], A. Visibile[117], C. Vittori[37], I. Vivarelli[24b,24a], E. Voevodina[112], F. Vogel[111], J.C. Voigt[51], P. Vokac[135], Yu. Volkotrub[87b], J. Von Ahnen[49], E. Von Toerne[25], B. Vormwald[37], V. Vorobel[136], K. Vorobev[38], M. Vos[166], K. Voss[144], M. Vozak[117], L. Vozdecky[123], N. Vranjes[16], M. Vranjes Milosavljevic[16], M. Vreeswijk[117], N.K. Vu[63d,63c], R. Vuillermet[37], O. Vujinovic[102], I. Vukotic[40], I.K. Vyas[35], S. Wada[160], C. Wagner[105], J.M. Wagner[18a], W. Wagner[174], S. Wahdan[174], H. Wahlberg[92], J. Walder[137], R. Walker[111], W. Walkowiak[144], A. Wall[131], E.J. Wallin[100], T. Wamorkar[6], A.Z. Wang[139], C. Wang[102], C. Wang[11], H. Wang[18a], J. Wang[65c], P. Wang[98], R. Wang[62], R. Wang[6], S.M. Wang[151], S. Wang[63b], S. Wang[14], T. Wang[63a], W.T. Wang[81], W. Wang[14], X. Wang[114a], X. Wang[165], X. Wang[63c], Y. Wang[63d], Y. Wang[114a], Y. Wang[63a], Z. Wang[108], Z. Wang[63d,52,63c], Z. Wang[108], A. Warburton[106], R.J. Ward[21], N. Warrack[60], S. Waterhouse[97], A.T. Watson[21], H. Watson[53], M.F. Watson[21], E. Watton[60,137], G. Watts[141], B.M. Waugh[98], J.M. Webb[55], C. Weber[30], H.A. Weber[19], M.S. Weber[20], S.M. Weber[64a], C. Wei[63a], Y. Wei[55], A.R. Weidberg[129], E.J. Weik[120], J. Weingarten[50], C. Weiser[55], C.J. Wells[49], T. Wenaus[30],

B. Wendland[50], T. Wengler[37], N.S. Wenke[112], N. Wermes[25], M. Wessels[64a], A.M. Wharton[93], A.S. White[62], A. White[8], M.J. White[1], D. Whiteson[162], L. Wickremasinghe[127], W. Wiedenmann[173], M. Wielers[137], C. Wiglesworth[43], D.J. Wilbern[123], H.G. Wilkens[37], J.J.H. Wilkinson[33], D.M. Williams[42], H.H. Williams[131], S. Williams[33], S. Willocq[105], B.J. Wilson[103], P.J. Windischhofer[40], F.I. Winkel[31], F. Winklmeier[126], B.T. Winter[55], J.K. Winter[103], M. Wittgen[146], M. Wobisch[99], T. Wojtkowski[61], Z. Wolffs[117], J. Wollrath[162], M.W. Wolter[88], H. Wolters[133a,133c], M.C. Wong[139], E.L. Woodward[42], S.D. Worm[49], B.K. Wosiek[88], K.W. Woźniak[88], S. Wozniewski[56], K. Wraight[60], C. Wu[21], M. Wu[114b], M. Wu[116], S.L. Wu[173], X. Wu[57], Y. Wu[63a], Z. Wu[4], J. Wuerzinger[112,aa], T.R. Wyatt[103], B.M. Wynne[53], S. Xella[43], L. Xia[114a], M. Xia[15], M. Xie[63a], S. Xin[14,114c], A. Xiong[126], J. Xiong[18a], D. Xu[14], H. Xu[63a], L. Xu[63a], R. Xu[131], T. Xu[108], Y. Xu[15], Z. Xu[53], Z. Xu[114a], B. Yabsley[150], S. Yacoob[34a], Y. Yamaguchi[85], E. Yamashita[156], H. Yamauchi[160], T. Yamazaki[18a], Y. Yamazaki[86], S. Yan[60], Z. Yan[105], H.J. Yang[63c,63d], H.T. Yang[63a], S. Yang[63a], T. Yang[65c], X. Yang[37], X. Yang[14], Y. Yang[45], Y. Yang[63a], Z. Yang[63a], W-M. Yao[18a], H. Ye[114a], H. Ye[56], J. Ye[14], S. Ye[30], X. Ye[63a], Y. Yeh[98], I. Yeletskikh[39], B.K. Yeo[18b], M.R. Yexley[98], T.P. Yildirim[129], P. Yin[42], K. Yorita[171], S. Younas[28b], C.J.S. Young[37], C. Young[146], C. Yu[14,114c], Y. Yu[63a], J. Yuan[14,114c], M. Yuan[108], R. Yuan[63d,63c], L. Yue[98], M. Zaazoua[63a], B. Zabinski[88], E. Zaid[53], Z.K. Zak[88], T. Zakareishvili[166], S. Zambito[57], J.A. Zamora Saa[140d,140b], J. Zang[156], D. Zanzi[55], O. Zaplatilek[135], C. Zeitnitz[174], H. Zeng[14], J.C. Zeng[165], D.T. Zenger Jr[27], O. Zenin[38], T. Ženiš[29a], S. Zenz[96], S. Zerradi[36a], D. Zerwas[67], M. Zhai[14,114c], D.F. Zhang[142], J. Zhang[63b], J. Zhang[6], K. Zhang[14,114c], L. Zhang[63a], L. Zhang[114a], P. Zhang[14,114c], R. Zhang[173], S. Zhang[108], S. Zhang[91], T. Zhang[156], X. Zhang[63c], X. Zhang[63b], Y. Zhang[63c], Y. Zhang[98], Y. Zhang[114a], Z. Zhang[18a], Z. Zhang[63b], Z. Zhang[67], H. Zhao[141], T. Zhao[63b], Y. Zhao[139], Z. Zhao[63a], Z. Zhao[63a], A. Zhemchugov[39], J. Zheng[114a], K. Zheng[165], X. Zheng[63a], Z. Zheng[146], D. Zhong[165], B. Zhou[108], H. Zhou[7], N. Zhou[63c], Y. Zhou[15], Y. Zhou[114a], Y. Zhou[7], C.G. Zhu[63b], J. Zhu[108], X. Zhu[63d], Y. Zhu[63c], Y. Zhu[63a], X. Zhuang[14], K. Zhukov[69], N.I. Zimine[39], J. Zinsser[64b], M. Ziolkowski[144], L. Živković[16], A. Zoccoli[24b,24a], K. Zoch[62], T.G. Zorbas[142], O. Zormpa[47], W. Zou[42], L. Zwalinski[37].

[1]Department of Physics, University of Adelaide, Adelaide; Australia.
[2]Department of Physics, University of Alberta, Edmonton AB; Canada.
[3](a)Department of Physics, Ankara University, Ankara;(b)Division of Physics, TOBB University of Economics and Technology, Ankara; Türkiye.
[4]LAPP, Université Savoie Mont Blanc, CNRS/IN2P3, Annecy; France.
[5]APC, Université Paris Cité, CNRS/IN2P3, Paris; France.
[6]High Energy Physics Division, Argonne National Laboratory, Argonne IL; United States of America.
[7]Department of Physics, University of Arizona, Tucson AZ; United States of America.
[8]Department of Physics, University of Texas at Arlington, Arlington TX; United States of America.
[9]Physics Department, National and Kapodistrian University of Athens, Athens; Greece.
[10]Physics Department, National Technical University of Athens, Zografou; Greece.
[11]Department of Physics, University of Texas at Austin, Austin TX; United States of America.
[12]Institute of Physics, Azerbaijan Academy of Sciences, Baku; Azerbaijan.
[13]Institut de Física d'Altes Energies (IFAE), Barcelona Institute of Science and Technology, Barcelona; Spain.
[14]Institute of High Energy Physics, Chinese Academy of Sciences, Beijing; China.

[15]Physics Department, Tsinghua University, Beijing; China.
[16]Institute of Physics, University of Belgrade, Belgrade; Serbia.
[17]Department for Physics and Technology, University of Bergen, Bergen; Norway.
[18](a)Physics Division, Lawrence Berkeley National Laboratory, Berkeley CA;(b)University of California, Berkeley CA; United States of America.
[19]Institut für Physik, Humboldt Universität zu Berlin, Berlin; Germany.
[20]Albert Einstein Center for Fundamental Physics and Laboratory for High Energy Physics, University of Bern, Bern; Switzerland.
[21]School of Physics and Astronomy, University of Birmingham, Birmingham; United Kingdom.
[22](a)Department of Physics, Bogazici University, Istanbul;(b)Department of Physics Engineering, Gaziantep University, Gaziantep;(c)Department of Physics, Istanbul University, Istanbul; Türkiye.
[23](a)Facultad de Ciencias y Centro de Investigaciónes, Universidad Antonio Nariño, Bogotá;(b)Departamento de Física, Universidad Nacional de Colombia, Bogotá; Colombia.
[24](a)Dipartimento di Fisica e Astronomia A. Righi, Università di Bologna, Bologna;(b)INFN Sezione di Bologna; Italy.
[25]Physikalisches Institut, Universität Bonn, Bonn; Germany.
[26]Department of Physics, Boston University, Boston MA; United States of America.
[27]Department of Physics, Brandeis University, Waltham MA; United States of America.
[28](a)Transilvania University of Brasov, Brasov;(b)Horia Hulubei National Institute of Physics and Nuclear Engineering, Bucharest;(c)Department of Physics, Alexandru Ioan Cuza University of Iasi, Iasi;(d)National Institute for Research and Development of Isotopic and Molecular Technologies, Physics Department, Cluj-Napoca;(e)National University of Science and Technology Politechnica, Bucharest;(f)West University in Timisoara, Timisoara;(g)Faculty of Physics, University of Bucharest, Bucharest; Romania.
[29](a)Faculty of Mathematics, Physics and Informatics, Comenius University, Bratislava;(b)Department of Subnuclear Physics, Institute of Experimental Physics of the Slovak Academy of Sciences, Kosice; Slovak Republic.
[30]Physics Department, Brookhaven National Laboratory, Upton NY; United States of America.
[31]Universidad de Buenos Aires, Facultad de Ciencias Exactas y Naturales, Departamento de Física, y CONICET, Instituto de Física de Buenos Aires (IFIBA), Buenos Aires; Argentina.
[32]California State University, CA; United States of America.
[33]Cavendish Laboratory, University of Cambridge, Cambridge; United Kingdom.
[34](a)Department of Physics, University of Cape Town, Cape Town;(b)iThemba Labs, Western Cape;(c)Department of Mechanical Engineering Science, University of Johannesburg, Johannesburg;(d)National Institute of Physics, University of the Philippines Diliman (Philippines);(e)University of South Africa, Department of Physics, Pretoria;(f)University of Zululand, KwaDlangezwa;(g)School of Physics, University of the Witwatersrand, Johannesburg; South Africa.
[35]Department of Physics, Carleton University, Ottawa ON; Canada.
[36](a)Faculté des Sciences Ain Chock, Université Hassan II de Casablanca;(b)Faculté des Sciences, Université Ibn-Tofail, Kénitra;(c)Faculté des Sciences Semlalia, Université Cadi Ayyad, LPHEA-Marrakech;(d)LPMR, Faculté des Sciences, Université Mohamed Premier, Oujda;(e)Faculté des sciences, Université Mohammed V, Rabat;(f)Institute of Applied Physics, Mohammed VI Polytechnic University, Ben Guerir; Morocco.
[37]CERN, Geneva; Switzerland.
[38]Affiliated with an institute covered by a cooperation agreement with CERN.
[39]Affiliated with an international laboratory covered by a cooperation agreement with CERN.
[40]Enrico Fermi Institute, University of Chicago, Chicago IL; United States of America.
[41]LPC, Université Clermont Auvergne, CNRS/IN2P3, Clermont-Ferrand; France.

[42]Nevis Laboratory, Columbia University, Irvington NY; United States of America.
[43]Niels Bohr Institute, University of Copenhagen, Copenhagen; Denmark.
[44](a)Dipartimento di Fisica, Università della Calabria, Rende;(b)INFN Gruppo Collegato di Cosenza, Laboratori Nazionali di Frascati; Italy.
[45]Physics Department, Southern Methodist University, Dallas TX; United States of America.
[46]Physics Department, University of Texas at Dallas, Richardson TX; United States of America.
[47]National Centre for Scientific Research "Demokritos", Agia Paraskevi; Greece.
[48](a)Department of Physics, Stockholm University;(b)Oskar Klein Centre, Stockholm; Sweden.
[49]Deutsches Elektronen-Synchrotron DESY, Hamburg and Zeuthen; Germany.
[50]Fakultät Physik , Technische Universität Dortmund, Dortmund; Germany.
[51]Institut für Kern- und Teilchenphysik, Technische Universität Dresden, Dresden; Germany.
[52]Department of Physics, Duke University, Durham NC; United States of America.
[53]SUPA - School of Physics and Astronomy, University of Edinburgh, Edinburgh; United Kingdom.
[54]INFN e Laboratori Nazionali di Frascati, Frascati; Italy.
[55]Physikalisches Institut, Albert-Ludwigs-Universität Freiburg, Freiburg; Germany.
[56]II. Physikalisches Institut, Georg-August-Universität Göttingen, Göttingen; Germany.
[57]Département de Physique Nucléaire et Corpusculaire, Université de Genève, Genève; Switzerland.
[58](a)Dipartimento di Fisica, Università di Genova, Genova;(b)INFN Sezione di Genova; Italy.
[59]II. Physikalisches Institut, Justus-Liebig-Universität Giessen, Giessen; Germany.
[60]SUPA - School of Physics and Astronomy, University of Glasgow, Glasgow; United Kingdom.
[61]LPSC, Université Grenoble Alpes, CNRS/IN2P3, Grenoble INP, Grenoble; France.
[62]Laboratory for Particle Physics and Cosmology, Harvard University, Cambridge MA; United States of America.
[63](a)Department of Modern Physics and State Key Laboratory of Particle Detection and Electronics, University of Science and Technology of China, Hefei;(b)Institute of Frontier and Interdisciplinary Science and Key Laboratory of Particle Physics and Particle Irradiation (MOE), Shandong University, Qingdao;(c)School of Physics and Astronomy, Shanghai Jiao Tong University, Key Laboratory for Particle Astrophysics and Cosmology (MOE), SKLPPC, Shanghai;(d)Tsung-Dao Lee Institute, Shanghai;(e)School of Physics and Microelectronics, Zhengzhou University; China.
[64](a)Kirchhoff-Institut für Physik, Ruprecht-Karls-Universität Heidelberg, Heidelberg;(b)Physikalisches Institut, Ruprecht-Karls-Universität Heidelberg, Heidelberg; Germany.
[65](a)Department of Physics, Chinese University of Hong Kong, Shatin, N.T., Hong Kong;(b)Department of Physics, University of Hong Kong, Hong Kong;(c)Department of Physics and Institute for Advanced Study, Hong Kong University of Science and Technology, Clear Water Bay, Kowloon, Hong Kong; China.
[66]Department of Physics, National Tsing Hua University, Hsinchu; Taiwan.
[67]IJCLab, Université Paris-Saclay, CNRS/IN2P3, 91405, Orsay; France.
[68]Centro Nacional de Microelectrónica (IMB-CNM-CSIC), Barcelona; Spain.
[69]Department of Physics, Indiana University, Bloomington IN; United States of America.
[70](a)INFN Gruppo Collegato di Udine, Sezione di Trieste, Udine;(b)ICTP, Trieste;(c)Dipartimento Politecnico di Ingegneria e Architettura, Università di Udine, Udine; Italy.
[71](a)INFN Sezione di Lecce;(b)Dipartimento di Matematica e Fisica, Università del Salento, Lecce; Italy.
[72](a)INFN Sezione di Milano;(b)Dipartimento di Fisica, Università di Milano, Milano; Italy.
[73](a)INFN Sezione di Napoli;(b)Dipartimento di Fisica, Università di Napoli, Napoli; Italy.
[74](a)INFN Sezione di Pavia;(b)Dipartimento di Fisica, Università di Pavia, Pavia; Italy.
[75](a)INFN Sezione di Pisa;(b)Dipartimento di Fisica E. Fermi, Università di Pisa, Pisa; Italy.
[76](a)INFN Sezione di Roma;(b)Dipartimento di Fisica, Sapienza Università di Roma, Roma; Italy.
[77](a)INFN Sezione di Roma Tor Vergata;(b)Dipartimento di Fisica, Università di Roma Tor Vergata,

Roma; Italy.
[78](a)INFN Sezione di Roma Tre;(b)Dipartimento di Matematica e Fisica, Università Roma Tre, Roma; Italy.
[79](a)INFN-TIFPA;(b)Università degli Studi di Trento, Trento; Italy.
[80]Universität Innsbruck, Department of Astro and Particle Physics, Innsbruck; Austria.
[81]University of Iowa, Iowa City IA; United States of America.
[82]Department of Physics and Astronomy, Iowa State University, Ames IA; United States of America.
[83]Istinye University, Sariyer, Istanbul; Türkiye.
[84](a)Departamento de Engenharia Elétrica, Universidade Federal de Juiz de Fora (UFJF), Juiz de Fora;(b)Universidade Federal do Rio De Janeiro COPPE/EE/IF, Rio de Janeiro;(c)Instituto de Física, Universidade de São Paulo, São Paulo;(d)Rio de Janeiro State University, Rio de Janeiro;(e)Federal University of Bahia, Bahia; Brazil.
[85]KEK, High Energy Accelerator Research Organization, Tsukuba; Japan.
[86]Graduate School of Science, Kobe University, Kobe; Japan.
[87](a)AGH University of Krakow, Faculty of Physics and Applied Computer Science, Krakow;(b)Marian Smoluchowski Institute of Physics, Jagiellonian University, Krakow; Poland.
[88]Institute of Nuclear Physics Polish Academy of Sciences, Krakow; Poland.
[89]Faculty of Science, Kyoto University, Kyoto; Japan.
[90]Research Center for Advanced Particle Physics and Department of Physics, Kyushu University, Fukuoka ; Japan.
[91]L2IT, Université de Toulouse, CNRS/IN2P3, UPS, Toulouse; France.
[92]Instituto de Física La Plata, Universidad Nacional de La Plata and CONICET, La Plata; Argentina.
[93]Physics Department, Lancaster University, Lancaster; United Kingdom.
[94]Oliver Lodge Laboratory, University of Liverpool, Liverpool; United Kingdom.
[95]Department of Experimental Particle Physics, Jožef Stefan Institute and Department of Physics, University of Ljubljana, Ljubljana; Slovenia.
[96]School of Physics and Astronomy, Queen Mary University of London, London; United Kingdom.
[97]Department of Physics, Royal Holloway University of London, Egham; United Kingdom.
[98]Department of Physics and Astronomy, University College London, London; United Kingdom.
[99]Louisiana Tech University, Ruston LA; United States of America.
[100]Fysiska institutionen, Lunds universitet, Lund; Sweden.
[101]Departamento de Física Teorica C-15 and CIAFF, Universidad Autónoma de Madrid, Madrid; Spain.
[102]Institut für Physik, Universität Mainz, Mainz; Germany.
[103]School of Physics and Astronomy, University of Manchester, Manchester; United Kingdom.
[104]CPPM, Aix-Marseille Université, CNRS/IN2P3, Marseille; France.
[105]Department of Physics, University of Massachusetts, Amherst MA; United States of America.
[106]Department of Physics, McGill University, Montreal QC; Canada.
[107]School of Physics, University of Melbourne, Victoria; Australia.
[108]Department of Physics, University of Michigan, Ann Arbor MI; United States of America.
[109]Department of Physics and Astronomy, Michigan State University, East Lansing MI; United States of America.
[110]Group of Particle Physics, University of Montreal, Montreal QC; Canada.
[111]Fakultät für Physik, Ludwig-Maximilians-Universität München, München; Germany.
[112]Max-Planck-Institut für Physik (Werner-Heisenberg-Institut), München; Germany.
[113]Graduate School of Science and Kobayashi-Maskawa Institute, Nagoya University, Nagoya; Japan.
[114](a)Department of Physics, Nanjing University, Nanjing;(b)School of Science, Shenzhen Campus of Sun Yat-sen University;(c)University of Chinese Academy of Science (UCAS), Beijing; China.

[115]Department of Physics and Astronomy, University of New Mexico, Albuquerque NM; United States of America.
[116]Institute for Mathematics, Astrophysics and Particle Physics, Radboud University/Nikhef, Nijmegen; Netherlands.
[117]Nikhef National Institute for Subatomic Physics and University of Amsterdam, Amsterdam; Netherlands.
[118]Department of Physics, Northern Illinois University, DeKalb IL; United States of America.
[119](a)New York University Abu Dhabi, Abu Dhabi;(b)United Arab Emirates University, Al Ain; United Arab Emirates.
[120]Department of Physics, New York University, New York NY; United States of America.
[121]Ochanomizu University, Otsuka, Bunkyo-ku, Tokyo; Japan.
[122]Ohio State University, Columbus OH; United States of America.
[123]Homer L. Dodge Department of Physics and Astronomy, University of Oklahoma, Norman OK; United States of America.
[124]Department of Physics, Oklahoma State University, Stillwater OK; United States of America.
[125]Palacký University, Joint Laboratory of Optics, Olomouc; Czech Republic.
[126]Institute for Fundamental Science, University of Oregon, Eugene, OR; United States of America.
[127]Graduate School of Science, Osaka University, Osaka; Japan.
[128]Department of Physics, University of Oslo, Oslo; Norway.
[129]Department of Physics, Oxford University, Oxford; United Kingdom.
[130]LPNHE, Sorbonne Université, Université Paris Cité, CNRS/IN2P3, Paris; France.
[131]Department of Physics, University of Pennsylvania, Philadelphia PA; United States of America.
[132]Department of Physics and Astronomy, University of Pittsburgh, Pittsburgh PA; United States of America.
[133](a)Laboratório de Instrumentação e Física Experimental de Partículas - LIP, Lisboa;(b)Departamento de Física, Faculdade de Ciências, Universidade de Lisboa, Lisboa;(c)Departamento de Física, Universidade de Coimbra, Coimbra;(d)Centro de Física Nuclear da Universidade de Lisboa, Lisboa;(e)Departamento de Física, Universidade do Minho, Braga;(f)Departamento de Física Teórica y del Cosmos, Universidad de Granada, Granada (Spain);(g)Departamento de Física, Instituto Superior Técnico, Universidade de Lisboa, Lisboa; Portugal.
[134]Institute of Physics of the Czech Academy of Sciences, Prague; Czech Republic.
[135]Czech Technical University in Prague, Prague; Czech Republic.
[136]Charles University, Faculty of Mathematics and Physics, Prague; Czech Republic.
[137]Particle Physics Department, Rutherford Appleton Laboratory, Didcot; United Kingdom.
[138]IRFU, CEA, Université Paris-Saclay, Gif-sur-Yvette; France.
[139]Santa Cruz Institute for Particle Physics, University of California Santa Cruz, Santa Cruz CA; United States of America.
[140](a)Departamento de Física, Pontificia Universidad Católica de Chile, Santiago;(b)Millennium Institute for Subatomic physics at high energy frontier (SAPHIR), Santiago;(c)Instituto de Investigación Multidisciplinario en Ciencia y Tecnología, y Departamento de Física, Universidad de La Serena;(d)Universidad Andres Bello, Department of Physics, Santiago;(e)Instituto de Alta Investigación, Universidad de Tarapacá, Arica;(f)Departamento de Física, Universidad Técnica Federico Santa María, Valparaíso; Chile.
[141]Department of Physics, University of Washington, Seattle WA; United States of America.
[142]Department of Physics and Astronomy, University of Sheffield, Sheffield; United Kingdom.
[143]Department of Physics, Shinshu University, Nagano; Japan.
[144]Department Physik, Universität Siegen, Siegen; Germany.

[145]Department of Physics, Simon Fraser University, Burnaby BC; Canada.
[146]SLAC National Accelerator Laboratory, Stanford CA; United States of America.
[147]Department of Physics, Royal Institute of Technology, Stockholm; Sweden.
[148]Departments of Physics and Astronomy, Stony Brook University, Stony Brook NY; United States of America.
[149]Department of Physics and Astronomy, University of Sussex, Brighton; United Kingdom.
[150]School of Physics, University of Sydney, Sydney; Australia.
[151]Institute of Physics, Academia Sinica, Taipei; Taiwan.
[152](a)E. Andronikashvili Institute of Physics, Iv. Javakhishvili Tbilisi State University, Tbilisi;(b)High Energy Physics Institute, Tbilisi State University, Tbilisi;(c)University of Georgia, Tbilisi; Georgia.
[153]Department of Physics, Technion, Israel Institute of Technology, Haifa; Israel.
[154]Raymond and Beverly Sackler School of Physics and Astronomy, Tel Aviv University, Tel Aviv; Israel.
[155]Department of Physics, Aristotle University of Thessaloniki, Thessaloniki; Greece.
[156]International Center for Elementary Particle Physics and Department of Physics, University of Tokyo, Tokyo; Japan.
[157]Department of Physics, Tokyo Institute of Technology, Tokyo; Japan.
[158]Department of Physics, University of Toronto, Toronto ON; Canada.
[159](a)TRIUMF, Vancouver BC;(b)Department of Physics and Astronomy, York University, Toronto ON; Canada.
[160]Division of Physics and Tomonaga Center for the History of the Universe, Faculty of Pure and Applied Sciences, University of Tsukuba, Tsukuba; Japan.
[161]Department of Physics and Astronomy, Tufts University, Medford MA; United States of America.
[162]Department of Physics and Astronomy, University of California Irvine, Irvine CA; United States of America.
[163]University of Sharjah, Sharjah; United Arab Emirates.
[164]Department of Physics and Astronomy, University of Uppsala, Uppsala; Sweden.
[165]Department of Physics, University of Illinois, Urbana IL; United States of America.
[166]Instituto de Física Corpuscular (IFIC), Centro Mixto Universidad de Valencia - CSIC, Valencia; Spain.
[167]Department of Physics, University of British Columbia, Vancouver BC; Canada.
[168]Department of Physics and Astronomy, University of Victoria, Victoria BC; Canada.
[169]Fakultät für Physik und Astronomie, Julius-Maximilians-Universität Würzburg, Würzburg; Germany.
[170]Department of Physics, University of Warwick, Coventry; United Kingdom.
[171]Waseda University, Tokyo; Japan.
[172]Department of Particle Physics and Astrophysics, Weizmann Institute of Science, Rehovot; Israel.
[173]Department of Physics, University of Wisconsin, Madison WI; United States of America.
[174]Fakultät für Mathematik und Naturwissenschaften, Fachgruppe Physik, Bergische Universität Wuppertal, Wuppertal; Germany.
[175]Department of Physics, Yale University, New Haven CT; United States of America.
[a] Also Affiliated with an institute covered by a cooperation agreement with CERN.
[b] Also at An-Najah National University, Nablus; Palestine.
[c] Also at Borough of Manhattan Community College, City University of New York, New York NY; United States of America.
[d] Also at Center for Interdisciplinary Research and Innovation (CIRI-AUTH), Thessaloniki; Greece.
[e] Also at CERN, Geneva; Switzerland.
[f] Also at CMD-AC UNEC Research Center, Azerbaijan State University of Economics (UNEC); Azerbaijan.
[g] Also at Département de Physique Nucléaire et Corpusculaire, Université de Genève, Genève;

Switzerland.
[h] Also at Departament de Fisica de la Universitat Autonoma de Barcelona, Barcelona; Spain.
[i] Also at Department of Financial and Management Engineering, University of the Aegean, Chios; Greece.
[j] Also at Department of Physics, California State University, Sacramento; United States of America.
[k] Also at Department of Physics, King's College London, London; United Kingdom.
[l] Also at Department of Physics, Stanford University, Stanford CA; United States of America.
[m] Also at Department of Physics, Stellenbosch University; South Africa.
[n] Also at Department of Physics, University of Fribourg, Fribourg; Switzerland.
[o] Also at Department of Physics, University of Thessaly; Greece.
[p] Also at Department of Physics, Westmont College, Santa Barbara; United States of America.
[q] Also at Hellenic Open University, Patras; Greece.
[r] Also at Imam Mohammad Ibn Saud Islamic University; Saudi Arabia.
[s] Also at Institucio Catalana de Recerca i Estudis Avancats, ICREA, Barcelona; Spain.
[t] Also at Institut für Experimentalphysik, Universität Hamburg, Hamburg; Germany.
[u] Also at Institute for Nuclear Research and Nuclear Energy (INRNE) of the Bulgarian Academy of Sciences, Sofia; Bulgaria.
[v] Also at Institute of Applied Physics, Mohammed VI Polytechnic University, Ben Guerir; Morocco.
[w] Also at Institute of Particle Physics (IPP); Canada.
[x] Also at Institute of Physics, Azerbaijan Academy of Sciences, Baku; Azerbaijan.
[y] Also at Institute of Theoretical Physics, Ilia State University, Tbilisi; Georgia.
[z] Also at National Institute of Physics, University of the Philippines Diliman (Philippines); Philippines.
[aa] Also at Technical University of Munich, Munich; Germany.
[ab] Also at The Collaborative Innovation Center of Quantum Matter (CICQM), Beijing; China.
[ac] Also at TRIUMF, Vancouver BC; Canada.
[ad] Also at Università di Napoli Parthenope, Napoli; Italy.
[ae] Also at University of Colorado Boulder, Department of Physics, Colorado; United States of America.
[af] Also at Washington College, Chestertown, MD; United States of America.
[ag] Also at Yeditepe University, Physics Department, Istanbul; Türkiye.
[*] Deceased